

**BIOBASED/BIODEGRADABLE/COMPOSTABLE
/ANTIBACTERIAL POLYMERIC MULCHING AND FOOD
PACKAGING FILMS**

**BİYOESASLI/BİYOBOZUNUR/KOMPOST EDİLEBLİR
/ANTİBAKTERİYAL POLİMERİK TARIMSAL ÖRTÜ VE
GIDA AMBALAJ FİLMLERİ**

KOUROUSH SALİMİ

Prof. Dr. ERHAN BİŞKİN

Supervisor

Submitted to Institute of Science of Hacettepe University
as a Partial Fulfillment to the Requirements
for the Award of the Degree of Doctor of Philosophy
in Chemical Engineering

2015

This work named “**Biobased/Biodegradable/Compostable/Antibacterial Polymeric Mulching and Food Packaging Films**” by **KOUROUSH SALİMİ** has been approved as a thesis for the Degree of **DOCTOR OF PHILOSOPHY IN CHEMICAL ENGINEERING** by the below mentioned Examining Committee Members.

Prof. Dr. Tülin KUTSAL

Head

.....

Prof. Dr. Erhan BİŞKİN

Supervisor

.....

Prof. Dr. Hülya YAVUZ ERSAN

Member

.....

Assoc. Prof. Dr. Halil Murat AYDIN

Member

.....

Asst. Prof. Dr. Sinan EĞRİ

Member

.....

This thesis has been approved as a thesis for the Degree of **DOCTOR OF PHILOSOPHY IN CHEMICAL ENGINEERING** by Board of Directors of the Institute for Graduate Studies in Science and Engineering.

Prof. Dr. Fatma SEVİN DÜZ

Director of the Institute of
Graduate Studies in Science

To my mother...

ETHICS

In this thesis study, prepared in accordance with the spelling rules of Institute of Graduate Studies in Science of Hacettepe University,

I declare that

- all the information and documents have been obtained in the base of the academic rules
- all audio-visual and written information and results have been presented according to the rules of scientific ethics
- in case of using others works, related studies have been cited in accordance with the scientific standards
- all cited studies have been fully referenced
- I did not do any distortion in the data set
- and any part of this thesis has not been presented as another thesis study at this or any other university.

26/01/2015

KOUROUSH SALİMİ

ABSTRACT

BIOBASED/BIODEGRADABLE/COMPOSTABLE/ ANTIBACTERIAL POLYMERIC MULCHING AND FOOD PACKAGING FILMS

Kouroush SALİMİ

Doctor of Philosophy, Department of Chemical Engineering

Supervisor: Prof. Dr. Erhan BIŞKİN

January 2015, 143 pages

The synthetic polymers have replaced metals, glasses, ceramics and wood in many products and are found in almost all aspects of technology, from simple household utilities to advanced polymeric composites in high-tech engineering such as computers, space ships, etc. Currently, most polymeric packaging/mulching materials are based on non-renewable fossil resources. Because of the disadvantages include the fact that they are expensive and non-biodegradable, and some are 'toxic' when compared to natural polymers, they release toxic components during fabrication and these materials do not allow composting and take long time to break down. Therefore, "green" plastic packaging materials that are based on renewable resources are required.

The effect of disposal plastics products raised significantly the environmental problems. For example, plastics packaging, being disposed of soon after their purchase. However, environmental concerns have raised significant

international interest in the using carbohydrate polymers to produce biodegradable plastics. Polysaccharides are relatively complex carbohydrates, with the general formula $(C_6H_{10}O_5)_n$. The polymer chains are made up of monosaccharide units linked together by glycoside bonds. Among polysaccharides, starch is one of the most widely produced biopolymer in the world. Because of biocompatibility and degradability, the biopolymers has been of interest in pharmaceuticals, filling agent in synthetic polymers, thermoplastics, paper, textile and several other applications.

Poly(lactic acid) (PLA) is an aliphatic polyester, biodegradable and compostable thermoplastic derived from renewable plant sources, such as starch and sugar. Recently, with the elevated environmental awareness of the general public, PLA has been considered as one of the solutions to decrease solid waste disposal problems. However, discovery of new polymerization techniques which allow the economical production of high molecular weight PLA, cause to decrease of the dependence on conventional plastics for consumer goods and packaging materials.

In the research described in this thesis, Novel bioengineering functional copolymer-*g*-biopolymer-based layered silicate nanocomposites were fabricated by catalytic interlamellar bulk graft copolymerization of L-lactic acid (LA) monomer onto alternating copolymer of maleic anhydride (MA) with 1-octadecene as a reactive matrix polymer in the presence of preintercalated LA...organo-MMT clay (reactive ODA-MMT and non-reactive DMDA-MMT) complexes as nanofillers under vacuum at 80°C. Additionally, the synthesis and characterization of novel functional copolymer-*g*-biopolymer layered silicate nanocomposites by bulk self-catalytic interlamellar graft copolymerization of preintercalated MMT...L-LA complexes onto poly(maleic anhydride-*alt*-1-octadecene) poly(MA-*alt*-1-OD) as a matrix polymer were fabricated. In this part, the development of a novel approach for the grafting/graft copolymerization of LA onto alternating copolymer of maleic anhydride and 1-octadecene in the presence of MMTs (Na^+ -MMT and Ag^+ -MMT) or organoclay (octadecyl amine modified MMT) as a catalyst-nanofiller (3.2 mass%) without use of hazardous conventional thin catalyst through ring opening monoesterification reaction of anhydride units with LA monomer and then its

graft copolymerisation to prepare the PLA grafted MMT/copolymer nanocomposites. Another aspect of this work is to evaluate the self-catalytic effects of different clays on graft copolymerization, as well as on chemical and physical structures, thermal properties and morphology of the CPNs.

In this thesis, novel biobased/biodegradable/compostable antibacterial St-*g*-PLA copolymers and St-*g*-PLA/organoclay nanocomposites were fabricated by using different “green” methods applying as a food packaging and mulching films. The development of new methods for graft copolymerization of L-lactic acid onto starch were evaluated for the first time in the literature for this kind of monomers, such as supercritical carbon dioxide media, microwave irradiation, shear mixing method, and reactive extrusion without using toxic solvents and investigation of the St-*g*-PLA based film properties.

Chemical and physical structures, thermal behavior and morphology of synthesized copolymers and nanocomposites, as well as some parameters were performed by FTIR and ¹³C CP/MAS NMR spectroscopy, MALDI-TOF-MS, XRD, TGA/DTG and SEM/TEM, respectively. The film extrusion in a lab-scale was carried out by using a twin-screw extruder equipped by a film extrusion die, blowing unit and rotating film-uptake. Mechanical properties were evaluated from the tensile stress-strain test data. The effect of St/LA ratio and in situ intercalation/exfoliation process of organoclay on water vapor, O₂ and CO₂ permeabilities were measured. Films were exposed degradation tests in natural buried soil. Additionally, antibacterial activities of the St-*g*-PLA based films were obtained and also the food contact analysis of the films were performed. Finally, the real field applications of the St-*g*-PLA and St-*g*-PLA/organoclay nanocomposite based films were performed to mulch tomato and pepper seed at greenhouse conditions.

Key words: interlamellar graft copolymerization, organoclay, nanocomposites, Graft copolymerization, Starch, Lactic acid, Supercritical carbon dioxide, microwave heating, shear mixing, reactive extrusion.

ÖZET

BİYOESASLI/BİYOBOZUNUR/KOMPOST EDİLEBLİR /ANTİBAKTERİYAL POLİMERİK TARIMSAL ÖRTÜ VE GIDA AMBALAJ FİLMLEİ

Kouroush SALİMİ

Doktora, Kimya Mühendisliđi Bölümü

Tez Danışmanı: Prof. Dr. Erhan BİŞKİN

Ocak 2015, 143 sayfa

Günümüzde sentetik polimerler pekçok üründe kullanılan metallerin, camların, seramiklerin ve ahşabın yerini almıştır. Basit, günlük evle ilgili materyallerde kullanımından, bilgisayarlar, uzay gemileri, vb. gibi üretimlerinde ileri teknolojik mühendislikten yararlanan ürünlerin eldesine kadar geniş bir yelpazede kullanımları bulunmaktadır. Mevcut durumda, birçok polimerik ambalaj/örtü materyallerinin üretimi yenilenebilir olmayan fosil kaynaklar bazlıdır. Bu kaynaklar pahalı ve biyobozunur olmamaları, doğal polimerlere göre barındırdıkları toksitite gibi dezavantajları beraberlerinde getirmektedirler. Üretimleri sırasında toksik içerikler salmaları, kompostlamaya izin vermemeleri ve bozulma sürelerinin uzunlukları diğer dezavantajlarındandır. Bu yüzden yenilenebilir kaynaklı yeşil plastik paketleme materyallerine ihtiyaç duyulmaktadır.

Tek kullanımlık plastik ürünlerin etkileri çevresel problemleri önemli ölçüde arttırmıştır. Örneđin; ürünlerin satışından sonra kullanım sonrası açığa çıkan

ambalaj malzemelerinin çok kısa bir sürede atık konumuna geçmesi bu problemlerin asıl sebeplerindendir. Tüm bu çevresel kaygılar, biyobozunur plastiklerin üretiminde karbonhidrat polimerlerin kullanımının uluslararası boyutta artmasını sağlamıştır. Tüm bu çevresel kaygılar, biyobozunur plastiklerin üretiminde karbonhidrat polimerlerin kullanımının uluslararası boyutta artmasını sağlamıştır. Polisakkaritler glikozidik bağla birbirine bağlanmış monosakkarit birimlerinden oluşan, $(C_6H_{10}O_5)_n$; kimyasal formülüne sahip nispeten kompleks moleküllerdir. Dünyada en fazla üretimi yapılan biyopolimerlerden bir tanesi de polisakkaritlerden nişastadır. Biyopolimerler biyoyumlulukları ve bozunabilirlikleri sayesinde farmakolojide, sentetik polimerlerde dolgu malzemesi olarak, termoplastiklerde, kağıt üretiminde, tekstil, vb. alanlarda yüksek oranda tercih edilmektedir.

Polilaktik asit (PLA) yenilenebilir bitki kaynaklarından türemiş olan, örneğin şeker ve nişasta gibi, kompost edilebilir termoplastik ve biyoyumlu, alifatik polyesterlerdir. Yakın zamanlarda, halkın çevreye artan ilgisinden dolayı, PLA bazlı polimerler katı atık sorunlarını azaltmak için çözümlerin biri olarak düşünülmektedir. Son zamanlarda, toplumun çevresel bakımdan artan duyarlılığı sayesinde, katı atık problemlerini azaltmak için yararlanılan çözümlerden bir tanesi de PLA kullanımına gidilmesi olmuştur. Ayrıca; yeni polimerizasyon tekniklerinin keşfiyle yüksek molekül ağırlıklı PLA'nın ekonomik şekildeki üretimi, tüketici eşyaları ve ambalaj malzemelerinde kullanılan geleneksel plastiklere olan bağımlılığın azalmasını da sağlamıştır.

Sonuç olarak, silikon tabakalı (reaktif ODA-MMT ve reaktif olmayan DMDA-MMT) yeni biyo-fonksiyonel kopolimer olarak poly(maleic anhydride-alt-1-octadecene)-g-biopolymer (poly(L-lactic acid) nanokompozitleri sentezlenmiştir. İşlem vakum altında 80°C'de, katalizör olarak kalay oktoat, nanofiller olarak ise önceden interkale edilmiş LA...organo-MMT organokiller (ODA-MMT and DMDA-MMT) kompleksi kullanılarak gerçekleştirilmiştir. Böylece LA...organo-MMT monomeri reaktif matris polimeri gibi alternatif kopolimer üzerine eklenerek, katalitik interlamellar bulk graft kopolimerizasyonu yapılmıştır. Bu bölümde ayrıca, geleneksel herhangi bir tehlikeli katalizör kullanılmadan; organokiller (ODA-MMT) ve montmorillonit (Na^+ ve Ag^+ iyonları taşıyan nanohibritler) katalizör nanodolgu varlığında graft kopolimerizasyon yöntemiyle

poly(MA-alt-1-OD)-g-PLA nanokompozitlerin sentezi ve karakterizasyonu gerçekleştirilmiştir.

Sunulan çalışmanın temel amacı biyoesaslı/biyobozunur/kompostedilebilir ve antibakteriyel özellikleri taşıyan nişasta-g-PLA ve nişasta-g-PLA/organokil nanokompozitlerinin farklı yeşil teknolojiler yardımıyla sentezi, karakterizasyonu ve buradan elde edilen filmleri gıda ambalajı ve toprak örtü malzemesi olarak kullanabilmeyi gerçekleştirmektir. Tez kapsamında kullanılan ana monomerler (nişasta ve laktik asit) için hiç bir toksik çözücünden yararlanılmaması ve sentezde süperkritik karbon dioksit, mikrodalga yöntemi, shear mixing ve reaktif ekstrüzyon yönteminden yararlanılması literatürde ilk defa rapor edilmiştir.

Tez kapsamında elden edilen kopolimerler ve nanokompozitler için kimyasal, fiziksel, termal ve morfoloji yapı analizleri FTIR, ¹³C CP/MAS NMR, MALDI-TOF-MS, XRD, TGA/ DTG ve SEM/TEM teknikleri ile gerçekleştirilmiştir. Film ekstrüzyonu, çift vidalı ekstrüdere bir üfleme-şişirme ünitesi monte edilerek film ekstrüzyon kafası ile gerçekleştirilmiştir. Elde edilen filmlerin mekanik özellikleri çekme uzama testleri ile değerlendirilmiştir. Kopolimerlerin sentezi esnasında kullanılan nişasta/LA oranı ve organokillerin interkalasyon/eksfolyasyon işleminin etkileri; su buharı, oksijen ve karbon dioksit geçirgenliklerinin ölçülmesiyle belirlenmiştir. Filmlerin biyodegradasyonunu incelemek amacıyla; filmlerin bozunma özellikleri doğal ortamda toprak varlığında gerçekleştirilmiştir. Ayrıca elde edilen filmlerin gıda ambalajı olarak uygun olup olmadığını incelemek için antibakteriyel testleri ve gıda ile temas testleri yapılmıştır. Son olarak sera koşullarında elde edilen filmler toprak örtü malzemesi olarak domates ve biber fideleri için denenmiştir.

Anahtar kelimeler: lamellar arası graft kopolimerizasyon, organokil, nanokompozit, graft kopolymerizasyon, nişasta, laktik asit, süper kritik karbondioksit, mikrodalga ile ısıtma, shear mixing, reaktif ekstrüzyon.

ACKNOWLEDGMENT

I sincerely thank my supervisor, Prof. Dr. Erhan Bişkin for advising my PhD study. It would not have been possible without your guidance, patience, understanding, and hard work throughout the process.

Special thanks is due to my academic grandfather, Prof. Dr. Zakir M.O. Rzayev, for supporting, encouraging, help and personal guidance throughout my study.

I am very much appreciative of the assistance given to me by the all the staff members of the Chemical Engineering Department especially Prof. Dr. Tülin Kutsal, Prof. Dr. Ali Tuncel, Prof. Dr. Hülya Yavuz Ersan, Assoc. Prof. Dr. Halil M.Aydın, and Asst. Prof. Dr. Sinan Eğri for their suggestions, comments, kindness and encouragement.

I thank Assoc. Prof. Dr. Ömür Çelikbıçak and Dr. Mehmet Yılmaz for their collaborating and assisting during my study.

This thesis becomes a reality with the kind support and help of my colleague, Duygu Deniz Usta and Selin Cansu Şen, during the extrusion of polymers and biodegradation tests. I would like to extend my sincere thanks to them.

My thanks and appreciations also go to my colleague, who have willingly helped out with their abilities; Behzad Nasserı, Erhan Şenlik, Elif Kayyalp, Lena Mahmoudi Azar, Ali Ebrahimi, Araz Norouz Dizaji, Dilek Özden, Erkan Karataş, Ehsan Sanattalab, Berkay Demirci.

I would also like to thank the staff members of Chemical Engineering Department, Belgin Aslan and Duygu Gülay, for their help in operational training initially and continuous support during the use of characterization instruments.

Thanks is also extended to the staff members of Turkish Ministry of Food, Agriculture and Livestock, Nihal Güler and Burcu Şengül, for antibacterial and food contacting tests of films through a national project supporting by Scientific and Technological Council of Turkey (TUBITAK-1003, No: 113O864).

Thanks is also extended to the staff members of NAKSAN PLASTİK factory during the SANTEZ project and characterization of films.

A special thanks is also extended to the Turkish Ministry of Science and Technology for supporting the SANTEZ project (No: 00875-STZ-2011-1) and PhD scholarship.

Finally, I do feel so deeply indebted to my family. Their infinite love, tender care and rear makes me as I am. They try every effort to keep me in better shape. Their persistently encouraging, supporting and thoroughly understanding is always inspiring me. With their endless patience this thesis has been brought into reality. I hereby contribute me deepest thanks and perpetual love to them...

Kouroush Salimi

TABLE OF CONTENTS

	Page
ABSTRACT	i
ÖZET	iv
ACKNOWLEDGMENT	vii
TABLE OF CONTENTS	viii
LIST OF TABLES	xiii
LIST OF FIGURES	xiv
SYMBOLS AND ABBREVIATIONS	xx
1. INTRODUCTION	1
2. GENERAL INFORMATION	4
2.1. Plastics and Environment	4
2.2. Global and Local Market of the Plastic Film	6
2.3. Polysaccharides	7
2.3.1. Starch	7
2.3.2. Grafting of Polysaccharides	8
2.4. Lactic acid	10
2.4.1. Properties of Polylactic acid	12
2.4.1.1. Structure and Characterization of PLA	12
2.4.2. Processing of PLA	13
2.5. Polylactic acid/Poly(maleic anhydride- <i>alt</i> -1-octadecene)/Organoclay Nanocomposites	21
3. MATERIALS AND METHODS	27
3.1. Materials	27
3.2. Manufacturing of PLA/Silicate Nanocomposites and Catalyst Nanofillers	28

3.2.1. Nanofabrication and Characterization of Poly(MA- <i>alt</i> -1-octadecene)-g-Poly L-lactic acid Layered Silicate Nanocomposites	28
3.2.2. Interlamellar Graft Copolymerization of L-lactic acid onto Poly(maleicanhydride- <i>alt</i> -1-octadecene) in the Presence of Different Clays as Catalyst-nanofillers	29
3.3. Graft copolymerization of starch with lactic acid using various methods	31
3.3.1. Synthesis of St- <i>g</i> -PLA copolymers in supercritical CO ₂ media.....	31
3.3.2. Microwave Assisted Grafting of St- <i>g</i> -PLA Copolymers	32
3.3.3. Processing of St- <i>g</i> -PLA Copolymers and St- <i>g</i> -PLA/Organoclay Nanocomposites Blends through Shear Mixing and Reactive Extrusion.....	34
3.3.4. Film Extrusion	36
3.4. Characterization	37
3.4.1. Chemical and Physical Properties.....	37
3.4.1.1. ATR-FTIR.....	37
3.4.1.2. ¹³ C/CP MAS-NMR and ¹ H-NMR.....	37
3.4.1.3. MALDI-TOF-MS	37
3.4.1.4. XRD	37
3.4.1.5. ζ-size and ζ-potential Analysis	37
3.4.1.6. UV/VIS Spectrophotometer.....	38
3.4.2. Thermal Behavior.....	38
3.4.2.1. DSC	38
3.4.2.2. TGA/DTG	38
3.4.2.3. DMA (Dynamic mechanical).....	38
3.4.3. Morphological Characterization.....	38
3.4.3.1. SEM and SEM/EDX.....	38
3.4.3.2. TEM and C-TEM	39
3.4.4. Mechanical Properties.....	39
3.4.4.1. Tensile Properties	39

3.4.5. Permeability Properties of Films.....	39
3.4.5.1. Gas (CO ₂ and O ₂) Permeability	39
3.4.5.2. H ₂ O Vapor Permeability	39
3.4.6. Biodegradation Properties.....	40
3.4.7. Microbiology Tests and Food Contact Properties	40
3.4.8. Agricultural Application of Films	41
4. RESULTS AND DISCUSSION.....	42
4.1. Characterization of Poly(MA- <i>alt</i> -1-octadecene)- <i>g</i> -Poly L-lactic acid Layered Silicate Nanocomposites	42
4.1.1. FT-IR Spectroscopy	42
4.1.2. ¹ H-NMR Analysis	43
4.1.3. MALDI-TOF-MS Analysis.....	44
4.1.4. X-ray Diffraction	46
4.1.5. SEM Surface Morphology	47
4.1.6. TEM Internal Morphology.....	50
4.1.7. ζ -size and ζ -potential Parameters of (Micro) Nanoparticles	54
4.1.8. Thermal Behaviors (DSC and TGA/DTG)	55
4.1.9. Dynamic Mechanical Properties.....	58
4.2. Characterization of Poly(MA- <i>alt</i> -1-octadecene)- <i>g</i> -Poly L-lactic/Clay Nanohybrids and Catalyst Nanofillers	60
4.2.1. Self-Catalytic Effects of Clay Nanofillers	60
4.2.2. FT-IR Spectroscopy	62
4.2.3. UV/VIS Spectrophotometer and Elemental (SEM/EDX) Analysis	64
4.2.4. ¹ H, ¹³ C and ¹³ C-DEPT-135 NMR Analysis	66
4.2.5. X-ray Diffraction Analysis	67
4.2.6. Parameters of Particles: Structure ζ -size (potential) Relationships	70
4.2.7. Effect of Clay Origin on the Morphology of Polymer Nanocomposites	71
4.2.8. Thermal Properties.....	77

4.3. Characterization of St- <i>g</i> -PLA Copolymers Synthesized Through Supercritical Carbon Dioxide.....	81
4.3.1. Optimization of the Operational Parameters and Evaluation of Their Effect on the Grafting Degree	81
4.3.2. ATR-FTIR Spectroscopy	85
4.3.3. ¹ H-NMR and ¹³ C CP/MAS-NMR Analysis of Graft Copolymers	86
4.3.4. Acid Number Analysis of the Precipitate Phase	89
4.3.5. X-ray Diffraction Analysis	90
4.3.6. Reaction Parameters-Morphology Relationships	91
4.3.7. Thermal Behavior of Graft Copolymers.....	93
4.4. Characterization of St- <i>g</i> -PLA Copolymers Synthesized by Microwave Irradiation	94
4.4.1. ATR-FTIR Analysis	94
4.4.2. ¹³ C CP/MAS-NMR Analysis	95
4.4.4. X-ray Diffraction	96
4.4.5. Surface Morphology: SEM Analysis	97
4.4.6. Thermal Behavior: TGA/DTG Analysis.....	98
4.4.7. Effect of Reaction Conditions on Graft Copolymerization	100
4.5. Characterization of St- <i>g</i> -PLA Copolymers and St- <i>g</i> -PLA/Organoclay Nanocomposites Synthesized Through Shear Mixing and Reactive Extrusion Methods	103
4.5.1. ATR-FTIR Spectroscopy	103
4.5.2. ¹³ C CP/MAS-NMR Analysis	105
4.5.3. X-ray Diffraction	106
4.5.5. SEM Analysis.....	108
4.5.6. Thermal Analysis, Influence of the Processing Parameters and Composition	110
4.5.7.1. Mechanical Properties.....	114

4.5.7.2. Permeability Properties	115
4.5.7.3. Biodegradation and Composting Properties.....	117
4.5.7.4. Microbiological Tests and Food Contact Properties.....	118
4.5.7.5. Real Field Application Properties	119
5. CONCLUSIONS.....	121
REFERENCES	127
CURRICULUM VITAE.....	143

LIST OF TABLES

Table. 4. 1. Nanoparticle structure–composition– ζ -size/ ζ -potential relationships.	55
Table. 4. 2. The ζ -size and ζ -potential of inorganic and organic mmt and their polymeric particles in CHCl_3 solution before and after sonication ($P = 400 \text{ W}$, $F = 40 \text{ KHZ}$, $T = 15 \text{ min}$)	61
Table. 4. 3. Effects of reaction parameters on grafting degree.....	83
Table. 4. 4. $^1\text{H-NMR}$ analysis data to determine the composition of St- <i>g</i> -PLA for different feed ratios.....	89
Table. 4. 5. End group analysis of st- <i>g</i> -pla in precipitated phase.	90
Table. 4. 6. Synthesis parameters of St- <i>g</i> -PLA copolymers under different conditions.	101
Table. 4. 7. degradation parameters of starch and St- <i>g</i> -PLA copolymers.	113
Table. 4. 8. Tensile properties of St- <i>g</i> -PLA and St- <i>g</i> -PLA/organoclay nanocomposite films	114
Table. 4. 9. O_2 permeability of St- <i>g</i> -PLA and St- <i>g</i> -PLA/organoclay nanocomposite films.....	115
Table. 4. 10. CO_2 permeability of St- <i>g</i> -PLA and St- <i>g</i> -PLA/organoclay nanocomposite films.....	116
Table. 4. 11. Water vapor permeability (WVP) of St- <i>g</i> -PLA and St- <i>g</i> -PLA/organoclay nanocomposite films.....	117
Table. 4. 12. Microbiological results of samples.	119

LIST OF FIGURES

Figure. 2. 1. Cyclic process by which agricultural products and fermentative routes can yield biodegradable polymers	5
Figure. 2. 2. Structures of selected biodegradable polymers.....	6
Figure. 2. 3. Production methods of PLA and simplified properties of PLA and its precursors with regard to polymer production and end-use possibilities.	11
Figure. 2. 4. Typical geometries of a screw for single-screw extruder.	15
Figure. 2. 5. Major components of an injection molding machine showing the extruder and clamp units.	16
Figure. 2. 6. Injection stretch blow molding of PLA bottle.	18
Figure. 2. 7. Biaxial oriented extrusion cast film machine.....	19
Figure. 2. 8. Extrusion blown film line	21
Figure. 3. 1. Synthetic pathways for preparation of the poly(maleic anhydride- <i>alt</i> -1-octadecene)- <i>g</i> -poly(L-lactic acid)/octadecyl amine-MMT clay nanocomposites: (i) grafted LA monomer onto alternating copolymer via esterification, (ii) preintercalated MMT-ODA...LA complex, (iii) octadecyl amide-MMT derivative of alternating copolymer (nanohybrid) and (iv) copolymer- <i>g</i> -PLA and its ODA-MMT layered nanocomposites.	29
Figure. 3. 2. Schematic representation of synthetic pathways for copolymer- <i>g</i> -PLA intercalated silicate nano-composites in the presence of Na ⁺ -MMT, Ag ⁺ -MMT and ODA-MMT as catalysts of graft copolymerisation of L-lactic acid onto poly(ma- <i>alt</i> -1-octadecene) and nanofillers: (i) mono-esterification, (ii) intercalation via hydrogen-bonding, (iii) intercalation via ion-exchange, (iv) intercalation via in situ amidisation and (v) interlamellar graft copolymerization.	30
Figure. 3. 3. The graft copolymerization of L-lactic acid onto a starch backbone in supercritical carbon dioxide.	32
Figure. 3. 4. Schematic representation of starch- <i>g</i> -PLA synthesis by microwave irradiation.....	34
Figure. 3. 5. Schematic representation of starch- <i>g</i> -pla/organoclay nanocomposites synthesis by “shear mixer” and “reactive extrusion”.....	35

Figure. 3. 6. (A, B) As prepared St- <i>g</i> -PLA and St- <i>g</i> -PLA/organoclay nanocomposites through reactive extrusion; (C) extruder and film blowing unit; (C, D) blowing die and the blown film.	36
Figure. 4. 1. FTIR spectra of (a) pristine graft copolymer and its (b) nanocomposite.	42
Figure. 4. 2. ¹ H NMR spectra of (a) pristine poly(MA- <i>alt</i> -1-octadecene)- <i>g</i> -PLA, (b) copolymer- <i>g</i> -PLA/ODA-MMT and (c) copolymer- <i>g</i> -PLA/DMDA-MMT nanocomposites in CHCL ₃ -D ₁ solution.	44
Figure. 4. 3. MALDI-TOF-MS spectra of (A) pristine copolymer and (B) copolymer- <i>g</i> -PLA in thf solution using α-ciyano-4-hidroxicinnamic acid (CHCA) as a matrix and NaTFA as a cationizing agent for ionization of the samples...	45
Figure. 4. 4. XRD patterns of (a) pristine graft copolymer, (b) copolymer- <i>g</i> -PLA/ODA-MMT, (c) copolymer- <i>g</i> -PLA/DMDA-MMT nanocomposites.	46
Figure. 4. 5. SEM images (A, B and C) pristine poly(MA- <i>alt</i> -1-octadecene)- <i>g</i> -PLA.	48
Figure. 4. 6. SEM images (A, B and C) copolymer- <i>g</i> -PLA/ODA-MMT and (D) copolymer- <i>g</i> -PLA/DMDA-MMT nanocomposites. effect of organoclay origin (intercalant).	49
Figure. 4. 7. TEM images of core–shell morphology of individual particles: (A) and (B) copolymer- <i>g</i> -PLA/ODA-MMT, (C) copolymer- <i>g</i> -PLA/DMDA-MMT and (D) pristine poly(MA- <i>alt</i> -1-octadecene) copolymer. scale: (A) 100 nm, (B), (C) and (D) 200 nm.	51
Figure. 4. 8. TEM images of copolymer- <i>g</i> -PLA/ODA-MMT nanocomposite. ...	52
Figure. 4. 9. TEM images of copolymer- <i>g</i> -PLA/DMDA-MMT clay nanocomposite.	53
Figure. 4. 10. Nanostructural model of (micro) nanoparticles with core-shell morphology.	54
Figure. 4. 11. DSC traces of (a) copolymer- <i>g</i> -PLA and its nanocomposites incorporated with (b) ODA-MMT and (c) DMDA-MMT clays. heating rate is 10°c/min under a nitrogen atmosphere.	56
Figure. 4. 12. TGA-DTG curves of (A) pristine graft copolymer and its (B) ODA-MMT AND (C) DMDA/MMT incorporated nanocomposites. heating rate is 10°c/min under a nitrogen atmosphere.	57

Figure. 4. 13. DMA spectra of (1) pristine copolymer- <i>g</i> -PLA, (2) copolymer- <i>g</i> -PLA/ODA-MMT and (3) copolymer- <i>g</i> -PLA/DMDA-MMT organoclays. plots of dynamic force (black curves) and complex modulus (blue curves) versus α -relaxation temperature (T_α).	59
Figure. 4. 14. Schematic representation of synthetic pathways for copolymer- <i>g</i> -PLA intercalated silicate nano-composites in the presence of Na ⁺ -MMT, Ag ⁺ -MMT and ODA-MMT as catalysts of graft copolymerization of L-lactic acid onto poly(<i>ma-alt</i> -1-octadecene) and and nanofillers.....	60
Figure. 4. 15. FT-IR spectra (KBr pellet) OF (a) Ag ⁺ -MMT and nano-composites containing copolymer- <i>g</i> -PLA matrix polymer incorporated with (b) Ag ⁺ -MMT, (c) Na ⁺ -MMT AND (D) ODA-MMT.....	64
Figure. 4. 16. (A) UV-VIS spectrum and (B) SEM/EDX composition analysis of Ag ⁺ -MMT.	65
Figure. 4. 17. ¹ H, ¹³ C and ¹³ C-DEPT-135 NMR spectra of copolymer- <i>g</i> -PLA fabricated with (a) tinooctoate catalyst (grafting time 5 h), (b) Na ⁺ -MMT catalyst-nanofiller (grafting time 56 min) and (c) ODA-MMT catalyst-reactive nanofiller (grafting time 35 min).....	67
Figure. 4. 18. XRD patterns of Ag ⁺ -MMT and lactic acid-MMT.....	68
Figure. 4. 19. XRD patterns of poly(MA- <i>alt</i> -1-octadecene)- <i>g</i> -PLA incorporated with (a) ODA-MMT, (b) Na ⁺ -MMT AND (c) Ag ⁺ -MMT nano-composites. loading clay is 3.2 wt %.....	69
Figure. 4. 20. SEM images of poly(MA- <i>alt</i> -1-octadecene)- <i>g</i> -PLA/ODA-MMT nano-composites. scale: (A) 1000 x, 10 μ m, (B) 2000 x, 10 μ m, (C) 20.000 x, 2 μ m and (D) 10.000 x, 2 μ m.....	72
Figure. 4. 21. SEM images of poly(MA- <i>alt</i> -1-octadecene)- <i>g</i> -PLA/Ag ⁺ -MMT nanocomposites at differents scales and magnifications.....	73
Figure. 4. 22. TEM images of individual particles of poly(MA- <i>alt</i> -1-octadecene)- <i>g</i> -PLA silicate layered nano-composites incorporated with (A and B) ODA-MMT, (C) Na ⁺ -MMT AND (D) Ag ⁺ -MMT organic and inorganic clays in the presence of pre-intercalated MMT...LA complexes.....	74
Figure. 4. 23. TEM images of poly(MA- <i>alt</i> -1-octadecene)- <i>g</i> -PLA/ODA-MMT nanocomposites. scale: (A) 1 μ m, (B) 500 nm and (C and D) 200 nm.	75
Figure. 4. 24. TEM images of poly(<i>ma-alt</i> -1-octadecene)- <i>g</i> -PLA/Ag ⁺ -MMT nanocomposites. scale: (A) 1 μ m, (B) 500 nm and (C and D) 200 nm.	76

Figure. 4. 25. TEM images of poly(MA- <i>alt</i> -1-octadecene)- <i>g</i> -PLA/Na ⁺ -MMT nanocomposites. scale: (A) 1 μm and (B) 200 nm.....	76
Figure. 4. 26. TGA-DTG curves of (A) Ag ⁺ -MMT, (B) Na ⁺ -MMT and (C) ODA-MMT. the heating rate is 10°C/min under nitrogen atmosphere.....	78
Figure. 4. 27. Thermal properties of copolymer- <i>g</i> -PLA/clay nano-composites. (A) DSC analysis of copolymer- <i>g</i> -PLA/Ag ⁺ -MMT, (B) DSC analysis of copolymer- <i>g</i> -PLA/ODA-MMT, (C) DSC analysis of copolymer- <i>g</i> -PLA/Na ⁺ -MMT, (a) TGA/DTG analysis of copolymer- <i>g</i> -PLA/Ag ⁺ -MMT, (b) TGA/DTG analysis of copolymer- <i>g</i> -PLA/ODA-MMT, (c) TGA/DTG analysis of copolymer- <i>g</i> -PLA/Na ⁺ -MMT.	79
Figure. 4. 28. The synthetic pathways of St- <i>g</i> -PLA copolymer.	81
Figure. 4. 29. Influence of variable conditions on grafted la mol percent. (A) polymerization temperature, (B) polymerization time, (C) scCO ₂ flow rate and (D) polymerization pressure.....	84
Figure. 4. 30. FTIR spectra of (A) starch and (B) St- <i>g</i> -PLA copolymer for the following reaction conditions; 1:3 polymer/monomer ratio, 100°C, 200 bar, 6 h (see table 4.3).....	86
Figure. 4. 31. ¹³ C CP/MAS NMR spectra of (A) starch and (B) St- <i>g</i> -PLA copolymer prepared at 100°C, 200 bar, 6 h with 1:3 St/LA feed ratio.....	87
Figure. 4. 32. ¹ H-NMR (400 MHz) spectra of St- <i>g</i> -PLA copolymers in CHCl ₃ -D ₁ at 100°C, 200 bar, 6h. (A) 1:5; (B) 1:3 and (C) 1:1 monomer ratio.	88
Figure. 4. 33. X-RAY diffraction patterns of (A) starch and (B) St- <i>g</i> -PLA copolymer prepared at optimized reaction conditions; 1:3 St/LA ratio, 200 bar, 100°C for 6 h.....	90
Figure. 4. 34. SEM images of (A) starch and St- <i>g</i> -PLA copolymers at (B) 1:1, (C, E and F) 1:3 and (D) 1:5 St/LA feed ratios. all of products were performed at 100°C, 200 bar, 6 h.	92
Figure. 4. 35. (a) TGA and (b) DTG thermograms of St- <i>g</i> -PLA copolymers prepared with the following different St/LA feed ratios: (A) 1:1, (B) 1:3 and (C) 1:5.....	93
Figure. 4. 36. IR spectra of (A) starch, (B) St- <i>g</i> -PLA at 150w, (C) St- <i>g</i> -PLA at 300w and (D) St- <i>g</i> -PLA at 450w microwave irradiation.	95
Figure. 4. 37. ¹³ C CP/MAS NMR spectra of (A) starch and (B) St- <i>g</i> -PLA at 450w microwave irradiation.	96

Figure. 4. 38. X-RAY diffraction patterns of (A) starch, (B) St- <i>g</i> -PLA at 300w and (c) St- <i>g</i> -PLA at 450 w microwave irradiation.....	97
Figure. 4. 39. SEM images of (A) St- <i>g</i> -PLA at 300w, (B) St- <i>g</i> -PLA at 450w, (C) St- <i>g</i> -PLA at 600w and (D) St- <i>g</i> -PLA at 750w microwave irradiation.	98
Figure. 4. 40. TGA and DTG diagrams of St- <i>g</i> -PLA copolymers. (A) at 150 W, (B) at 300 W, (C) at 450 W and (D) at 600 W microwave irradiation.	99
Figure. 4. 41. The effect of power of radiation (A) and monomer ratio (B) on duration of radiation and grafted pla mole fraction (%).	102
Figure. 4. 42. Microstructural model of St- <i>g</i> -PLA copolymers synthesized by microwave irradiation.....	102
Figure. 4. 43. FTIR spectra of (A) St- <i>g</i> -PLA copolymer synthesized through shear mixer, (B) St- <i>g</i> -PLA copolymer blending by twin-screw extruder (1 st step), (C) St- <i>g</i> -PLA copolymer blending by twin-screw extruder (2 nd step), (D) St- <i>g</i> -PLA copolymer blending by twin-screw extruder (3 rd step), St- <i>g</i> -PLA copolymer blending by twin-screw extruder (4 th step).	104
Figure. 4. 44. FTIR spectra of St- <i>g</i> -PLA/organoclay nanocomposite.....	104
Figure. 4. 45. ¹³ C CP/MAS-NMR spectra of St- <i>g</i> -PLA copolymer.	105
Figure. 4. 46. ¹³ C CP/MAS-NMR spectra of St- <i>g</i> -PLA/organoclay nanocomposite.	106
Figure. 4. 47. X-RAY diffraction patterns of (A) St- <i>g</i> -PLA copolymer and (B) St- <i>g</i> -PLA/organoclay nanocomposite.....	107
Figure. 4. 48. SEM images of St- <i>g</i> -PLA copolymers. scale: (A) St- <i>g</i> -PLA copolymer synthesized through shear mixer; 2.00k x, 10 μm, (B) St- <i>g</i> -PLA copolymer synthesized through shear mixer; 10.00k x, 1 μm, (C) St- <i>g</i> -PLA copolymer blending by twin-screw extruder (1 st step); 2.00k x, 10 μm, (D) St- <i>g</i> -PLA copolymer blending by twin-screw extruder (1 st step), 5.00k x, 2 μm, (E) St- <i>g</i> -pla copolymer blending by twin-screw extruder (4 th step); 2.00k x, 10 μm and (f) St- <i>g</i> -PLA copolymer blending by twin-screw extruder (4 th step); 10.00k x, 1 μm.....	109
Figure. 4. 49. TGA-DTG curves of pristine starch.....	110
Figure. 4. 50. TGA-DTG curves of St- <i>g</i> -PLA copolymers. (A) blending by twin-screw extruder (1 st step), (B) blending by twin-screw extruder (2 nd step), (C) blending by twin-screw extruder (3 rd step), (D) blending by twin-screw extruder (4 th step).	112

Figure. 4. 51. TGA-DTG curves of St-g-PLA/organoclay nanocomposite.....	113
Figure. 4. 52. The biodegradability and time relationship; (A) St-g-PLA (sample 1), (B) St-g-PLA (sample 2).	118
Figure. 4. 53. Real field applications of St-g-PLA mulching films.....	120

SYMBOLS AND ABBREVIATIONS

St	: Starch
LA	: L-lactic Acid
PLA	: Poly lactic Acid
St- <i>g</i> -PLA	: Starch grafted Polylactic acid
MMT	: Montmorillonit
ASTM	: American Society for Testing and Materials
FTIR	: Fourier Transform Infrared Spectroscopy
NMR	: Nuclear Magnetic Resonance
MALTI-TOF-MS	: Matrix-Assisted Laser Desorption/Ionization Time-of-Flight Mass Spectrometer
XRD	: X-ray Diffraction
SAXS	: Small-Angle X-ray Scattering
WAXS	: Wide-Angle X-ray Scattering
TGA/DTG	: Thermogravimetric Analysis
SEM	: Scanning Electron Microscope
TEM	: Transmission Electron Microscopy
T _g	: Glass Transition Temperature
T _m	: Melting Temperature
T _c	: Crystallization Temperature
PET	: Poly Ethylene Terphetalate
PVC	: Poly Vinyl Chloride
PCL	: Poly ε-Caprolactone
DSC	: Differential Scanning Calorimetry

PP	: Polypropylene
PS	: Polystyrene
MA	: Maleic Anhydride
DOM	: Dioctyl Maleate
LDPE	: Low Density Poly Ethylene
DMSO	: Dimethyl Sulfoxide
scCO ₂	: Supercritical Carbon Dioxide
MeOH	: Methanol
UV	: Ultra Violet
KPS	: Potassium Persulfate
PEGD	: Polyethylene Glycol Diacrylate
PAM	: Polyacrylamide
AFM	: Atomic Force Microscope
SIMS	: Secondary-ion Mass Spectrometry
GPC	: Gel Permeation Chromatography
GPC-MALLS	: GPC Coupled to Multiangle Laser Light Scattering
THF	: Tetrahydrofuran
ΔH_{rel}	: Endothermic Enthalpy Relaxation Value
ISBM	: Injection Stretch Blow Molding
OPS	: Oriented Polystyrene
OPP	: Oriented Polypropylene
PEO	: Polyethylene Oxide
VMT	: Vermiculite
DMDA	: Dimethyldidodecyl Ammonium Cation

AgNPs	: Silver Nanoparticles
NaOH	: Sodium Hydroxide
DMA	: Dynamic Mechanical
WVTRs	: Water Vapor Transmittion
CHCl ₃ -d ₁	: Deuterated Chloroform
RSD	: Relative Standard Deviation

1. INTRODUCTION

The 21st century is witnessing a huge demand of fossil reserves along with a rapid reduction in oil feedstocks, so there are possibilities to making the world exposed to geopolitical risk because the present energy demand in the world is not fulfilled from fossil fuel sources. Recently, concerns regarding the environmental impacts have resulted in an ever-increasing shift of global energy policies to replacement of an alternative technologies and sustainable sources of energy, value-added, and environmentally friendly products. Furthermore, the need for development of an economy based on renewable resources has been recognized by governments, and diverse R&D activities have started to be funded to perform this aim. Among this materials, it is difficult to imagine the modern life without plastics; however these versatile materials are often seen to be in conflict with an increasing focus on the employment of renewable biomass feedstocks leading to a search for more acceptable/alternative sources. One of the most visible and promising solutions are bioplastics (plastics that are biodegradable and/or compostable), which are the only sustainable options to substitute for fossil fuel resources, as sources of organic compounds over a relatively short time scale and with limitless supply.

Thermoplastic polymers exhibit many ideal properties such as light weight, variable barrier properties to match endues applications, good printability, heat sealable, and ease of conversion into different forms for use in packaging and mulching products. Today, most plastics are derived from non-renewable crude oil and natural gas resources. While some plastics are being recycled and reused, the majority are disposed in landfills due to end-use contamination.

Starch is an α -linked polysaccharide composed of two components with various molecular masses: 20–30% linear amylose and 70–80% 1,6- α -linked branched amylopectin. Commercial granular starch has been used in polyolefins as a filling agent and blended with synthetic polymers to produce biodegradable materials with desired properties [1]. Earlier publications [2, 3] have indicated that blends of functional anhydride polymers and starch could lead to products with useful end properties.

Poly(lactic acid) or PLA is one of the most commercially important biodegradable and biocompatible polymers. It can be derived from renewable sources, environmentally friendly and it exhibits a combination of physical properties that meet the requirements for many applications, notably for packaging and mulch films. To improve the mechanical and thermal properties of PLA and limit its degradation, different polymer/silicate nanocomposites have been explored.

In recent years, polymer/layered silicate (PLS) nanocomposites, especially various types of synthetic and natural polymer nanocomposites and nanomaterials reinforced with different types of nanoparticles have taken attention of many researchers both from industry and academia. In addition to these nanocomposites, polymer nanocomposites reinforced with functionalized nanoparticles, namely organoclays, functionalized graphene and carbon nanotubes are relatively new areas of research in Macromolecular Nanotechnology. Most of the recently developed new approaches and nanotechnological methods in polymer synthesis and processing are related to various synthetic pathways and mechanisms for the formation of nanostructures in polymer/nanofiller hybrids and nanocomposites, predominantly containing anhydride/carboxyl functionalized copolymers such as alternating, random and graft copolymers of maleic anhydride and its isostructural analogues. Plackett [4] synthesized and used maleated PLA as an interfacial compatibilizer in biocomposites. Similar hydrogen abstraction on the PLA backbone was recently reported by Avella et al. [5] in the case of radical polymerization of butyl acrylate in the presence of modified PLA. Hawker et al. [6] reported synthesis and characterization of molecularly defined (L)-lactic acid oligomers and polymers. They demonstrated a close correlation between the molecular structure of the well-defined LA oligomers and their physical properties.

In this thesis, novel biobased/biodegradable/compostable/antibacterial St-g-PLA copolymers and St-g-PLA/organoclay nanocomposites were fabricated by using different green methods applying as a food packaging and mulching films. In the design of different types of modified organoclays as a partner polymer for fabrication of St-g-PLA/organoclay nanocomposites, a facile and effective strategy was carried out for synthesis of functional alternating

copolymer-*g*-poly(L-lactic acid)/organoclays nanocomposites using an interlamellar bulk graft copolymerization of lactic acid (LA) monomer onto poly (MA-*alt*-1-octadecene) in the presence of organoclays and tin(oct)₂ catalyst. Furthermore, a new approach for the synthesis of functional copolymer-*g*-biopolymer layered silicate nanocomposites incorporated with different clays was performed which are executed the dual functions as a catalyst and nanofiller. To characterize the functional copolymer layered silicate nanocomposites and understand the mechanism of in situ processing, interfacial interactions and nanostructure formation in these nanosystems, a combination of various methods such as FT-IR spectroscopy, X-ray diffraction (XRD), dynamic mechanical (DMA), thermal (DSC and TGA-DTG), SEM and TEM morphology were applied. It was found that in situ graft copolymerization occurred through the following steps: (i) esterification of anhydride units of copolymer with LA; (ii) intercalation of LA between silicate galleries; (iii) intercalation of matrix copolymer into silicate layers through in situ amidization of anhydride units with octadecyl amine intercalant; and (iv) interlamellar graft copolymerization via in situ intercalating/exfoliating processing.

In the main part of this thesis, development of new methods for graft copolymerization of L-lactic acid onto starch, such as supercritical carbon dioxide media, microwave irradiation, shear mixing method, and reactive extrusion without using toxic solvents were carried out. Chemical and physical structures, thermal behavior and morphology of synthesized copolymers, as well as some parameters were performed by FTIR and ¹³C CP/MAS NMR spectroscopy, XRD, TGA/ DTG and SEM, respectively. The film extrusion in a lab-scale was carried out by using a twin-screw extruder equipped by applying a film extrusion die, blowing unit and rotating film-uptake. Mechanical properties were evaluated from the tensile stress-strain test data. The effect of St/LA ratio and in situ intercalation/exfoliation process of organoclay on water vapour, O₂ and CO₂ permeabilities were measured. Films were exposed degradation tests in buried soil media. Finally, antibacterial activities of the St-*g*-PLA based films were obtained and also the food contact analysis of the films were performed.

2. GENERAL INFORMATION

2.1. Plastics and Environment

Conventional polymers such as Polyethylene (PE), Poly(propylene) (PP), Polystyrene (PS) and Poly(vinyl chloride) (PVC) persist for many years after disposal. These polymers seem not-suitable for applications in which plastics are used for short time periods and then disposed include films, flexible bags and rigid containers in packaging industry. However, these materials are indispensable materials of modern life, but in a short time, the after-use fates of these products has led to a waste disposal problem [7]. Furthermore, conventional plastics are often soiled by food and other biological substances, physical recycling of these materials take a long time to break down , so this method is impractical and generally undesirable [8]. The development of environment-friendly materials based on natural and renewable resources (i.e., biobased) have arisen as the most attractive and popular approach to overcome this problem [9].

In contrast, biodegradable polymers have a potential to degrade in biobactive environments by the enzymatic action of microorganisms such as bacteria, fungi, and algae and the non-enzymatic process by chemical hydrolysis may also broke the polymer chain. Biobased/biodegradable polymers are naturally derived from plant processing of atmospheric CO₂ and recycled by biological processes and converts to CO₂, CH₄, water, biomass, humic matter (Figure. 2.1.). Among this, carbohydrate polymers have raised significant international interest in the using to produce biodegradable plastics [10].

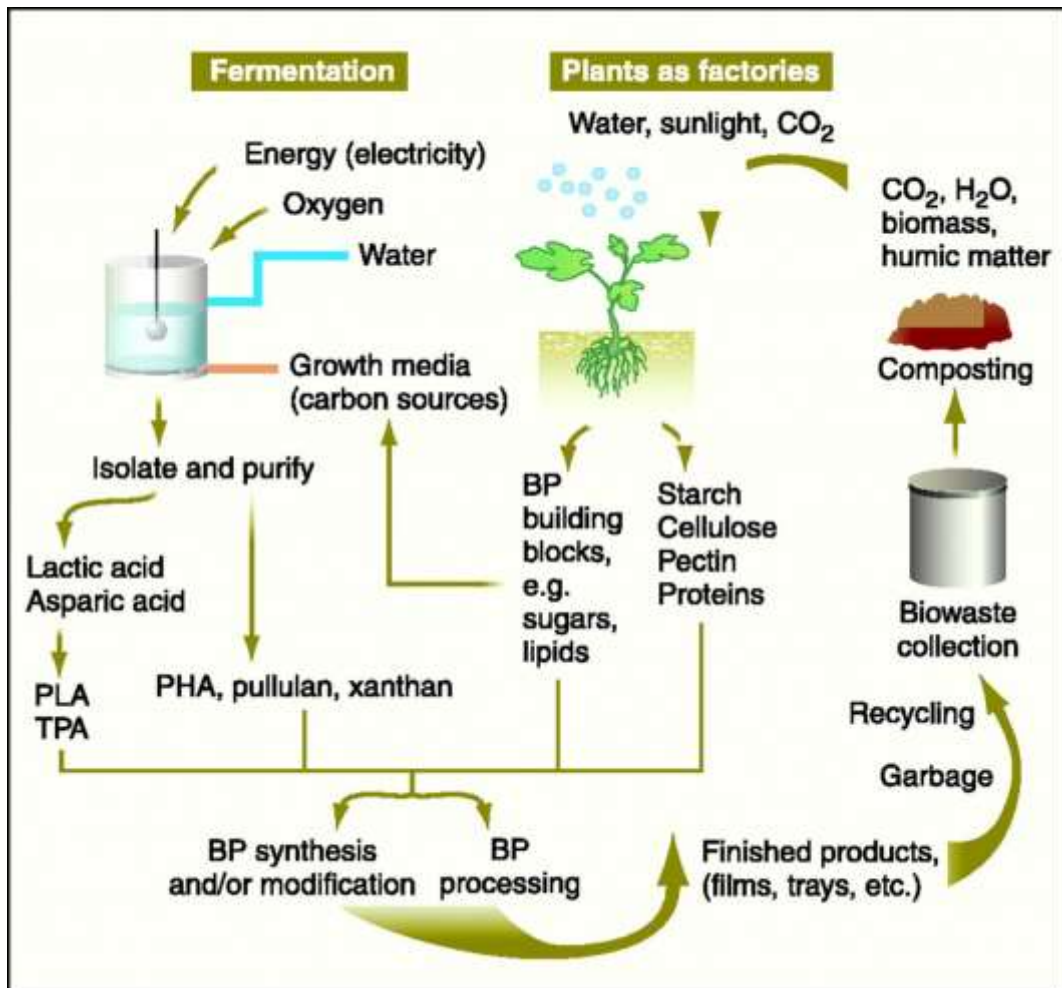


Figure. 2. 1. Cyclic process by which agricultural products and fermentative routes can yield biodegradable polymers

While worldwide consumption of biopolymers has increased from 14 million kg in 1996 to an estimated 68 million kg in 2001, nowadays this data represent well under one percent of the approx. 290 million tons of plastics produced annually. In 2012, the global production capacity reported to around 1.4 million tones. By 2017, the production capacity is expected to multiply to more than 6 million tones. Packaging materials (trash bags, wrappings, loose-fill foam, food containers, film wrapping, laminated paper), disposable nonwovens (engineered fabrics) and hygiene products (diaper back sheets, cotton swabs), consumer goods (fast-food tableware, containers, egg cartons, razor handles, toys), and agricultural tools (mulch films, planters) are the main target markets for Biopolymers [8]. The competition of biopolymers with conventional polymers

hampered the commercialization of this biobased materials which are inexpensive and familiar to the customer.

2.2. Global and Local Market of the Plastic Film

Crude oil or gas, predicted to decline over the next few decades which are necessary to the manufacture of conventional plastics. An early replacement to renewable sources is important to the plastics industry. Although only four percent of the global oil consumption is used to produce plastics, and a further four percent is used to generate the energy in plastic industry for production line and sufficient time is required to develop the new technologies needed to process renewable sources. In contrast of conventional plastics, biobased plastics such as corn, cereals and sugar beets or perennial cultures (cassava and sugar cane) are predominantly annual crops to production of renewable resources (Figure. 2.2.). Furthermore, generation of new markets and industries while enhancing the sustainability of production and consumption of the biobased products is the aim of european bioeconomy to activate the potential of this field and in future bioplastics will be an important part of bioeconomy [11].

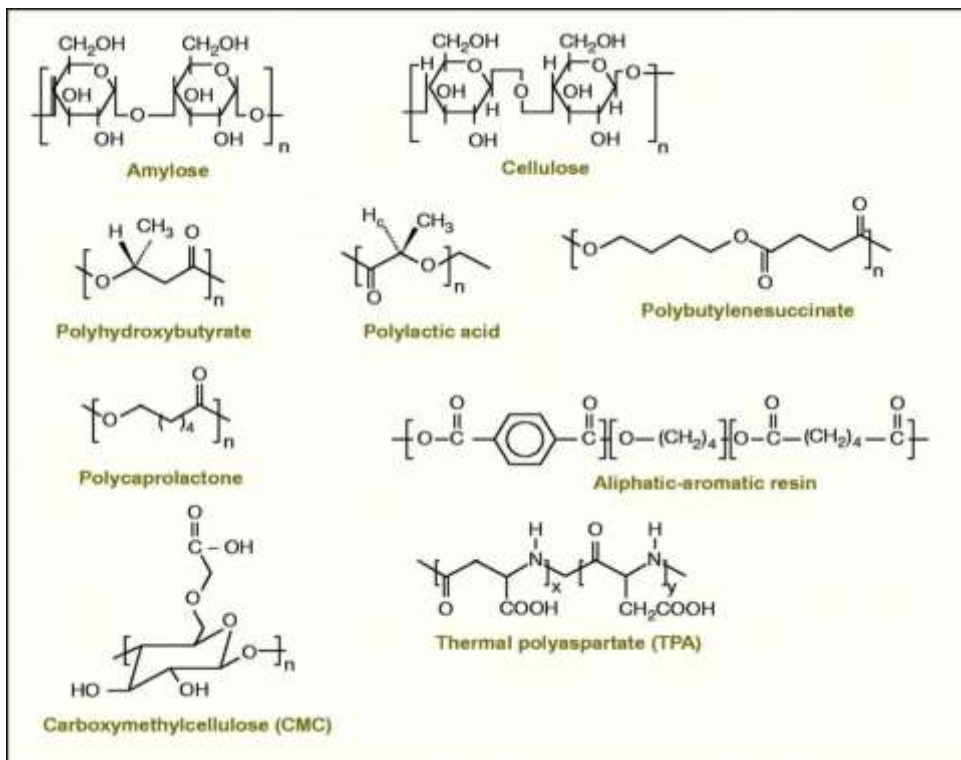


Figure. 2. 2. Structures of selected biodegradable polymers.

Poly(lactic acid) (PLA) is a thermoplastic polyester derived from renewable feedstock such as corn starch, sugarcane, wheat and tapioca roots. The global PLA market is expected to reach a market size of \$5.2 billion by 2020, growing at a CAGR of 19.5% during 2013 to 2020. Reduction in oil resources and rising fossil fuel are the key factors changing the market. Growing environmental concerns, environment pollution, and government regulations is further assisting in preferring of PLA by end users of final products as well as manufacturers in industries such as medical, coating, textile, packaging, transportation, electronics, etc.

2.3. Polysaccharides

2.3.1. Starch

Starch is the most abundant renewable biopolymer in the world, and it is relatively inexpensive which consists of a mixture of two components: amylose (mainly a linear (1→4)- α -D-glucopyranan units) and amylopectin (highly ordered semi-crystalline, contains (1→4)- α -D-glucopyranan units). This variation provides a natural mechanism for regulating starch material properties. The biodegradation of starch products recycles atmospheric CO₂ trapped by starch-producing plants. Starch-based bioplastics can be produced by blending or mixing them with synthetic polymers by a wide range of synthetic blend components the morphology and hence the properties can be regulated efficiently [12, 13].

The use of starch in the manufacturing of bioplastics began in the 70's, this day it can be found in several forms. Starch is not a thermoplastic polymer, but, in the presence of a plasticizer (water, glycerol, sorbitol, etc.), temperature (90-180°C) and shear can be used such as a synthetic plastics by injection, extrusion and blowing processes. Blends containing thermoplastic starch may be blended or grafted with biodegradable polyesters [such as polycaprolactone (PCL), polylactic acid (PLA), etc.] and vinyl monomers (e.g., methyl acrylate) to increase flexibility and resistance to moisture while this materials are mainly formed into films and sheets by foaming and injection molding. The final product can be used as loose-fill in place of polystyrene.

2.3.2. Grafting of Polysaccharides

The development of environmentally friendly materials based on natural and renewable resources (i.e., biobased) have arisen as the most attractive and popular approach to overcome this problem [9]. Starch is the most abundant renewable biopolymer in the world, and it is relatively inexpensive [12, 13]. Commercial granular starch has been used in polyolefins as a filling agent and blended with synthetic polymers to produce biodegradable materials with desired properties [1]. Earlier publications [2] have indicated that blends of functional anhydride polymers and starch could lead to products with useful end properties. Research on blending polysaccharides (e.g., starch and cellulose) and synthetic polymers (e.g., polyolefins) has a long history, but poor compatibility limits the production of these blends. To improve the poor compatibility, many approaches have been proposed, such as the chemical modification of both starch [14, 15] and polyolefins (LDPE) [16] and/or the introduction of compatibilizer [17, 18] into the blends of starch and polyethylene (PE). Grafting hydrophobic thermoplastic polymers with more hydrophilic monomers (e.g., maleic anhydride (MA) and dioctyl maleate (DOM)) has been presented as an effective approach to fabricate compatible and biodegradable polymer materials [19, 20]. Zhang et al. have used MA as a nontoxic reactive compatibilizer to improve the compatibility and properties of poly(lactic acid) (PLA)/starch blends for extrusion [21]. According to Heinze and Liebert, starch in a granular state was modified by chemical deviation grafting processes that improve the properties of the starch [22]. In the starch modification by grafting, acrylic monomers (e.g., methyl acrylate) were grafted onto the starch backbone leading to modified starch that can be injected or extruded into films [23].

In the conventional methods, to produce grafted starch materials, organic solvents such as dimethylsulfoxide (DMSO) and pyridine have been employed, and that is a major drawback of these materials, especially when they are used as food packaging. Moreover, this bottleneck creates environmental problems and obstructs the industrialization and commercialization of the production method [24]. Well-known techniques utilize highly toxic organic solvents as mediums in polymerization reactions. This problematic issue forced

researchers to propose alternative approaches and reaction mediums. Supercritical carbon dioxide (scCO₂), with its high abundance, inexpensive cost and chemically inert nature, has emerged as a suitable reaction medium instead of toxic organic solvents in the last two decades [25, 26]. Furthermore, recently scCO₂ has become a green solvent for polymer synthesis without requiring the use of any conventional solvents, especially in the processing of the products for biomaterial applications and biodegradable polymers, such as the production of drug delivery systems and highly porous scaffolds for tissue engineering, which would be very difficult to achieve using the traditional system [27-29]. Additionally, Condo et al. reported the effect of compressed scCO₂ fluid acting as a plasticizing agent on the T_g behaviour of polymers (Condo, Paul & Johnston, 1994). scCO₂ has proven to be an ideal solvent for polymerization reactions, especially in the chemical or physical modification of polysaccharides [24, 30-32]. Moreover, scCO₂ has a clear advantage over traditional solvents in that it acts as a plasticizer for crystalline polymer derivatives of starch. Recently, the utilization of scCO₂ in condensation without any organic solvents led to removal of small molecules from the condensate (e.g., water, MeOH and phenol) and an increase in the degree of polycondensation [25, 33].

Recently, new methods have improved the synthesis process of grafted polysaccharide copolymers, and they involve free radical initiators, gamma rays, UV radiation and electron beam and microwave irradiation [34-38]. Using microwave energy in organic reactions has found widespread applications in polymer laboratories for developing novel materials. Microwave-assisted heating has been performed in various polymerization techniques, such as radical polymerization, step-growth polymerization and ring opening polymerization (ROPs), thanks to more efficient energy transfer than conventional heating [39, 40]. In microwave-assisted polymerization methods, microwave reactors allow fast and accurate monitoring of important process parameters, such as temperature and pressure, for the production of materials in different forms and with high purity [39].

Grafting onto polysaccharides by microwave irradiation has been performed in different conditions (i) in completely homogeneous solutions where all the

reaction contents are fully miscible with no phase separation; (ii) in suspension where the reactants are not fully miscible; either the polysaccharide and/or monomer/catalyst are immiscible; (iii) in solid phase where the polysaccharide monomers and initiator are impregnated on neutral solid support. These materials have diverse applications in the fields of science and technology such as flocculant for wastewater treatment and controlled drug delivery [38, 41-44].

In recent decades, microwave irradiation has been used actively as a “green” approach for the chemical modification of starch. Chang et al. reported the microwave irradiation for one-pot grafting of ϵ -caprolactone (ϵ -CL) onto starch via ROP at 255W for 3 min in the presence of tin octanoate [$\text{Sn}(\text{oct})_2$] as a catalyst [45]. Singh and coworkers modified starch by acrylonitrile grafting using peroxodisulfate as an initiator, at 1200W in a domestic microwave oven [46]. Mishra and coworkers prepared polyacrylamide grafted starch (St-g-PAM) by performing microwave radiation in the presence of a free radical initiator (ceric ammonium nitrate) [43]. Zheng et al. grafted sodium acrylate on cornstarch by using polyethylene glycol diacrylate (PEGD) as a crosslinker and potassium persulfate (KPS) as a catalyst, at 85-90W for 10 min in a microwave oven. In these studies, microwave power was accepted as a significant factor affecting the swelling ratio and solubility of the product [47].

2.4. Lactic acid

In the 21st century, because of the increasing environmental consciousness, renewable resource based and naturally biodegradable/compostable polymers gain more and more role. One of the most promising renewable resources to produce biopolymers is starch. Its fermentation allows the production of lactic acid and poly(lactic acid) [48].

The present industrial production of lactic acid is based on microbial carbohydrate fermentation because it is chemically and economically more feasible compared with the chemical method and enables the production of optically pure lactic acid [49].

The manufacture of polyester from lactic acid was pioneered by Carothers in 1932 [50] and further developed by Dupont and Ethicon [51]. Prohibitive production costs restricted the applicability of these polymers outside the

medical field until the late 1980s. Two chemical methods have been afforded to produce lactic acid in high molecular weight PLA. Cargill Dow LLC uses a solvent-free continuous process and a novel distillation method. In contrast, Mitsui Toatsu produce directly high molecular weight PLA by using a solvent based process with the azeotropic removal of water by distillation.

The most important factors that affected the careful control of the production of high molar mass polylactic acid are summarized in figure. 2.3 [8].

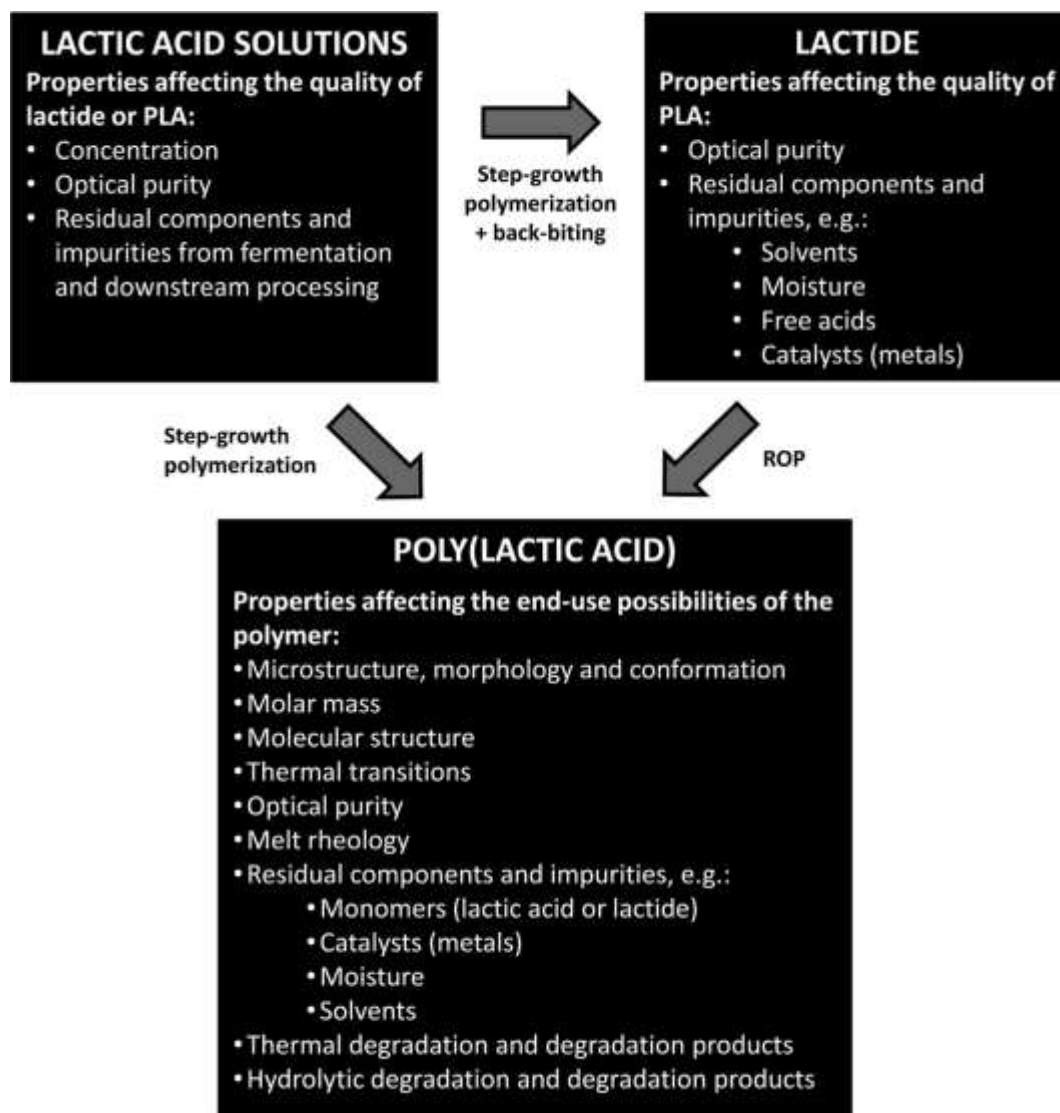


Figure. 2. 3. Production methods of PLA and simplified properties of PLA and its precursors with regard to polymer production and end-use possibilities.

2.4.1. Properties of Polylactic acid

2.4.1.1. Structure and Characterization of PLA

Microstructure, Morphology, and Conformation are the most important properties of PLA that often reflect and indicate changes in polymer composition. These changes may due to the different types of factors include degradation reactions, interactions, or immiscibility between blend components. Polylactic acid (PLA) is a thermoplastic derived from renewable resources that has a wide range of applications. A lot of different processing methods and storage environments affected the microstructure and morphology of PLA which are analyzed by a variety of analysis methods [52].

To study the morphology and interactions of PLA, PLA and filler, reinforcement in blends or composites, scanning electron microscopy (SEM) [53-55] and atomic force microscopy (AFM) [56, 57] have been used. Secondary-ion mass spectrometry (SIMS) is also a typical method for characterization of thin layers of PLA on silicon with different monatomic and polyatomic primary ions.

PLA with stereocomplex structure has a good thermal properties including thermal and hydrolytic stability. In the field of controlled delivery and pharmaceutical applications, PLA with heterostereocomplex structure, between a lactic-acid and another polymer or polypeptide, having a suitable complementary structure, described as promising materials. Infrared spectroscopy (IR), Raman spectroscopy, and near-infrared are typical methods used for studying the heterostereocomplexes (e.g., PDLA and L-configured leuprolide, respectively) of PLA [58]. The PLA stereocomplex related to the thermal transitions, morphological and conformational properties are often studied by ^1H NMR or vibrational spectroscopies, that is, Raman spectroscopy or Fourier-transform infrared spectroscopy (FT-IR), and ultraviolet (UV) spectroscopy, respectively [59, 60].

The processability, mechanical properties, and degradation properties of PLA are a variety of parameters that affected by the molar and molar mass distribution. Gel permeation chromatography (GPC) or dilute solution viscometry and GPC coupled to multiangle laser light scattering (GPC-MALLS) are often used to determine the molar mass of PLA [6, 61]. Two of the most

common solvents used in the GPC analysis of PLA are chloroform and tetrahydrofuran (THF). To analyze the end groups of the polymers in addition to the composition of individual chains, matrix-assisted laser desorption/ionization time-of-flight mass spectrometry (MALDI-TOF-MS), is one of the most recently developed characterization method for PLA and related lactic acid based copolymers. Thermal transition properties of PLA based thermoplastic polymers, are typically transformed into the desired morphology above the melting temperature, are dependent on the molar mass and optical purity of the polymer. The thermal transition behavior (glass transition temperature (T_g), crystallization temperature (T_c), and melting temperature (T_m) of PLA are the most common reported properties that largely affected the suitability of this polymer in the fields of packaging and biomedical materials [62]. Differential scanning calorimetry (DSC), thermogravimetric analysis (TGA), typically at a heating rate of 10°C/min and N₂ atmosphere, are useful in characterization of thermal transitions of PLA based polymers [62].

Small-angle X-ray scattering (SAXS), wide-angle X-ray scattering (WAXS), often in combination with DSC techniques, have been applied to characterization of crystalline morphology of PLA, biaxially oriented PLA films [63], PLA stereocomplexes [64, 65], or random copolymers of poly(L-lactide-co-meso-lactide) [66].

PLA based polymers show good mechanical, physical, and barrier properties. This important parameters have attracted the attention of polymer scientists to produce this materials in industrial scale as a packaging and mulching films. However, the understanding of the above mentioned properties of PLA is necessary before it can be fully adopted by the packaging industry. The literature reports a wide variety of factors that effects the mechanical properties of PLA such as molecular weight, orientation of molecular chains, crystallinity that develop during the processing, and chain branching architecture.

2.4.2. Processing of PLA

Thermoplastic PLA dominates the required mechanical and barrier properties desirable for a wide range of applications to compete and be a good replacement for existing petroleum-based thermoplastics. Nowadays, melt

processing is the main conversion methods for PLA [62]. This approach involves heating the polymer above its melting point, shaping it to the desired scale, and cooling to stabilize its shape. The reported methods for melt processing of PLA are injection molded disposable cutlery, thermoformed containers and cups, injection stretch blown bottles, extruded cast, oriented films, and melt spun fibers for nonwovens, textiles and carpets [67]. Recently, PLA has also been processed in conjunction with other filler materials to form bio/nano-composites which possess various unique properties, including nanoclays [68-71], biofibers [72, 73], glass fibers [74] and cellulose [75, 76].

In processing of PLA by drying and extrusion method, to prevent the decrease of the physical properties (molecular weight drop) the polymer must be dried to less than 250 ppm (0.025%, w/w) moisture before extrusion. The drying process takes place in the temperature range of 80–100°C and the drying time is dependent on the drying temperature. Extrusion is the most important technique for continuously melt processing of PLA. The plasticizing extruder can be part of the forming machine systems for injection molding, blow molding, film blowing and melt spinning as a major methods for molding. A typical screw consists of three parts: (1) feed section, (2): transition section and (3) metering section (Figure. 2.4). Commercial grade PLA resins can typically be processed using a conventional extruder equipped with a general purpose screw of L/d ratio of 24–30. Extruder screws that used for processing of PET, which are typically low-shear for gentle mixing (minimizing the resin degradation) and acetaldehyde generation, are also suitable for processing PLA resin. Another important screw parameter that is reported in the literature is the compression ratio, which is the ratio of the flight depth in the feed section to the flight depth in the metering section. It is obvious that the greater the compression ratio a screw possesses, the greater the shear heating it provides. For plasticizing the PLA resins, the pellets fed from a hopper and the screw, driven by an electric or hydraulic motor, rotates and transports the material towards the discharge point in the barrel. The heat required for melting is provided by the heat zones wrapped around the barrel. By the rotating of screw, the shear start and push the polymer against the wall of the barrel which also provides frictional heat for melting the polymer. The important parameter is

the combination of thermal energy from the zones and frictional heat due to the shear between the polymer and the screw and barrel, that is caused to the rising of the PLA polymer above its melting point (170–180°C) during a period of time when it reaches the end of the barrel [62].

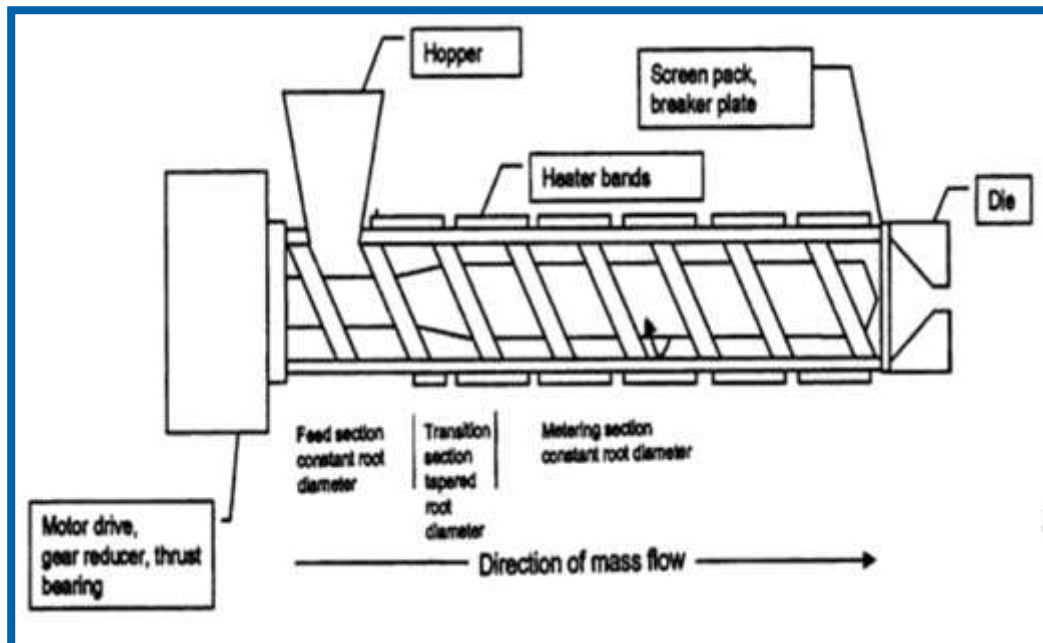


Figure. 2. 4. Typical geometries of a screw for single-screw extruder.

In the case of materials that are complex in shape and require high dimensional precision, injection molding is the most used processing technique for thermoplastic polymers. All injection molding machines have an extruder designed such the screw can reciprocate within the barrel to provide enough injection pressure to discharge the polymer melt into the mold cavities (Figure. 2.5). A typical cycle for an injection molding machine is summarized as follow: Immediately after the molds clamp up, the nozzle opens and the screw moves forward to injecting the polymer melt into the mold cavity. To prevent material shrinkage during cooling in the mold, the screw is maintained by a holding pressure in the forward position. At the end of the holding phase by shutting off of the nozzle the screw begins to recover, while the part continues to be cooled in the mold. The most important process parameter which is minimized to maximize the production is cycle time. To provide an extended cooling of the part outside and to reduce the cycle time, the transfer of the partially cooled injection molded part to a post mold cooling device is necessary. In this

technique, minimizing the duration for non-process events, such as mold opening, part ejection and mold closing are also important for reducing the cycle time. Generally the injection molded PLA based materials are brittle that is due to the rapid physical aging of the polymer since ambient temperature is only about 25°C below the T_g [77-79]. Endothermic enthalpy relaxation value (ΔH_{rel}), measured by DSC, is the parameter for evaluating of the aging of PLA at T_g region. Several reported articles in the literature showed that as the aging temperature increased towards the T_g , the rate of physical aging also became faster. However, when the aging temperature went above the T_g (60°C), the excess enthalpy relaxation was reduced, indicating that physical aging was no longer taking place when the aging temperature was above T_g [80]. However, process parameters include mold temperature, packing pressure, cooling rate, and post-mold cooling treatment playing an important role in PLA aging behavior.

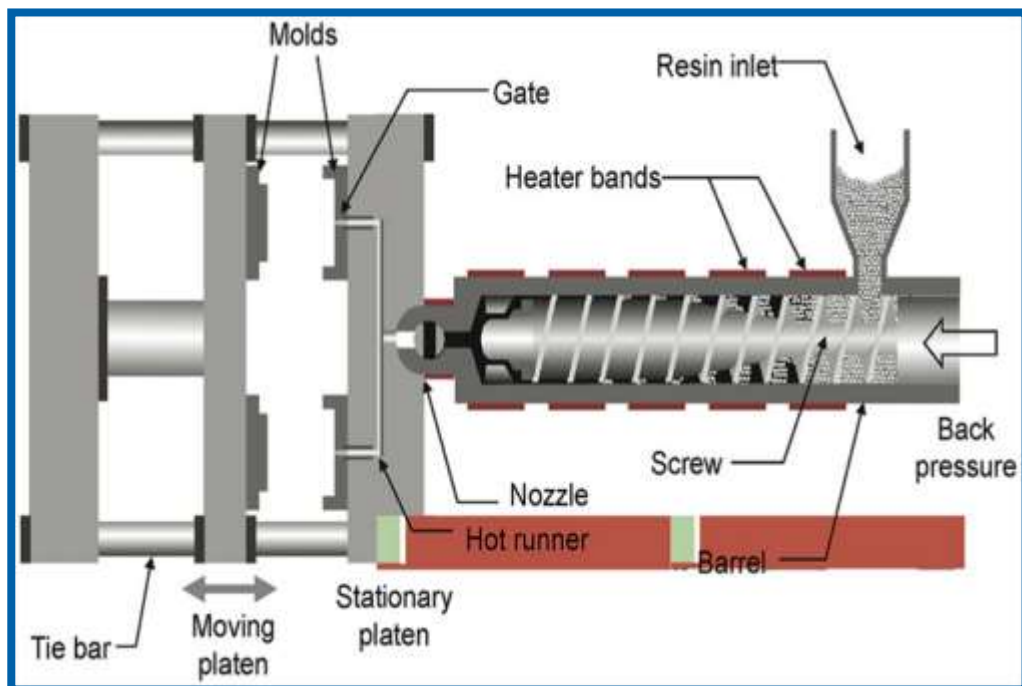


Figure. 2. 5. Major components of an injection molding machine showing the extruder and clamp units.

PLA based materials have attracted the attention of industry as a packaging material in addition to their biodegradability characteristics, they show good mechanical, physical, and barrier properties. There is a frequent interest from the food industry to replace the existing non-biodegradable thermoplastics with

biodegradable/antibacterial PLA for certain food packaging and beverage products. Recently, PLA bottles are predominantly used for beverages which are not sensitive to oxygen (e.g., flat water beverages, pasteurized milk). While barrier properties of PLA bottles may be improved by various technologies (multilayer structures, nanofillers and nanocomposites, external coating, internal plasma deposition, oxygen scavenger), but the generalizing of this materials is currently limited due to higher production costs.

Injection stretch blow molding (ISBM) technique is used for production of PLA bottles. The ISBM process for PLA bottles is illustrated in figure. 2.6. At first the formation of preform actualized in an injection molding machine. As prepared preform transferred to a blow molding machine where it is stretched in the axial direction and blown in the hoop direction to obtain biaxial orientation of the polymer. In the blow molding machine, the preform is heated in front of several banks of infrared heater to temperatures (85–110°C) suitable for blow molding. The stretching behavior of PLA is similar to PET but not entirely the same. Conversion of the existing PET systems may be practicable, but it needs to required modifications to obtain an optimized bottle.

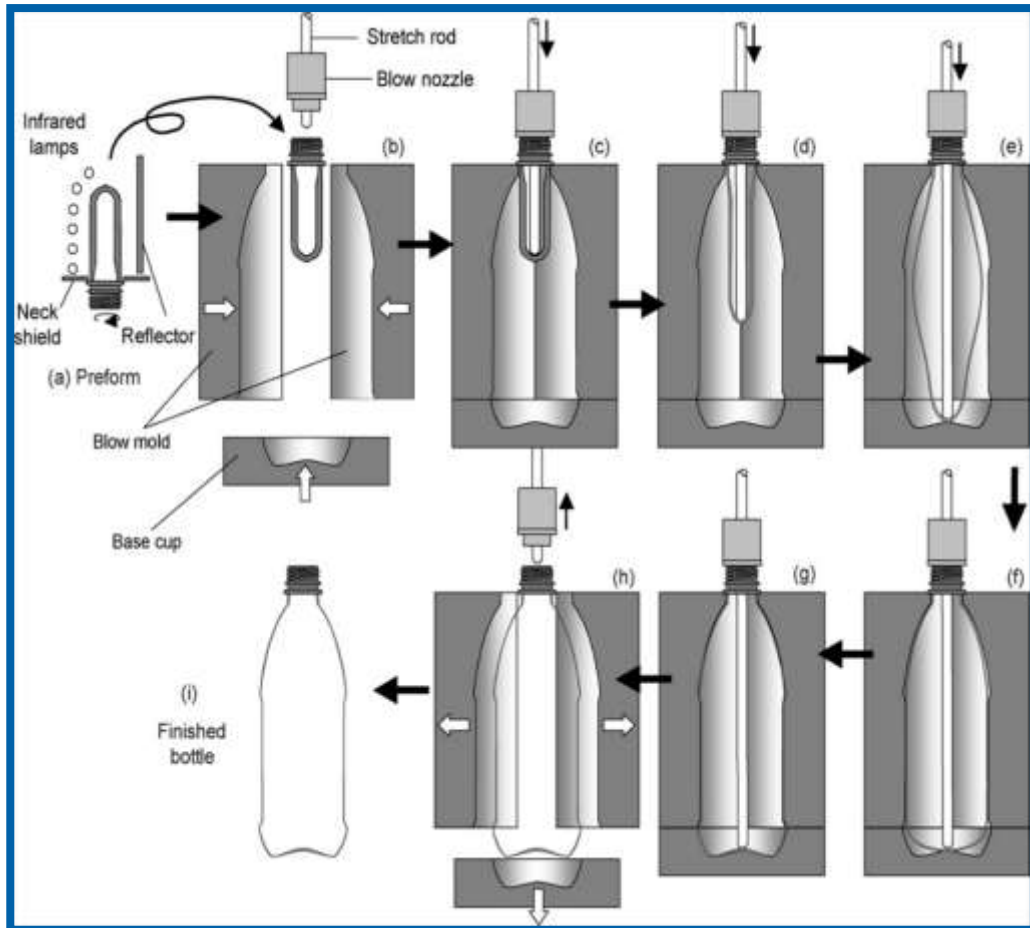


Figure. 2. 6. Injection stretch blow molding of PLA bottle.

By using of conventional extruders PLA has been successfully extruded. The production of PLA film and sheet is technically the same, but the main difference between them is their stiffness and flexibility because of the difference in their thicknesses (films: $\leq 0.076\text{mm}$ (0.003 in.) and sheets: $\geq 0.25\text{mm}$ (0.01 in.)). In the cast film technique (Figure. 2.7), PLA is extruded through a sheet die and cooled on polished chrome rollers that are quenched with circulating water. Because of the thermal sensitivity of PLA based materials, the use of external deckles on the die should be avoided since the degraded polymer behind the deckles may be caused to edge instability [81].

Uniaxial orientation of PLA films through the cast film process can enhance the physical properties similar to PP, PET and PS films by conventional machine direction orientation (MDO) rolls. During the drawing of films, nipped rolls are usually used to eliminate the PLA tends to neck. Through this mechanical drawing, the thermal and impact resistance of the PLA film enhanced similar to

oriented polystyrene (OPS), oriented polypropylene (OPP) or polyester. An oriented PLA film can be obtained by stretching it to two to ten times its original length at 60–80 °C [82].

The orientation in PLLA films depends on the draw rate, temperature and ratio, so high strain rate, low temperature and high stretch ratio favor strain-stimulate crystallization during orientation. Lee and coworkers reported that the optimal drawing temperature to achieve highly oriented PLLA films (Mw of 190,000 g/mol) is about 80°C [83]. In contrast, Gruber et al. used somewhat lower temperatures for biaxial orientation of 100,000–150,000 Mn PLA polymer with 10–20% mesolactide content [84].

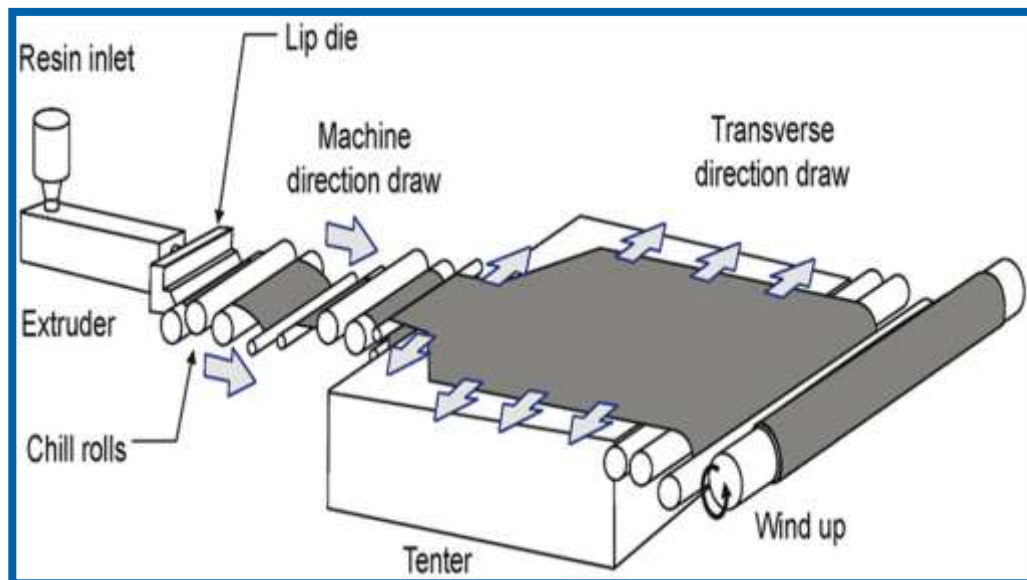


Figure. 2. 7. Biaxial oriented extrusion cast film machine.

In extrusion blow film process, PLA has been successfully extruded using an annular die. By blowing air through the die head, the tube is gathered and inflated into a thin tubular bubble and cooled. As prepared tube flattened in the nip rolls and taken up by the winder (Figure. 2.8). The ratio of bubble diameter to the die diameter is called the blow-up-ratio (BUR). BUR ratios of 2:1–4:1 with the die temperature of 190–200°C have been used for extrusion blowing of PLA films [85, 86]. Different thickness (~10–150 μm) and degree of orientation can be obtained by varying the BUR, screw speed, air pressure, and winder speed.

The specific density of PLA (1.24 g/cm³) is much higher than polyolefins (0.91–0.96 g/cm³). It is possible to process the PLA in extruders that designed for polyolefins while the extruder is already operating at close to maximum power of the screw drive [87]. PLA has weaker melt strength in compare of polyolefins, this parameter directly affected the production of stable bubble during extrusion. Most of the recently developed techniques reported that the extrusion of PLA film requires the use of additives such as viscosity enhancers which protect the polymer from degradation and/or couple polymer chains to attenuate overall loss of molecular weight and viscosity of the polymer melt [86].

Incorporation of fillers and PLA during extrusion is a way to overcome the lower elongation properties of PLA. Hiltunen et al. blended PLA with triacetin plasticizer (glycerol triacetate), and also various anti-adhesion agents, such as talc, TiO₂ and CaCO₃ to prevent the adhesion between films, They reported that the bursting strengths of the resulting blown films were better than typical polyethylene and PP films [88].

From the environmental viewpoint, the biodegradable/compostable characteristics of PLA are well suited for a variety of applications, while the source of the PLA (agricultural feedstock) will create a positive impact on the global agricultural economy. However, some of the properties of PLA still need to be improved, especially in applications where PLA is intended to be used as a replacement for existing thermoplastics. For example, in food packaging where high barrier protection (water vapor, CO₂, and O₂ permeability) is important, replacement of PET by PLA packaging may not be possible, because the barrier properties of PLA are not the same with PET. The biodegradability of PLA in some areas may cause to unpredictable performance of the final product if the polymer is exposed to uncontrollable high temperature and humidity conditions.

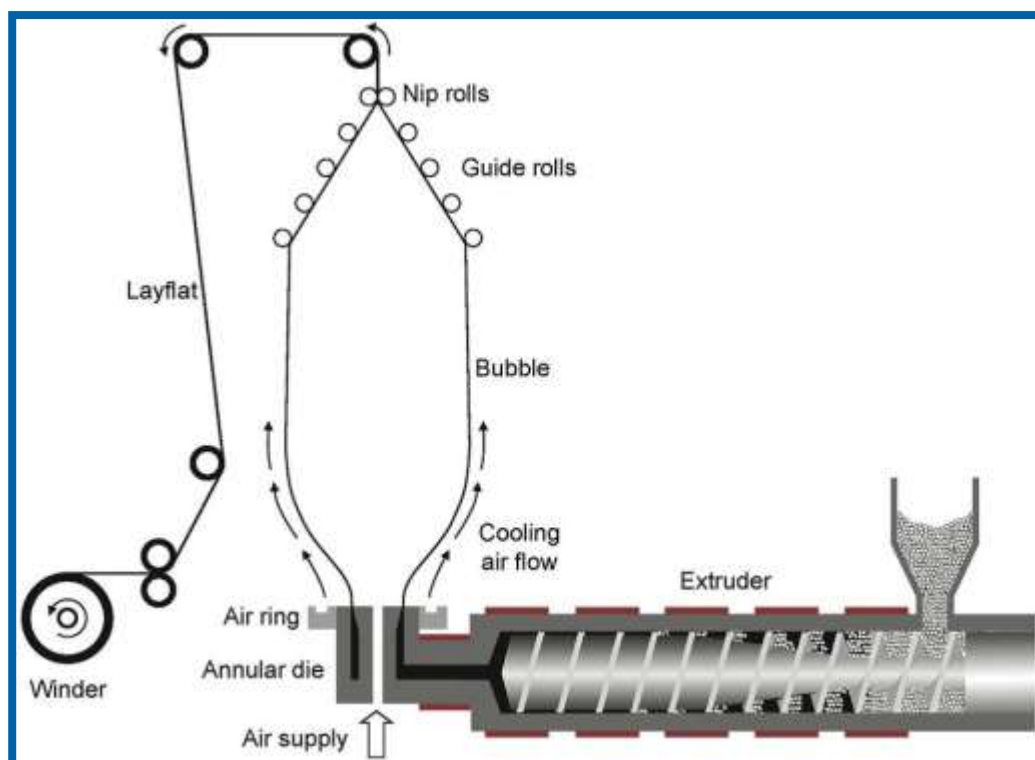


Figure. 2. 8. Extrusion blown film line

2.5. Polylactic acid/Poly(maleic anhydride-*alt*-1-octadecene)/Organoclay Nanocomposites

Various types of synthetic and natural polymer nanocomposites and nanomaterials reinforced with different types of nanoparticles have taken attention of many researchers both from industry and academia. In addition to these nanocomposites, polymer nanocomposites reinforced with functionalized nanoparticles, namely organoclays, functionalized graphene and carbon nanotubes, are relatively new areas of research in Macromolecular Nanotechnology. Most of the recently developed new approaches and nanotechnological methods in polymer synthesis and processing are related to various synthetic pathways and mechanisms for the formation of nanostructures in polymer/nanofiller hybrids and nanocomposites, predominantly containing anhydride/carboxyl functionalized copolymers such as alternating, random and graft copolymers of maleic anhydride and its isostructural analogues. The results of these studies, in particular, on polymer layered silicate nanocomposites have already been summarized by several excellent reviews [89-94]. Smectic clays, particularly montmorillonite (MMT)

minerals and their organic derivatives, serve as good nanoclay fillers owing to their ease of dispersion in the organic matrix. Nano-scale particles and effective in situ processing within these systems can be formed by the use of preintercalated monomer...organoclay complexes or intercalated functional monomers [95, 96] or polymers containing exchangeable and/or reactive groups such as, carboxyl, amine, epoxide, urethane and etc [97, 98].

Maleic anhydride (MA) reactive copolymers, including poly(MA-*alt*- α -olefin)s are being widely used to prepare high performance engineering, bioengineering and nanoengineering materials [19, 20, 99-103]. Nano methods in polymer synthesis and processing were the subject of our group recent review publication [103]. All these methods, especially interlamallar polymerization methods provide the formation of nanosystems with controlled structures. Recently, we have reported the preparation of polypropylene and EPDM rubber silicate layered nanocomposites in melt by reactive extrusion using poly(MA-*alt*-1-octadecene) as a reactive compatibilizer [99, 100]. Poly(maleic anhydride-*alt*-1-octadecene) is a new commercially available polymer and was used to water-solubilize colloidal nanocrystals with various compositions, morphologies, and sizes. Highly pure nanoparticles with homogeneous distributions of sizes and surface charges were obtained by Di Corato et al. after a single purification step of the polymer-coated particles by ultracentrifugation [104]. According to the authors, the inclusion of the hydrophobic nanoparticle in an amphiphilic polymeric shell is perhaps more advantageous with respect to the others, as the nanoparticles are simply wrapped in a polymeric shell due to favorable interactions between the alkyl chains of the surfactant.

This reactive copolymer like the other alternating copolymers of maleic anhydride easily undergoes various chemical reactions with hydroxyl-, epoxide- and amine-containing compounds. Schmidt et al. [105] prepared thin films of poly(maleic anhydride-*alt*-1-octadecene) on top of silicon wafers and glass plates by modification of anhydride units with different functional amines to be used in future studies on the relevance of certain molecular surface properties for the covalent immobilization of proteins. Highly pure nanoparticles of this copolymer with homogeneous distributions of sizes and surface charges were obtained by Di Corato et al. [104]. Some modified nanoparticles show both a

sufficient negative charge and a good stability in buffers, allowing further studies of virus-like particle formation with these modified cores. Besides water solubility of the nanoparticles, copolymers with longer hydrophobic branches and their diamine cross-linked networks [104, 106] provide a stable nanoparticles shell and hydrophobic double layer. Amphiphilic alternating copolymers such as poly(MA-*alt*-1-tetradecene), poly(MA-*alt*-1-octadecene) and their poly(ethylene oxide) (PEO) grafted derivatives were also used for the surface functionalization and encapsulation of magnetic nanoparticles [104, 106-108]. Donescu et al. [109] reported synthesis of cross-linked copolymer of maleic anhydride and divinylbenzene, containing a Fe₃O₄...oleic acid complex, by dispersion polymerization. Authors prepared the magnetic nanoparticles with an average size about 23 nm dispersed in micrometer size copolymer spherical particles.

Poly(lactic acid) (PLA) related to the class of natural polyesters is an important biodegradable polymer which has been used in various publications as medical implants [110], sutures [111], and controlled drug delivery systems [112]. According to the authors of a review [52], PLA polymers have been known for a relatively long time, but the interest in these materials is still accelerating. They described relevant and up-to-date information on characterization of LA-based polymers and highlighted the importance of monomer quality and different characterization methods and quality control steps for mechanical properties of the final products. Functionalization of PLA paves the way to prepare composites, laminates, coated items, and blends with improved properties and cost effectiveness. Functionalized matrix polymer and the fiber/filler with highly reactive groups is perhaps the most successful strategy, leading to a variety of commercial composites prepared by reactive extrusion processing [113]. MA was first used as a monomer to graft onto biodegradable PLA by several researchers [4, 114, 115]. The MA functionalization of PLA proved to be very efficient in promoting strong interfacial adhesion with corn native starch in composites as obtained by melt blending. Thus, improved interfacial adhesion could be obtained in PLA/starch blends via chemical modification of PLA with low levels of MA monomer [115]. Carlson et al. [114] performed free radical-initiated grafting of MA onto a PLA backbone at 180-200°C with 2 weight % of

MA concentration by using twin screw reactive extruder. Authors proposed that the formation of a radical in the first step of grafting can occur by hydrogen abstraction from -CH group, producing a PLA radical which can easily react with MA.

Recently, the attentions of many researchers were also focused on poly(lactic acid) (PLA) based nanocomposites [116-119]. Exfoliated PLA/organoclay (Cloisite 30B) nanocomposites were prepared by both in melt-processing, solution casting and in situ intercalative polymerization methods [120]. Preparation of PLA/organoclay blends by the solution casting method was first reported by Ogata et al. [70] The authors found only tactoids containing several stacked silicate layers. The ordered and well dispersed PLA/octadecylammonium-MMT nanocomposites and PLA/organoclay-phosphonium modified porous ceramic nanocomposites were prepared by Maiti et al. [121, 122] PLA based nanocomposites have received increasing attention in recent years due to their biocompatibility, degradability and possibility of their wide environment friendly applications such as eco-films for food packaging and clinical medicine. [123, 124]. New approaches related to the preparation, characterization, properties and applications of nanocomposites containing biodegradable polymers (PLA, poly(ϵ -caprolactone), poly(hydroxy-alkanoate) and natural renewable polymers) as matrix polymers and various nanoparticles (clays, nanotubes, magnetites, Au and Ag, hydroxyapatite, and etc.) were reported by Yang et al. [125].

Recently, the attention of many industrial and academic researchers was focused on PLA-based nanocomposites [122, 126-133]. Gacitua and Zhang [130] reported the results of a preliminary study using a biopolymer, PLA as the matrix polymer, and two fillers with 'nano' size (clays and calcium carbonate) to prepare nanocomposites. According to the authors, an important effort is now conducted to improve the general properties of PLA, which has a tremendous future as a polymer or reinforced polymer for automotive and other durable applications. Using only 2.5 % of nanoclay or nano calcium carbonate particles, they found a significant improvement in physical and mechanical properties of these nanocomposites. Fukushima et al. [64] prepared PLA nanocomposites by adding organically modified MMTs and one sepiolite obtained by melt

compounding. They found that all clays showed a good dispersion level and the highest thermo-mechanical improvements with PLA matrices due to a higher PLA/filler compatibility. Kontou et al. [131] investigated the effects of two different types of nanofillers (silica and MMT) at three different weight fractions as well as their mixtures on the thermomechanical properties of PLA. The authors suggested that silica and MMT clay have different reinforcing and toughening effects on PLA, while the combination of these two different nanofillers has a detrimental effect on the tensile properties of the PLA material. Several researchers consider that MMT clay mineral as a catalyst has played an important role in synthesis, selecting, protecting and concentrating of biomacromolecules in the natural conditions for the origin of the first life. MMT adsorbing organic compounds can also catalyzed a variety of organic reactions critical to the scenarios of life's origins [122, 125, 126]. Ferris demonstrated that MMT intercalated with RNA molecules can catalyze the formation of biomacromolecules with relatively higher molecular weight. He also found that MMT having alkali and alkaline earth metal ions as exchangeable cations is catalytically more active than pristine MMT with iron and other transition metal ions as exchangeable cations [127, 128]. Naturally occurred halloysite (Hal) nanotubes compounded with polylactide (PLA) via melt mixing formed biodegradable and biocompatible clay polymer nanocomposites (CPN). The hydrogen bonding interactions between Hal and PLA were confirmed by FTIR analysis. The prepared Hal-PLA nanocomposites had potential applications in biodegradable plastic and biomedical areas [132]. Souza et al. reported the synthesis, rheological and thermal properties of organofluoromica/PLA nanocomposites [134]. Vermiculite (VMT) was successfully modified by cationic exchange of hexadecyltrimethyl ammonium ions, covalent grafting of glycidoxypropyl trimethoxy silane, and combining grafting and intercalation [135]. According to the authors, the complete removal of excess surfactant from VMT resulted in a change in the interlayer structure and higher thermal stability of the organoclay mineral; the organosilane grafted on the clay mineral edges improved the thermal stability of the organoclay mineral. They evaluated the effects of clay surface modification and organoclay purity on microstructure and thermal properties of PLA/vermiculite nanocomposites. Bianchi et al. synthesized and characterized ODTMA-MMT and HDTMA-MMT organoclays.

Physical structures of these clays were investigated by WAXS, SAXS and surface charge methods [136]. Authors demonstrated that particle apparent diameters (determined by laser), zeta potential values and SEM images, indicate the presence of assorted d001 values (which depend on storage conditions), aggregate formation and charge reversal (which varied with loading and cation length) for samples obtained with 1 and 2 CEC. According to the authors, obtained them results will help attain better conditions to functionalize highly charged MMT making them suitable to be used as nanocomposite precursors for different applications.

Even though the most promising methods for the synthesis of polymer/clay nanocomposites are the melt-processing and intercalative (co)polymerization of various functional monomers, the interlamellar graft copolymerization of L-LA monomer onto alternating copolymers of maleic anhydride in the presence of organoclay has not been investigated yet. Complex-radical interlamellar solution copolymerization of maleic anhydride/acid with acrylic comonomers (acrylic acid, acrylamide and butyl methacrylate) in the presence of preintercalated complexes of reactive and non-reactive organoclays with functional monomers was a subject of our recent publications [137-140].

3. MATERIALS AND METHODS

3.1. Materials

Corn starch (22–28% amylose and 72–78% amylopectin) was supplied by Cargill (USA). L-Lactic acid (20 wt% aqueous solution, density 1.209 g/cm³, reflection index 1.427) was purchased from Purac (The Netherlands). Sodium hydroxide and stannous 2-ethyl hexanoate Sn(Oct)₂ were purchased from Sigma-Aldrich (Germany). High purity scCO₂ (99.9%) was obtained from Linde (Germany).

Commercially available poly(maleic anhydride-*alt*-1-octadecene), Poly(MA-*alt*-1-OD) was purchased from Sigma-Aldrich (Germany) and used as a matrix polymer having the following characteristics: density 0.97 g/cm³, acid number (AN) 310–315 mg KOH/g, Mw~40.000 Da, T_g (softening)=120–130°C (by DSC); ¹H NMR spectra (δ, ppm):3.42 and 3.38 (backbone CH–CH from anhydride unit), 1.69–1.34 (–(CH₂)_n– from olefin branch), 1.25 and 1.10 (backbone CH₂ and CH from olefin unit), and 1.10 (pendant CH₃ from olefin branch); ¹³C NMR spectra (δ, ppm): 151.95 (C–O of anhydride unit), 40.62 and 40.41 (backbone CH–CH of anhydride unit), 22.55 and 31.75 (backbone CH₂ and CH from olefin unit), 29.44–29.16 (–(CH₂)_n– from olefin branch), and 14.41 (pendant CH₃ from olefin branch). Na⁺-MMT (K-10) was purchased from Sigma-Aldrich: ζ-size=2.54 μm, and ζ-potential= 73.3 mV; Ag⁺-MMT was synthesised by intercalation and ion-exchange reaction of AgNO₃ with Na-salt of MMT in aqueous medium: ζ-size=0.98 μm, and ζ-potential=74.9 mV; ODA-MMT organoclay was obtained from Sigma-Aldrich: content of octadecyl amine 25–30%; particle size 8–10 μm, bulk density 0.41 g/cm³, crystallinity 52.8% (by XRD), glass-transition temperature (T_g) 108.4 °C (by DSC for the surface alkyl (C18) amine fragment), temperature of decomposition for T_d(onset) 275°C and T_d(max) 380°C (by TGA); particle parameters: ζ-size=1.47 μm, and ζ-potential = 94.2 mV. All other solvents and reagents were of analytical grade and used without purification. Dimethyldidodecyl ammonium cation (DMDA-MMT) (Viscobent SB-1) was purchased from Bensen (Enez, Turkey) having the following average parameters: specific surface area 43.6 m²/g, specific mesopore volume 0.14 cm³/g, contents of N 1.12 wt.% and C 32.56 wt.% [141]

and crystallinity 58.2% (by XRD). Bis(2-ethylhexanoic acid) tin(II) salt [Sn(oct)₂] was purchased from Goldschmidt, diluted with dry toluene and stored under nitrogen atmosphere. All other solvents and reagents were of analytical grade and used without purification.

3.2. Manufacturing of PLA/Silicate Nanocomposites and Catalyst Nanofillers

3.2.1. Nanofabrication and Characterization of Poly(MA-*alt*-1-octadecene)-*g*-Poly L-lactic acid Layered Silicate Nanocomposites

The nanocomposites were synthesized by bulk interlamellar graft copolymerization of LA monomer onto poly(MA-*alt*-1-OD) as a matrix polymer in the presence of reactive ODA-MMT (which tends towards a chemical reaction via intercalated and complexed primary amine group) and non-reactive DMDA-MMT (capable of forming in situ strong H-bonding via ammonium cation) organoclays (3.2 wt.%) and tin 2-ethylhexanoate, [CH₃(CH₂)₃CH(C₂H₅)-COO]₂Sn (24 mmol, 0.003%) as a catalyst under vacuum (600 mm/Hg) at 80 ± 0.1°C using a carousel-type micro reactor with intensive mixing up to the formation of a homogeneous ODA-MMT and finely dispersed DMDA-MMT solutions (Figure. 3.1). Then, the prepared viscose solutions were cooled up to room temperature, treated with a large amount of methanol with intensive mixing up to full precipitation of powder product, which was isolated by filtration, and purified by twice treatment with methanol through extraction–ultracentrifugation and dried under vacuum at 40°C.

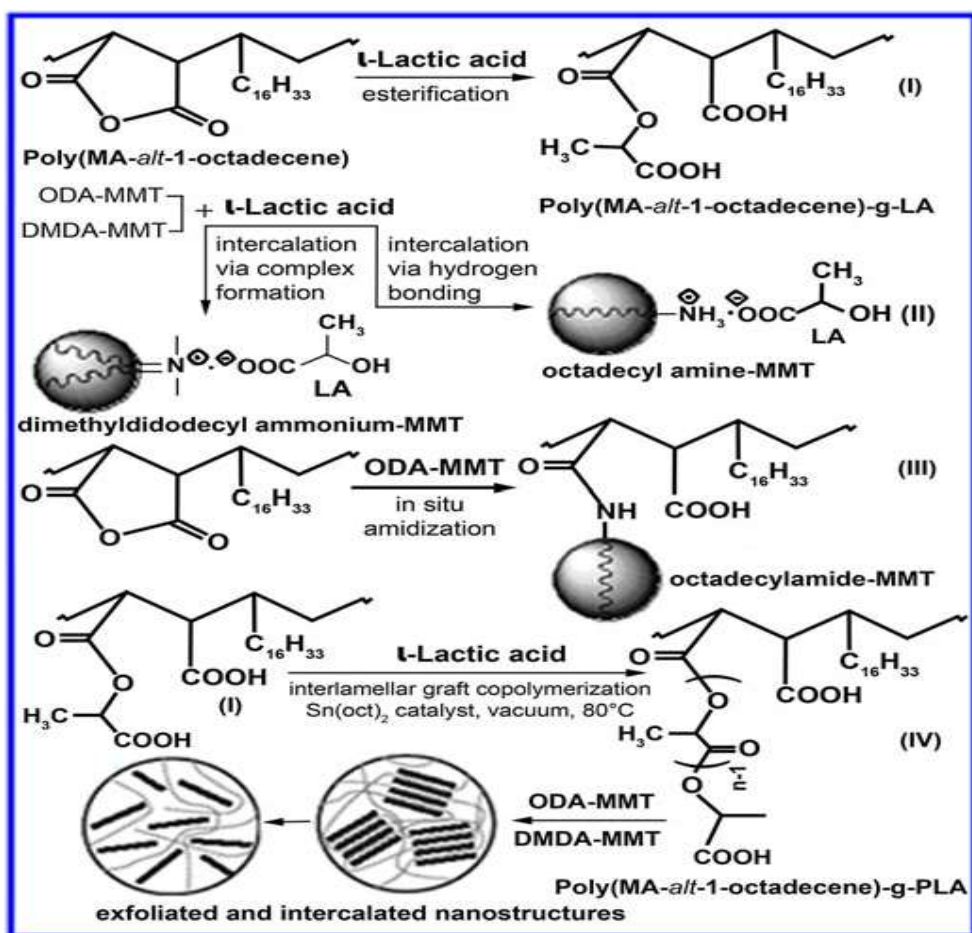


Figure 3. 1. Synthetic pathways for preparation of the poly(maleic anhydride-*alt*-1-octadecene)-*g*-poly(L-lactic acid)/octadecyl amine-MMT clay nanocomposites: (I) grafted LA monomer onto alternating copolymer via esterification, (II) preintercalated MMT-ODA...LA complex, (III) octadecyl amide-MMT derivative of alternating copolymer (nanohybrid) and (IV) copolymer-*g*-PLA and its ODA-MMT layered nanocomposites.

3.2.2. Interlamellar Graft Copolymerization of L-lactic acid onto Poly(maleicanhydride-*alt*-1-octadecene) in the Presence of Different Clays as Catalyst-nanofillers

Synthesis of Ag⁺-MMT was carried out by intercalation and ion exchange reaction of AgNO₃ with Na salt of MMT in aqueous medium (Figure 3.2). Approximate amounts of AgNO₃ and Na⁺-MMT are separately dissolved and dispersed in double distilled water to prepare solutions at 0.4 and 0.1 g/mL concentrations, respectively. Then 10 mL of silver nitrate solution is added to Na⁺-MMT dispersion drop by drop by stirring at 40 °C for 3 h up to turn of reaction solution to yellow. The light yellow water solution of Ag⁺-MMT indicates the formation of intercalated silver nanoparticles [142], which was also

confirmed by UV and XRD analyses. After cooling the reaction mixture up to room temperature, Ag^+ -MMT (intercalated via ion-exchange interaction) was isolated by precipitation with methanol and extraction–centrifugation. The prepared steel gray powder product undergoes a treatment at 150°C for 5min under nitrogen flow and dried under vacuum at 80°C to fully in situ generation of the intercalated AgNO_3 cations to silver nanoparticles (AgNPs). After this thermal treatment, the formation of light-brown powder product as a result of in situ generation processing confirmed significantly riching MMT clay with intercalated AgNPs. This method (annealing or UV-irradiation) is well known and widely used for the fabrication of AgNPs in various polymer nanocomposites.

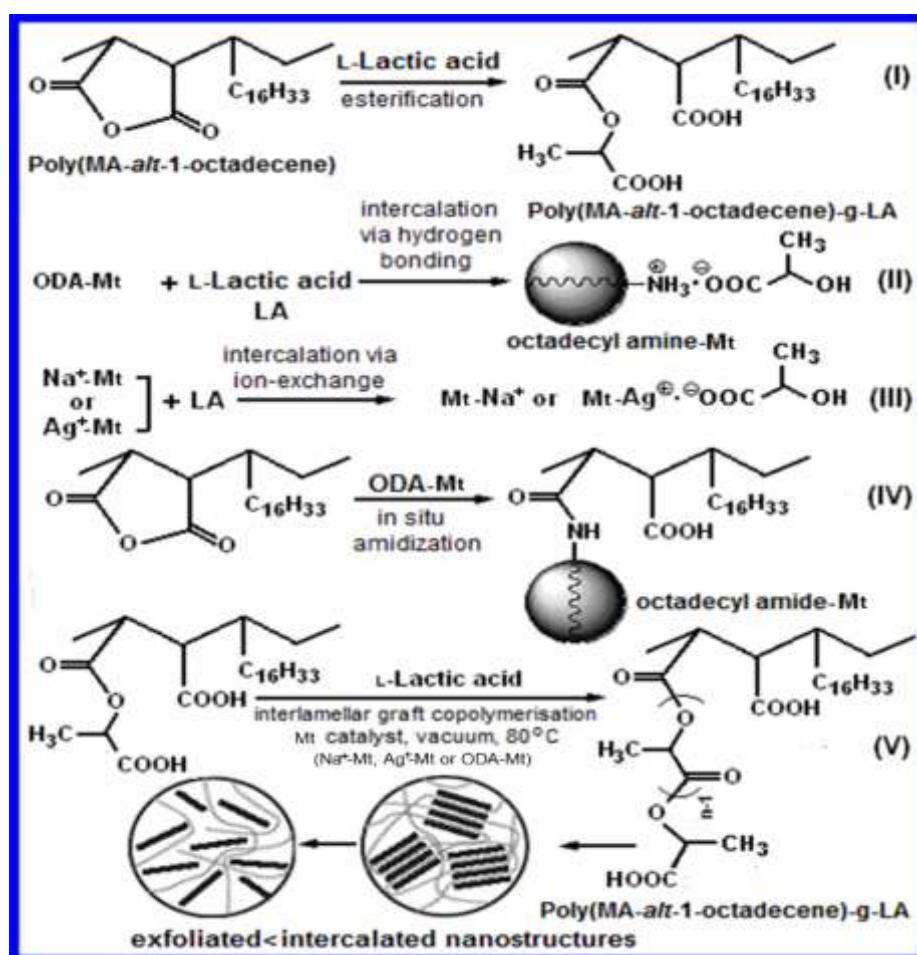


Figure. 3. 2. Schematic representation of synthetic pathways for copolymer-g-PLA intercalated silicate nano-composites in the presence of Na^+ -MMT, Ag^+ -MMT and ODA-MMT as catalysts of graft copolymerisation of L-lactic acid onto poly(MA-*alt*-1-octadecene) and nanofillers: (I) mono-esterification, (II) intercalation via hydrogen-bonding, (III) intercalation via ion-exchange, (IV) intercalation via in situ amidisation and (V) interlamellar graft copolymerization.

Synthesis of copolymer-*g*-PLA layered silicate includes the following steps: (1) 3.5 g of copolymer was dissolved in 20 mL LA by intensive mixing at 40°C up to the formation of a homogeneous viscous product; (2) 0.175 g of any clay (Na⁺-MMT, Ag⁺-MMT or ODA-MMT as catalyst-nanofillers) was dissolved in 5 mL LA by intensive mixing at room temperature for 6 h up to full intercalation of LA monomer between silicate interlayer species, and (3) both solutions of copolymer and inorganic or organic clays, were placed in a specially constructed vacuum (600 mm-Hg) micro-reactor with Dean-Stark unit and mixed at 80 °C up to a previously fixed phase separation time for each clay around 25–56 min (for ODA-MMT 56 min, Na⁺-MMT 35 min and Ag⁺-MMT 25 min). Then, powder polymer particles were isolated from the reaction mixture by precipitation with methanol, twice extraction–ultracentrifugation and dried under vacuum at 40 °C.

3.3. Graft copolymerization of starch with lactic acid using various methods

3.3.1. Synthesis of St-*g*-PLA copolymers in supercritical CO₂ media

Graft copolymerization was conducted by the following two steps: (1) gelatinization of the starch according to a related study [143] and (2) grafting in the scCO₂ reactor (Figure 3.3). For the gelatinization, 5 g of starch was dispersed in 30 mL of 0.40 M NaOH in a three-necked reactor at 70°C for 1 h. The gelatinized starch was transferred into a 250 mL high pressure stainless reactor (Thar R100, USA) consisting of two sapphire windows on both sides with a high-pressure pump (Thar, P series) to pressurize CO₂, an automated back pressure regulator (Thar, ABPR 200), a temperature controller (Thar, CN6), a mechanic mixer (Minarik Corporation, MM23101C) with four blades and a computer control system. The graft copolymerization was initiated with an excess amount of LA and catalyst (Sn(oct)₂) under different reaction conditions (70–110°C, 70–300 bar, 1.5–9 h and 1–15 g/min, see Table 4.3) under mechanical stirring (700 rpm). The reactor was cooled to room temperature to terminate the reaction, and the product was isolated by venting with CO₂. The product was then washed twice with methanol to remove the

unreacted LA and oligo (lactic acid), and it was dried under vacuum at 70°C. Additionally, to eliminate the presence of PLA in the product, an extraction procedure was applied as a further purification step for 12 h using methanol as an extraction solvent in a soxhlet system. Finally, the extracted polymer was dried at 70°C under vacuum.

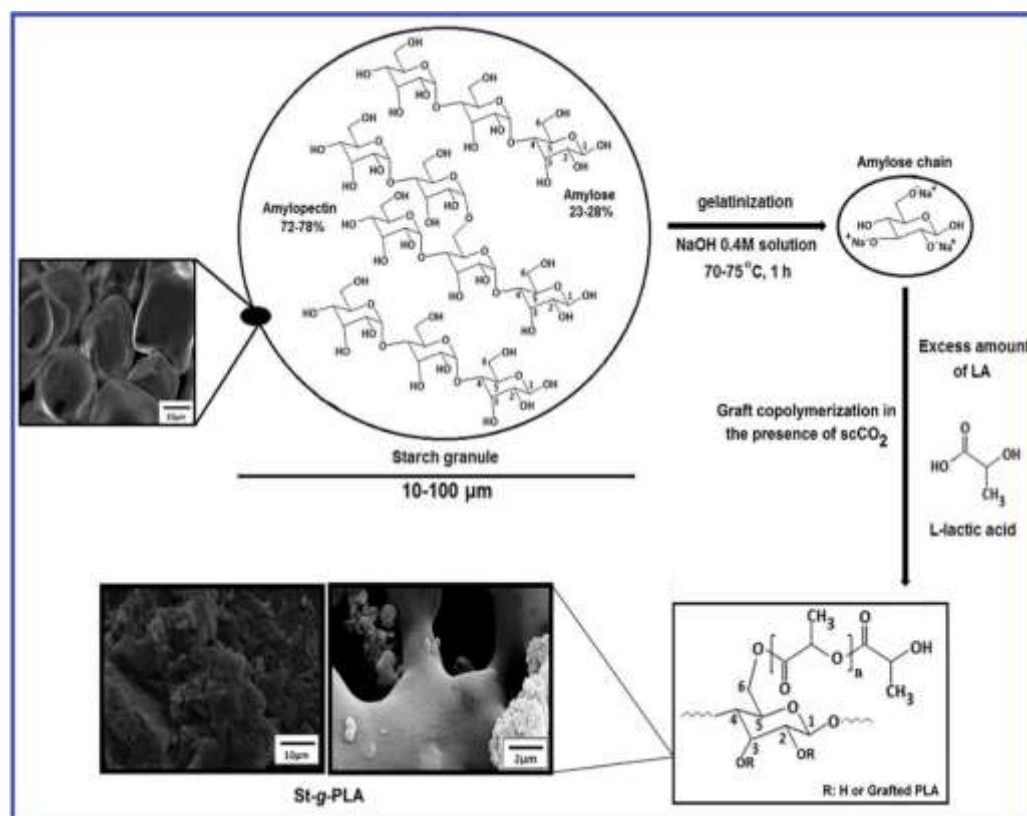


Figure. 3. 3. The graft copolymerization of L-lactic acid onto a starch backbone in supercritical carbon dioxide.

3.3.2. Microwave Assisted Grafting of St-g-PLA Copolymers

Graft copolymerization was performed in two steps (Figure 3.4). During the first stage, 5 g cornstarch was dispersed in 30 ml of 0.40 M NaOH solution in a three-necked reactor. Gelatinization of starch was carried out by increasing the temperature to 70°C and holding the system at this temperature for 1 h. During the second stage, the as-prepared slurry was transferred into three-necked round bottom flask using a vacuum system (-600 mm-Hg) to remove the water from the reaction media. The microwave irradiation was optimized by using the following process: an excess amount of L-lactic acid and stannous octoate (0.3 wt% of LA amount) were mixed with a magnetic stirrer. Varying reaction

conditions such as power, duration of radiation, concentration of LA and NaOH, (Table 4.6) were applied to graft LA on starch. The mixture was heated to 100°C by increasing the power outputs from 150 W to 750 W. Since the maximum grafted PLA (mole %) was achieved at 450 W irradiation, the optimal irradiation power was determined as 450 W. During the synthesis procedure, microwave irradiation was periodically paused before the mixture reached boiling point (not exceeding 100°C) and was kept for a while to allow the mixture to collapse in order to prevent the quit of slurry by the vacuum system and so that there was a formation of vapor which contained LA and starch mixture. This process was repeated until a highly viscous polymer (light brown) was obtained. After completion, the irradiation time was recorded and the sample was kept undisturbed for 12 h to complete the grafting reaction. After the specified conditions were fulfilled, the product was washed with excess methanol to remove the unreacted lactic acid and polylactic acid (PLA) homopolymers, and dried under vacuum at 70°C. To remove the unreacted PLA in the final product, an extraction procedure was carried out for 12h by using methanol as the extraction solvent in a soxhelet system. Finally, the extracted polymer was dried at 70°C under vacuum.

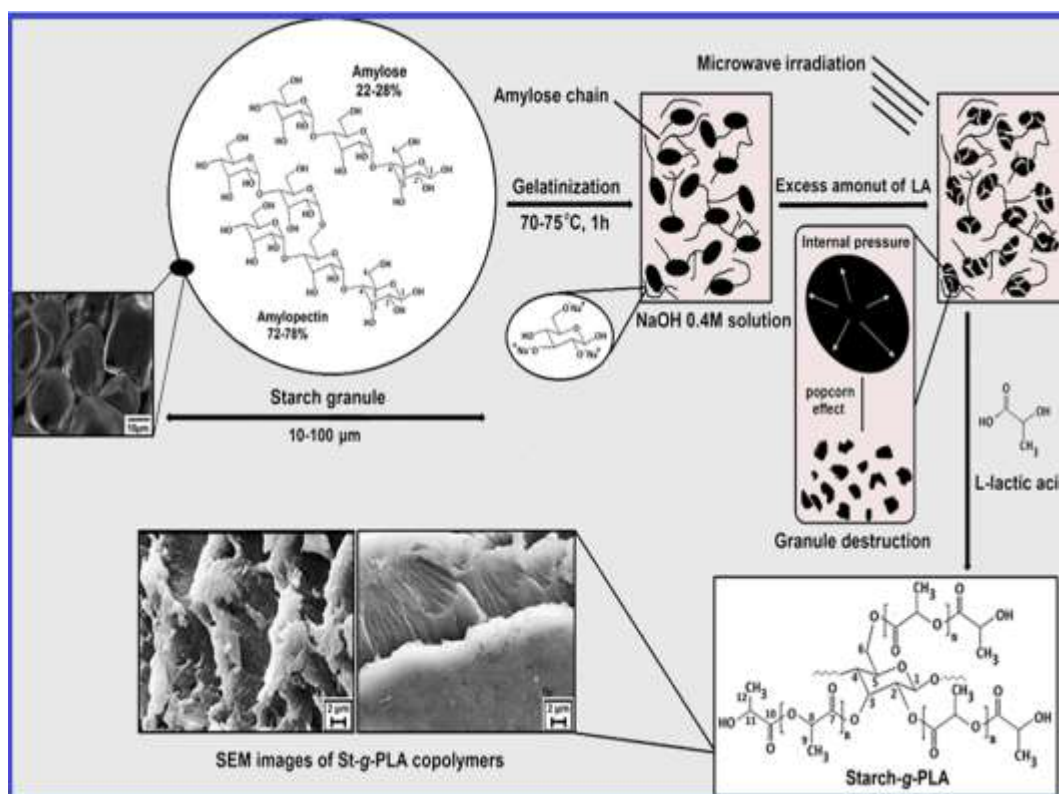


Figure. 3. 4. Schematic representation of starch-g-PLA synthesis by microwave irradiation.

3.3.3. Processing of St-g-PLA Copolymers and St-g-PLA/Organoclay Nanocomposites Blends through Shear Mixing and Reactive Extrusion

Processing of St-g-PLA copolymers and St-g-PLA/organoclay nanocomposites were carried out according to the following procedures (Figure 3.5). At first, native starch was weighed and dried in an oven (Memmert, Germany) at 60°C overnight. The LA/organoclay (MMT-Na) organomodification was done by an intercalation/exfoliation technique using mechanical stirring for 24 h [68, 69]. Starch was transferred in a High-shear mixer (Zeppelin, FML10, Germany) and Lactic acid was added slowly by using a variable speed peristaltic pump feeder (Watson Marlow, England) while the starch was slowly mixed. After completion of LA addition, the mixture was dispersed at high speed (~1500-2000 rpm) to obtain a homogenous St-LA or St-LA/organoclay paste. The shape and morphology of the blades in the mixer at high speed caused to increasing of temperature, allowing vaporization of water from the bulk and diffusion of LA and oligo-LA into the starch amylose part. In parallel, graft copolymerization process was continued for 4 h by applying vacuum (~600-mm Hg). After

cooling, St-g-PLA copolymers were ground by a laboratory mill into about 50 mm powder prior to blending in extrusion in order to increase the graft copolymerization degree.

Extrusion of copolymers were done in a twin-screw extruder (Rondol, England) at a mass flow rate of about 200 g/min. The length to diameter ratio of the screws was 21 mm. Five different extruder temperature profiles were used. After reaching steady state, as prepared copolymer granules with a variety of compositions were fed manually into the extruder at screw speed of 60 rpm in a random order and the products were obtained using a coil die. This process was continued for several times to obtain a high value of grafting degree. During extrusion, the temperature of the viscous melt, pressure and torque inside the barrel were monitored and recorded by a computer. The extruded coils granulated and then placed into linear low density polyethylene (LDPE) bags for blown film production step.

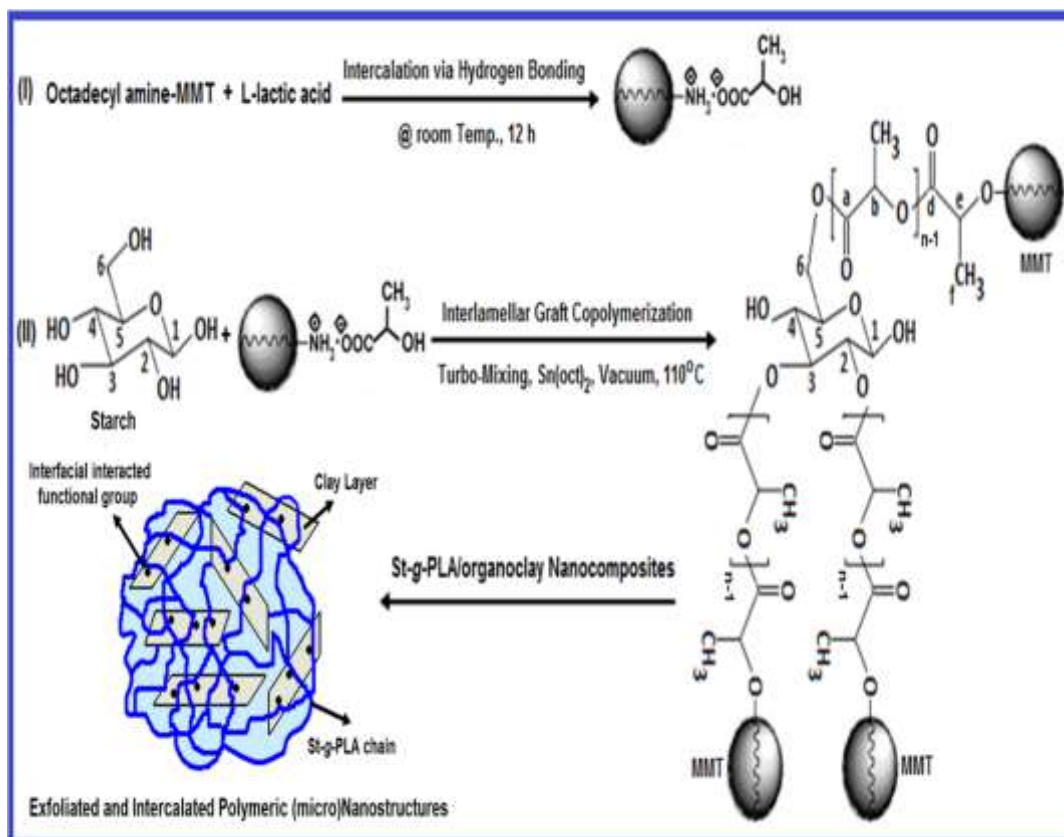


Figure. 3. 5. Schematic representation of starch-g-PLA/organoclay nanocomposites synthesis by “shear Mixer” and “Reactive Extrusion”.

3.3.4. Film Extrusion

The St-*g*-PLA and St-*g*-PLA/organoclay based films were produced in a lab-scale twin-screw extruder (Rondol, England), equipped with a film blowing die (0.6-mm thick and 25-mm wide), macro-compounder and rotating film-uptake rolls. The film quality was examined by selection the extrusion parameters based on the conditions of optimal extrusion trials. The extrusion process was carried out by running a macro-compounder to feeding the granules (70 rpm), temperature (5 different zone) and using a blowing die temperature at 140°C to obtain films with uniform thickness (Figure 3.6). The film blowing was done at constant air flow cooling after the die and collected by a rotating roll (a speed equal to the extrusion through the blowing die). The final film thickness was measured by a micrometer at several points of the film during the extrusion.

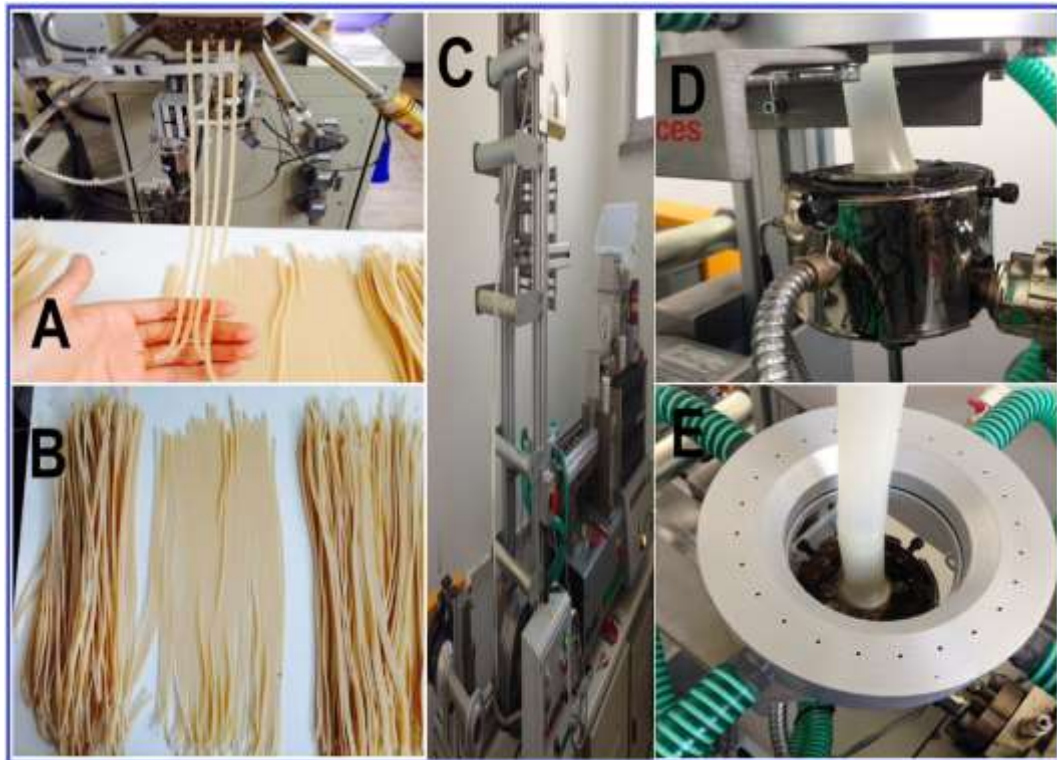


Figure. 3. 6. (A, B) As prepared St-*g*-PLA and St-*g*-PLA/organoclay nanocomposites through reactive extrusion; (C) Extruder and film blowing unit; (C, D) Blowing die and the blown film.

3.4. Characterization

3.4.1. Chemical and Physical Properties

3.4.1.1. ATR-FTIR

Attenuated total reflectance Fourier transform infrared spectroscopy (ATR-FTIR) analysis was employed by using an ATR-equipped spectrophotometer (FTIR-SMART-IR, THERMO Scientific, USA) throughout the wavenumber range of 4000 to 500 cm^{-1} .

3.4.1.2. ^{13}C /CP MAS-NMR and ^1H -NMR

The ^1H -NMR spectra were performed on a JEOL 6X-400 (400 MHz) spectrometer in $\text{CHCl}_3\text{-d}_1$ solution at 25 °C. The ^{13}C -NMR analysis was carried out using a Bruker AVANCE300 (Germany) spectrometer operating at a 300.13 MHz proton frequency with a 4-mm Bruker spinning probe and zirconia rotors. Spectra were obtained using the standard CP/MAS (cross polarization magic angle spinning) technique with 1400 scans. The magic angle was adjusted by maximizing the side bands of the 79Br signal of a KBr sample. The samples were rotated at 4000 ± 1 Hz.

3.4.1.3. MALDI-TOF-MS

The molecular mass of pristine copolymer and copolymer-*g*-PLA was performed by matrix-assisted laser desorption/ionization mass spectrometry (MALDI-TOF-MS, Applied Biosystems Voyager DE PRO model), in THF solution α -cyano-4-hydroxycinnamic acid (CHCA) as a matrix and NaTFA as a cationizing agent for ionization of the samples.

3.4.1.4. XRD

The X-ray powder diffraction (XRD) patterns were performed with a PANANALYTICAL X-ray diffractometer equipped with a $\text{CuK}\alpha$ tube and Ni filter ($\lambda=1.5406$ Å). The XRD diffractograms were measured at 2θ , in the range 1–50°. The Bragg equation was used to calculate the interlayer spacing (d): $n\lambda=2d\sin\theta$, where n is the order of reflection, and θ is the angle of reflection.

3.4.1.5. ζ -size and ζ -potential Analysis

The particle ζ -size and ζ -potential parameters were measured by Nanosizer 3000HSA instrument (Malvern, UK) in chloroform solution with 0.01% concentration of samples.

3.4.1.6. UV/VIS Spectrophotometer

The UV–vis spectra of Ag⁺-Mt was recorded by UV/VIS spectrophotometer (Jasco, USA).

3.4.2. Thermal Behavior

3.4.2.1. DSC

Differential scanning calorimetric (DSC) analyses were performed using DSC Perkin Elmer Thermal Analyzers and a linear heating rate of 10°C/min under nitrogen flow. Samples were measured in a sealed alumina pan with a mass of about 10 mg.

3.4.2.2. TGA/DTG

To investigate the thermal stability of the starch and graft copolymer, thermogravimetric analysis (Perkin Elmer Diamond, USA) was performed at a heating rate of 10°C/min in the range of 25 to 600°C under a nitrogen atmosphere.

3.4.2.3. DMA (Dynamic mechanical)

Dynamic mechanical analysis (DMA) was performed with Dynamic Mechanic Analyzer (TA Instruments, Q800, USA). Powdered mixtures of polymer nanohybrid and Al₂O₃ (50:50 wt.%) were loaded into the DMA using powder holder. The holder was clamped directly into the Analyzer dual cantilever. DMA parameters were measured at a constant frequency of 1 Hz and a heat rate of 3°C.min⁻¹.

3.4.3. Morphological Characterization

3.4.3.1. SEM and SEM/EDX

The surface morphology of nanocomposites was examined using a brief description of the ZEISS SUPRA 40 Field Emission Scanning Electron Microscope (FESEM) with image scales: 2 μm, ×2000 and 10 μm, ×10.000 magnifications using an acceleration voltage 20 kV. All specimens were freeze-dried and coated with a thin layer of platin before testing by using a QUORUM-Q150R ES surface coating device. SEM/EDX elemental analysis technique (acceleration voltage 20 kV, takeoff angle 35° and elapsed live-time 10min) was used.

3.4.3.2. TEM and C-TEM

The internal morphology of nanocomposites was performed by FEI Tecnai G2 Spirit Biotwin Model High Contrast Transmission Electron Microscopy (CTEM) with Lantan Hexaboron Electron Gun at 120 kV. Powder polymer sample was suspended in ethanol solution with 0.1% concentration, then was sonicated up to the formation of homogeneously dispersed solution. Prepared solution (3–5 μ l) was dropped on the surface of carbon coated grid and dried up to the formation of full solid phase on grid surface before testing.

3.4.4. Mechanical Properties

3.4.4.1. Tensile Properties

Mechanical standard tests were done using an Instron machine Model 1026 modified by connection with a computer allowing for control of the apparatus and analysis of the results using an ASTM Method D 882-88. Initial grip separation was set at 50 mm and cross-head speed at 5 mm/min. The average ultimate tensile strength (δ , MPa) and elongation at break (ϵ , %) were calculated on the basis of 10 measurements for the same sample type.

3.4.5. Permeability Properties of Films

3.4.5.1. Gas (CO₂ and O₂) Permeability

CO₂ and O₂ Permeability were measured by using the VAC-VBS gas permeability tester (Labthink, China) in accordance with ASTM D1434 standard. The films were cut into discs (7.5 cm diameter) and mounted in a gas transmission cell to form a sealed barrier between two chambers. CO₂ and O₂ were introduced into the evacuated high-pressure chamber and permeates into the lower-pressure chamber and the permeation was indicated by an increase in pressure on the lower-pressure side of the films.

3.4.5.2. H₂O Vapor Permeability

Water vapor transmission rates (WVTRs) were measured using a Labthink Transmission Rate Tester (PERME® W3/030, China) in accordance with ASTM D1653. Before testing, the specimens were cut into discs (7.5 cm diameter) and conditioned for 2 weeks at 50%RH and 23°C. The air flow rate during the test was supplied by a compressor and set to 100 cm³/min. Measurements

were carried out at 25°C under 90%RH and finished after values of WVTR reached a steady state, usually after 6–8 h.

3.4.6. Biodegradation Properties

Biodegradation tests were carried out using the simple soil burial test to find the biodegradation of films. All samples were buried in the soil of natural environment without any enzyme activity or any man-made composting materials and located outside natural environment with an average temperature of around 5-15°C and 80% relative humidity. All sample were covered by soil under the land surface of 10 cm at different stages of biodegradation (every 5 days for 10 times) and after the testing period completed the samples took out and washed by distilled water. After removing of the soil and sand from the surface of the samples, the samples were dried in an oven (55°C) to reach a constant weight. The weight loss of the films were evaluated as a degradation rate and calculated by using the following equation:

$$\text{Weight Loss (\%)} = ((W_o - W_f) / W_o) \times 100 \quad (1)$$

Where W_o and W_f are sample weights before and after the test, respectively.

3.4.7. Microbiology Tests and Food Contact Properties

The microbiology test of St-g-PLA and St-g-PLA/organoclay nanocomposite films were evaluated by applying the horizontal method for the enumeration of microorganism according to the ISO 4833-1:2013 standard technique. This method is suitable for products intended for human consumption, food packaging, and handling. During the test, colony count of salmonella at 30°C under aerobic incubation by the pour plate technique were carried out to evaluate the antibacterial properties of films. All of microbiology tests were done in the Turkish Ministry of Food, Agriculture and Livestock packaging control laboratory.

The best way to determine possible consumer exposure for package/cover added to a food is to experimentally measure migration from food contact material and its concentration in a food during the storage under prescribed

conditions. Film was tested to determine the amount of migration that occurs into food-simulating liquids (especially for meat and cheese) and the characteristics of the migration. Migration characteristics of film contents were examined according to BRITISH EN 1186/1-15 method. Before testing, the films were cut with 100 dm² area and using different simulants (10% ethyl alcohol, 50% ethyl alcohol, 95% ethyl alcohol, and iso-octane) performed at 5°C for 10 days.

3.4.8. Agricultural Application of Films

Two types of films (St-g-PLA and St-g-PLA/organoclay nanocomposite films) and a standard film (Novamont Mulch Film, Italy) were used to mulch potato and pepper seed in the southwest region of Turkey (Köyceğiz, Muğla). The seeds were sown in the middle of November, 2014. To compare the agricultural effect of the as prepared films, standard mulch film, and no film mulch were carried out as a control group, respectively.

4. RESULTS AND DISCUSSION

4.1. Characterization of Poly(MA-*alt*-1-octadecene)-*g*-Poly L-lactic acid Layered Silicate Nanocomposites

4.1.1. FT-IR Spectroscopy

FT-IR spectroscopy was used to detect various functional groups and understand the chemical structure of nanocomposites. FT-IR spectra of graft copolymer and its nanocomposites, as well as detected absorption bands and their assignments were illustrated in figure 4.1. The observed absorption bands at 1850 (m), 1778 (s), 1709 (vs) (Figure 4.1-a) and 1640 (m) cm^{-1} (amide band) are associated with C=O groups from anhydride, maleate and maleamide (Figure 4.1-a) units.

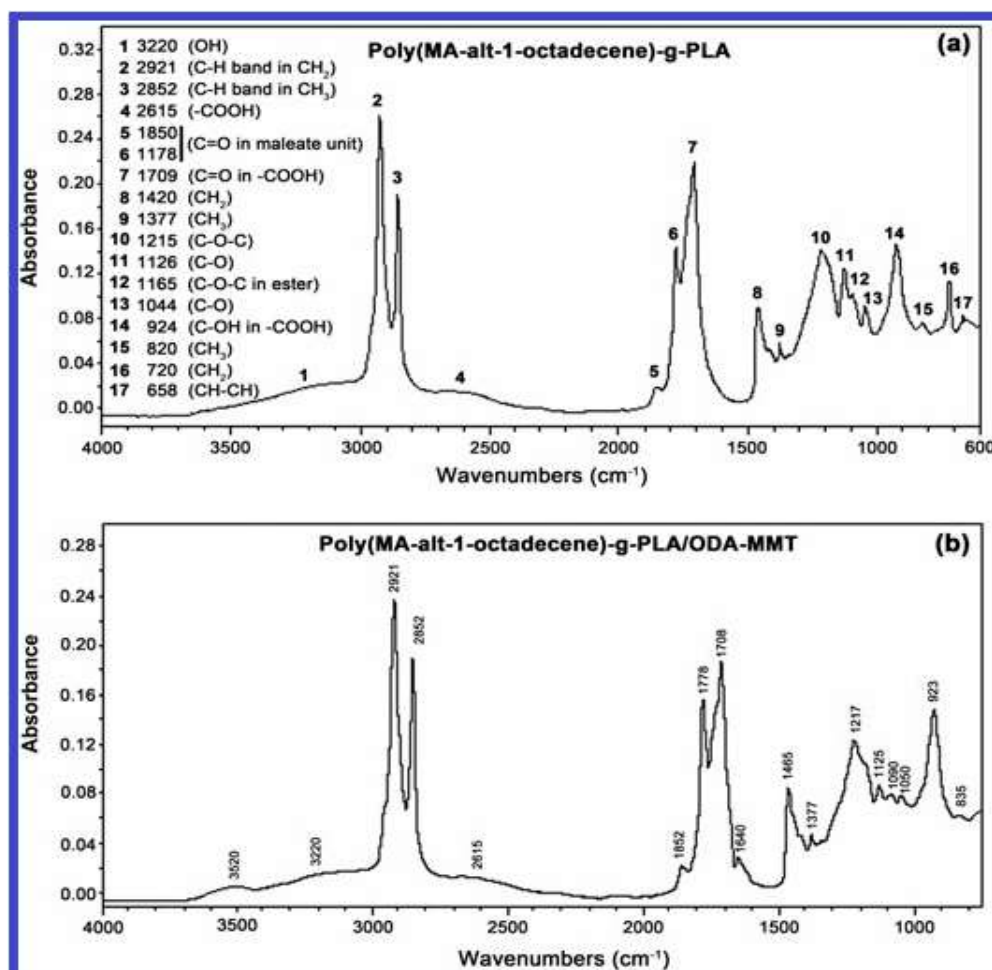


Figure. 4. 1. FTIR spectra of (a) pristine graft copolymer and its (b) nanocomposite.

The peaks at 3220 (broad), 2615 (broad) and 924 (s) cm^{-1} are related to OH groups in $-\text{COOH}$ and $-\text{C}-\text{OH}$. The bands for the CH_3 and ester groups at 2852 (s), 1377 (m) and 1165 (m) cm^{-1} , respectively, are related to the grafted PLA units. The new appeared peaks at 1090 and 1050 cm^{-1} are associated with Si–O and Si–O–Si stretching vibrations and the new broad peak at 3520 cm^{-1} is related to Si–OH stretching vibrations in nanocomposites (Figure 4.1-b). Absorption bands at 1496 and 1640 cm^{-1} are a consequence of the interfacial complexed octadecyl amine cationic surfactant–intercalant with free carboxylic groups and its chemical reaction (amidization) with anhydride unit in situ processing.

4.1.2. $^1\text{H-NMR}$ Analysis

Chemical structures of graft copolymer and its nanocomposites were also confirmed by $^1\text{H-NMR}$ analysis (Figure 4.2). Appearance of pristine graft copolymer and all nanocomposites characteristic peaks at 0.82 ppm (protons of CH_3 group from branched PLA) in the spectra indicates the occurrence of graft copolymerization in these systems.

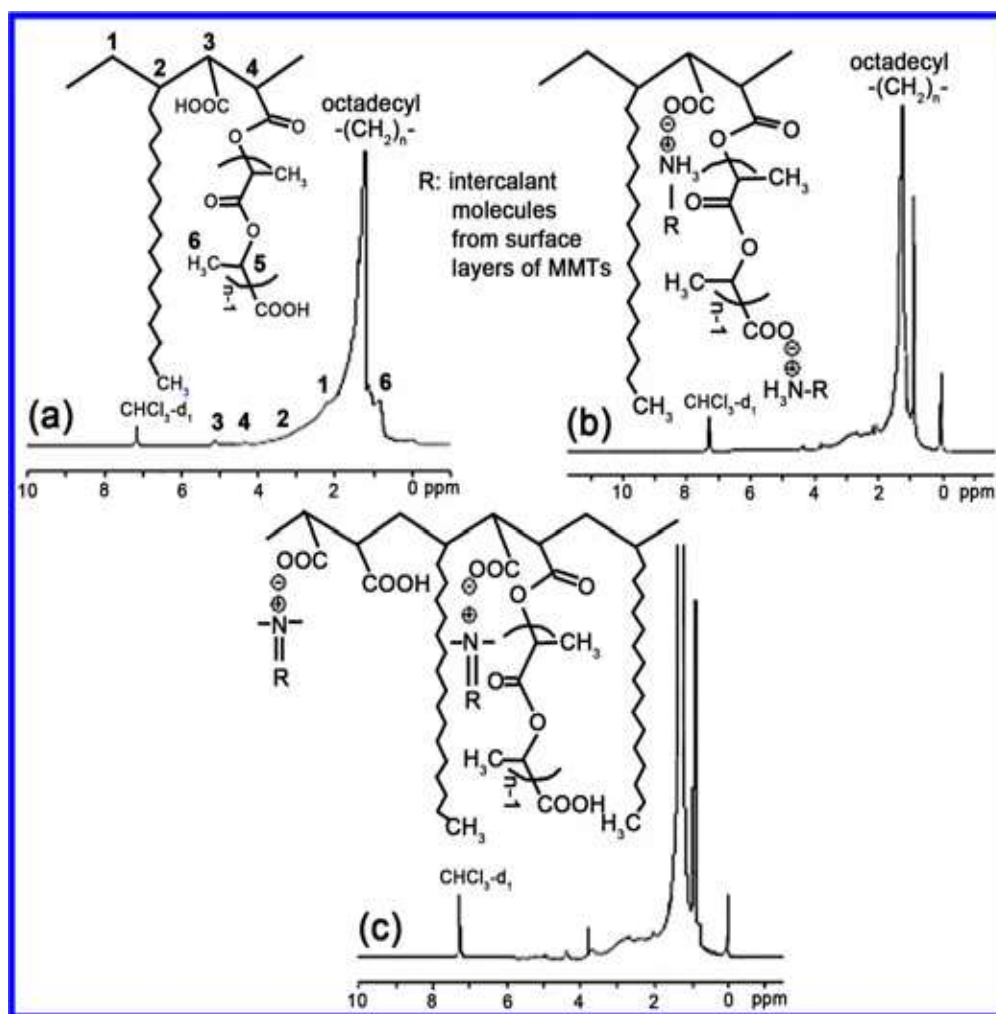


Figure. 4. 2. ^1H NMR spectra of (a) pristine poly(MA-*alt*-1-octadecene)-*g*-PLA, (b) copolymer-*g*-PLA/ODA-MMT and (c) copolymer-*g*-PLA/DMDA-MMT nanocomposites in $\text{CHCl}_3\text{-}d_1$ solution.

Intensity of this proton signal increases significantly with formation of nanostructures and indicates an increase in the number of branched fragments, and therefore, increase in the molecular weights of grafted PLA in nanocomposites as compared with those for pristine graft copolymer. Relatively higher intensity of peaks for LA units was observed in copolymer-*g*-PLA/DMDAMMT nanocomposite (Figure 4.2-c). This fact can be explained by co-catalytic effect of ammonium cations from intercalant on graft copolymerization.

4.1.3. MALDI-TOF-MS Analysis

The formation of graft copolymer is also confirmed with obtained values of molecular mass for the pristine copolymer (molecular mass=12.740 m/z) and

copolymer-*g*-PLA (molecular mass=21.900 m/z) using MALDI-TOF-MS m/z spectrometry method. These results were illustrated in Figure 4.3. Comparative analysis of these results showed the formation of graft copolymer with relatively higher molecular mass than those for pristine copolymer. Observed difference between molecular mass of graft copolymer and pristine copolymer (9.160 m/z) can be taking to molecular mass of branched PLA oligomer chain in the repeated units of graft copolymer.

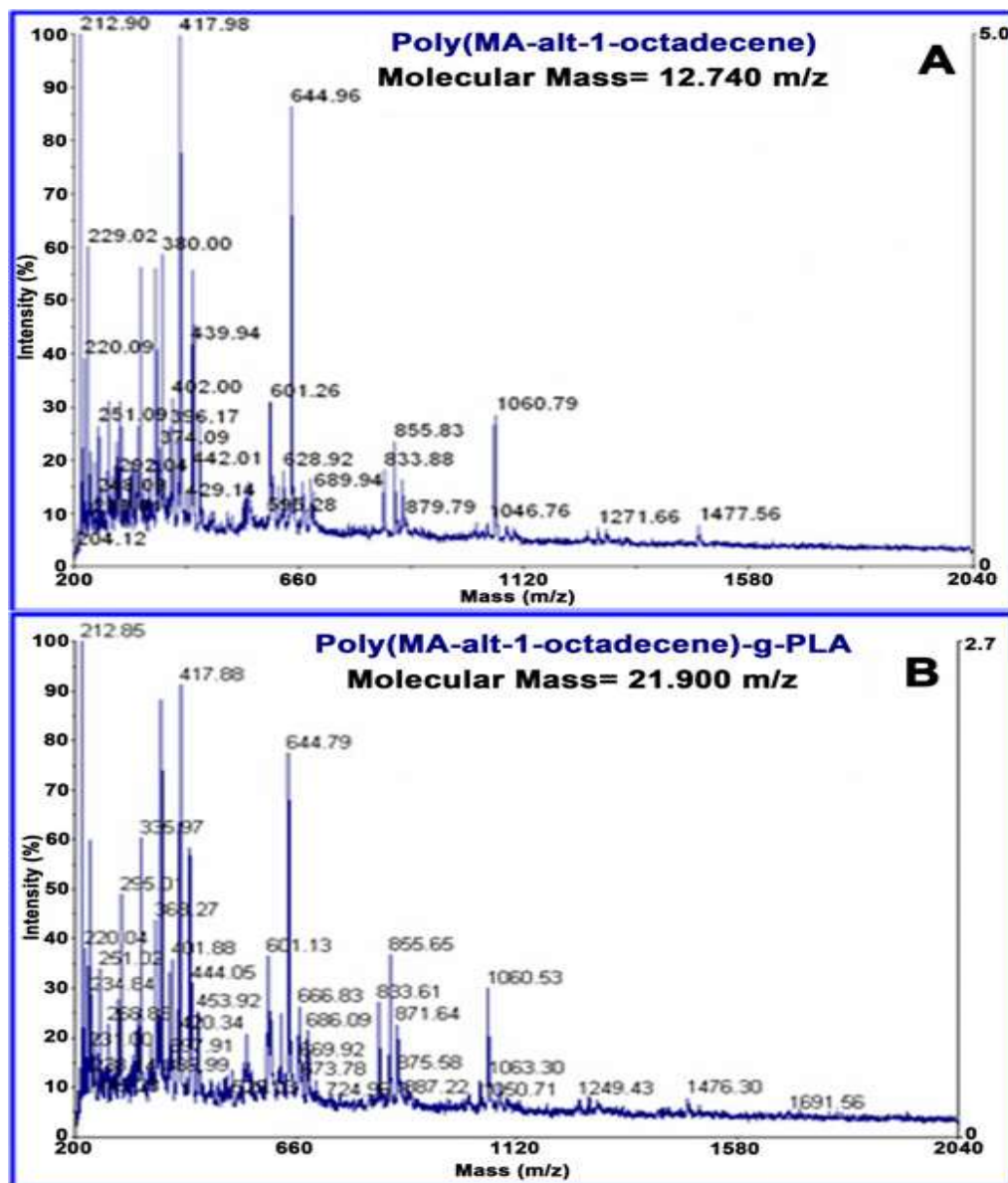


Figure. 4. 3. MALDI-TOF-MS spectra of (A) pristine copolymer and (B) copolymer-*g*-PLA in THF solution using α -cyano-4-hydroxycinnamic acid (CHCA) as a matrix and NaTFA as a cationizing agent for ionization of the samples.

4.1.4. X-ray Diffraction

Physical structure of nanocomposites was evaluated by X-ray diffraction (XRD) method. It is well known that XRD analysis of the polymer/organoclay nanosystems provides access to the interlayer stacking distance between clay plates and, therefore, to quantitatively determine the intercalating/exfoliating degree, crystallinity and ratio of amorphous and crystalline areas in the nanocomposites patterns. The results of our previous investigation [138, 140] showed that XRD patterns corresponding to organoclays indicate that surface modification not only changes surface property but also expands the interlayer d-spacing as a distance between clay platelets. Pristine graft copolymer shows predominantly amorphous structure with weak crystalline peaks at 2θ around $19\text{--}26^\circ$ due to branched PLA fragment (Figure 4.4-a).

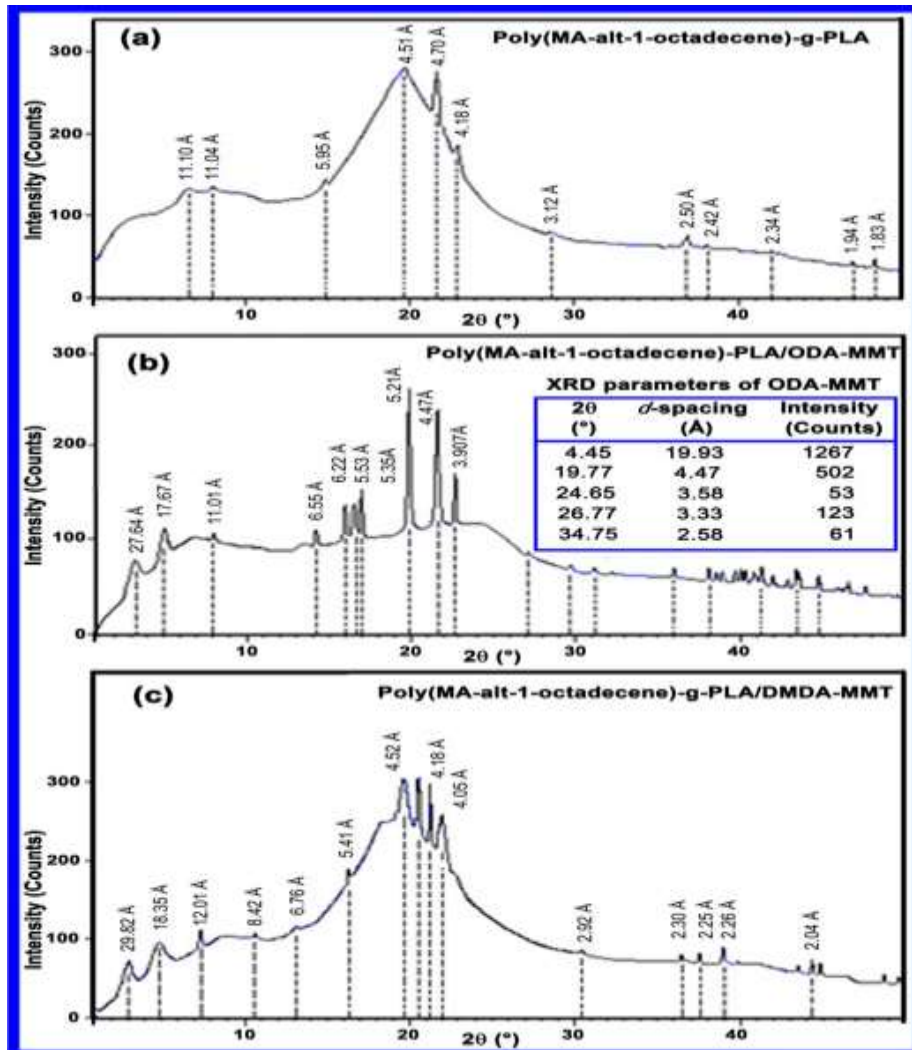


Figure 4. 4. XRD patterns of (a) pristine graft copolymer, (b) copolymer-g-PLA/ODA-MMT, (c) copolymer-g-PLA/DMDA-MMT nanocomposites.

It is well known that PLA with high molecular weight predominantly exhibits amorphous structure while PLA with lower molecular weight (oligomer) shows crystalline structure. This observation is agreed with obtained above mentioned values of MW values for graft copolymer. While graft copolymer/organoclay nanocomposites with low ODA-MMT loadings (3.2 wt.%) (Figure 4.4-b) exhibit semi-crystalline structure with diffraction peaks from layered silicate and PLA branched units. The nanocomposites incorporated with ODA-MMT and DMDA-MMT clays (Figs. 5b and 5c) show a weak diffraction peak due to layered silicate fragments. XRD patterns of pristine ODA-MMT (table in Figure 4.4-b) contain characteristic diffraction peak at 4.45° 2θ with $d(002)$ -spacing 19.93 Å and intensity 1267 count. Diffraction parameters of this peak are significantly changed when ODA-MMT clay was incorporated with graft copolymer; shift of peak from 4.45° to 3.43° 2θ and increase of $d(002)$ -spacing from 19.93 to 27.64 Å were observed. This fact allows us to suggest that graft copolymer/ODA-MMT composite predominantly exhibits intercalated nanostructure. Similar changes were observed for graft copolymer/DMDA-MMT clay composite. In situ processing changes the d -spacing parameters of 2:1 layered platelets $d(002)$ significantly, and from that of layers containing surface $\equiv\text{Si-OH}$ groups ($d(003)$), which are able to participate in the chemical and physical interfacial interactions with anhydride and carboxyl groups of graft copolymer. Comparative analysis of the XRD patterns of two nanocomposites incorporated with different organoclays indicates the relatively high crystallinity of nanocomposite prepared with reactive ODA-MMT than those for non-reactive DMDA-MMT-based nanocomposites. This observation can be explained by a chemical character of in situ interfacial interactions. Appearance of new peaks (around $16\text{--}17^\circ 2\theta$) in XRD spectra (Figure 4.4-b) can be related to hydrogen bonded amide crystalline fragments as a result of in situ amidization of anhydride units of graft copolymer with octadecyl amine intercalant of organoclay.

4.1.5. SEM Surface Morphology

The surface morphologies of the copolymer-*g*-PLA and its silicate layered nanocomposites using two types of MMT clays modified with alkyl ammonium

captions (octadecyl amine and dimethyldidodecyl ammonium) were investigated by Scanning Electron Microscopy (SEM) analysis method. Agreeing with obtained results, SEM images of powder copolymer-*g*-PLA showed a porous surface morphology as illustrated in Figure 4.5 (A, B and C).

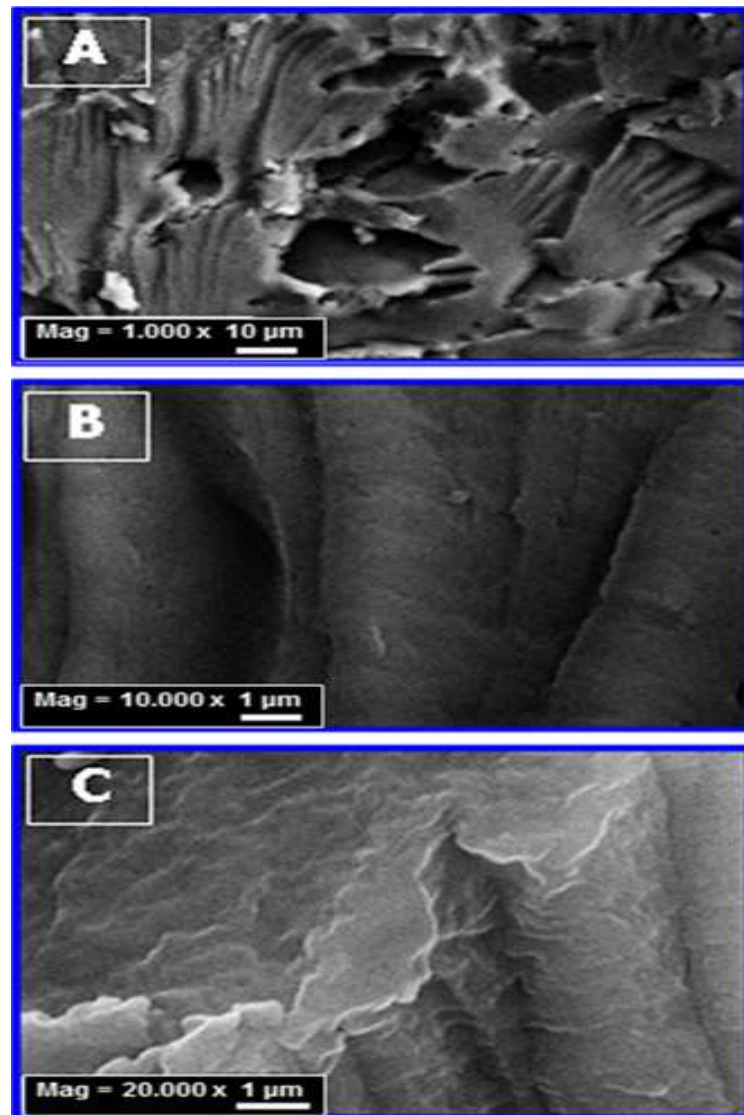


Figure. 4. 5. SEM images (A, B and C) pristine poly(MA-*alt*-1-octadecene)-*g*-PLA.

While powder copolymer-*g*-PLA/ODA-MMT (reactive organoclay) nanocomposite predominantly exhibits dual-porosity structure (micro and nanoporous) and some compact shell (Figure 4.5-A, B and C). Nanocomposite incorporated with non-reactive DMDA-MMT organoclay exhibits layered

morphology structures (Figure 4.6). It can be proposed that the multi-porous surface structures are formed due to the diffusion of the absorbed water by clay and eliminated water molecules as a result of graft copolymerization reaction (nano-porous surface) and remaining LA monomer (micro-porous surface) as fast transport paths in the formation of finely distributed nanoporous structures. These nanoporous formations may as well as continue during future thermal treatment under vacuum drying. It can be proposed that the two long dodecyl groups of intercalant of DMDA-MMT are preferred to avoid high steric hinderances between the neighboring side-chain octadecyl groups of alternating graft copolymer. On the other hand, organoclay ammonium cations may play the role of a co-catalyst in graft copolymerization to provide the controlled elimination of water molecules from the system, followed by the formation of a nanoporous surface morphology.

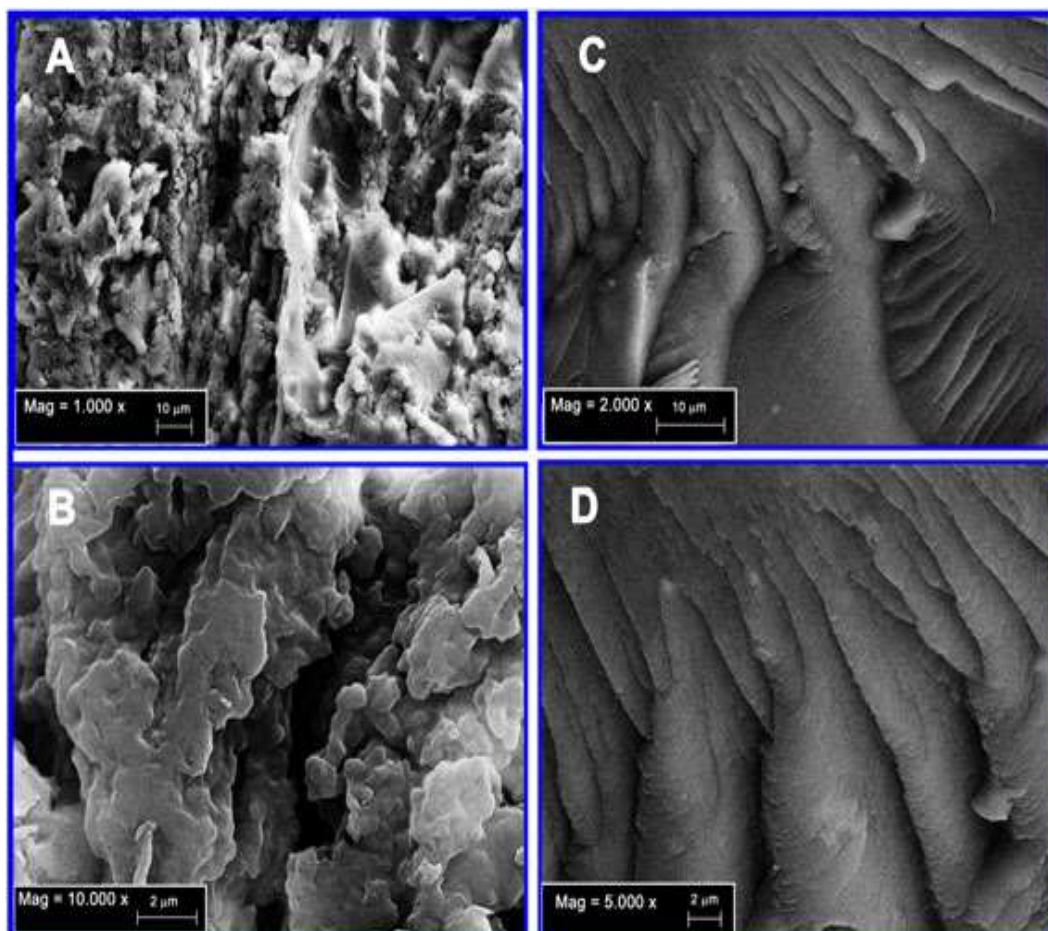


Figure. 4. 6. SEM images (A, B and C) copolymer-*g*-PLA/ODA-MMT and (D) copolymer-*g*-PLA/DMDA-MMT nanocomposites. Effect of organoclay origin (intercalant).

The results of comparative analysis indicated that the origin of loading organoclay and structural factors dramatically influenced the surface morphology of nanocomposites due to different types and degrees of in situ physical and chemical interfacial interactions during the formation of nanocomposites. As evidenced from these results, organic intercalants which more affectively participate in situ graft copolymerization via chemical (ODA-MMT) and physical (DMDA-MMT) interfacial interactions and their chosen volume fraction exhibit high compatibilizing effect in the formation of homogeneous polymer–clay blends with thermodynamically stable surface morphologies.

4.1.6. TEM Internal Morphology

It is well known that Transmission Electron Microscopy (TEM) is used to access to the size distribution of the platelets diameter and thickness particles in polymer/organoclay nanosystems, and to evaluate the nanostructures, predominantly in the form of core-shell morphology in polymer/silica nanocomposites. Moreover, TEM method allows a qualitative understanding of the internal structure, spatial distribution of the various phases and direct visualization of defect structure in the nanocomposites. The self-assembly of functional block and random copolymers with hydrophobic and hydrophilic units to enable micro phase separation has been intensively investigated due to their ability to form nanostructures like micelles, vesicles and capsules [144-148]. However, the association of alternating copolymers/organoclay nanosystems, especially the formation of self-assembled core–shell morphology in similar systems, has scarcely been studied. Type and content of the used clays, structure of matrix polymer and reaction medium significantly influence the morphological properties of nanocomposites. To evaluate core-shell morphology by TEM, we used coatings prepared from 0.1% dispersed ethanol solution of powder samples. TEM images illustrated in Figure 4.7, 4.8 and 4.9 confirm that the copolymer-*g*-PLA/organoclay nanocomposites tend to form encapsulated organoclay with graft copolymer matrix, dispersed core–shell micro- and nanoparticles and partially agglomerated core-shell structures.

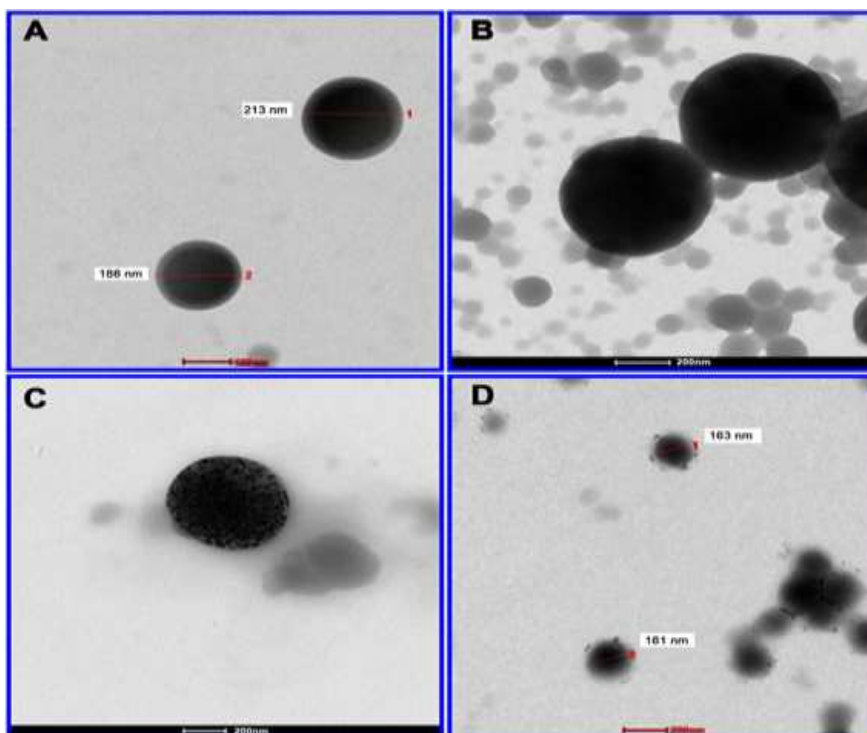


Figure. 4. 7. TEM images of core–shell morphology of individual particles: (A) and (B) copolymer-*g*-PLA/ODA-MMT, (C) copolymer-*g*-PLA/DMDA-MMT and (D) pristine poly(MA-*alt*-1-octadecene) copolymer. Scale: (A) 100 nm, (B), (C) and (D) 200 nm.

Therefore, we have demonstrated that the poly(MA-*alt*-1-octadecene)-*g*-PLA (Figure 4.7) and its layered silicate nanocomposites (Figure 4.8 and 4.9) similar to well-known polymer/SiO₂ nanosystems exhibit self-assembly behaviors due to their surfactant properties and structural peculiarity, especially tendency to form hydrophobic/hydrophilic balance in situ processing. Some individual particles from copolymer-*g*-PLA/organoclay systems (Figure 4.7-C) showed nanoporous structure with pore size around 15–20 nm, the formation of which can be explained by the elimination of water molecules from inner layers in the particle formation and thermal treatment under vacuum via drying processing. TEM images of the poly(MA-*alt*-1-octadecene)-*g*-PLA/organo-MMT clay nanocomposites showed that the clay crystals clustered together regularly to form spherical particles covered with matrix graft copolymer in the form of core–shell morphology. This phenomenon can be explained by the formation of better hydrophilic/hydrophobic balance in the used reactive copolymer-*g*-PLA/organoclay mixture and, therefore, the occurrence of self-organized in situ

chemical and physical interfacial interactions under selected interlamellar graft copolymerization conditions. Origin of used organoclays significantly influenced the internal morphology of copolymer-*g*-PLA/ODA-MMT (Figure 4.7) and copolymer-*g*-PLA/DMDA-MMT (Figure 4.8) nanocomposites.

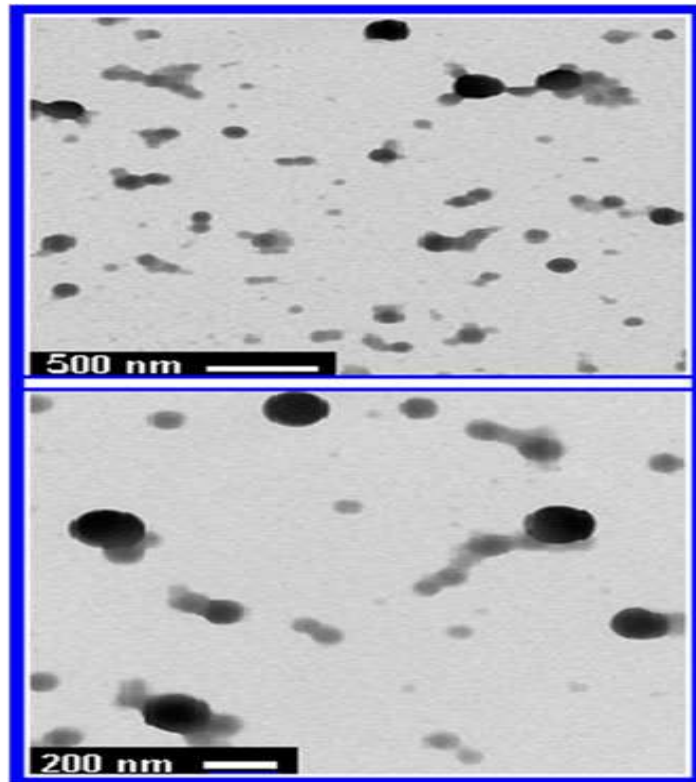


Figure. 4. 8. TEM images of copolymer-*g*-PLA/ODA-MMT nanocomposite.

Agreeing with TEM images, the strong chemical interfacial interactions between the copolymer-*g*-PLA and the reactive ODA-MMT clay provide the occurrence of the effective in situ intercalation/exfoliation processing, which lead to the formation of the finely dispersed polymer and organoclay phases with higher self-organized core-shell morphology. However, physical in situ interactions of graft copolymer with DMDA-MMT, being a non-reactive nanofiller, lead to a partially agglomerated antisymmetric core-shell structure. Better self-assembled morphology structure with nano-scale particle size around 25–100 nm, as well as some microparticles (300–400 nm), as a result of water absorption-swelling processes, were observed in the first nanosystem (Figure 4.8). Partially agglomerated spherical core-shell structures of particles were also formed in the second nanosystem (Figure 4.9).

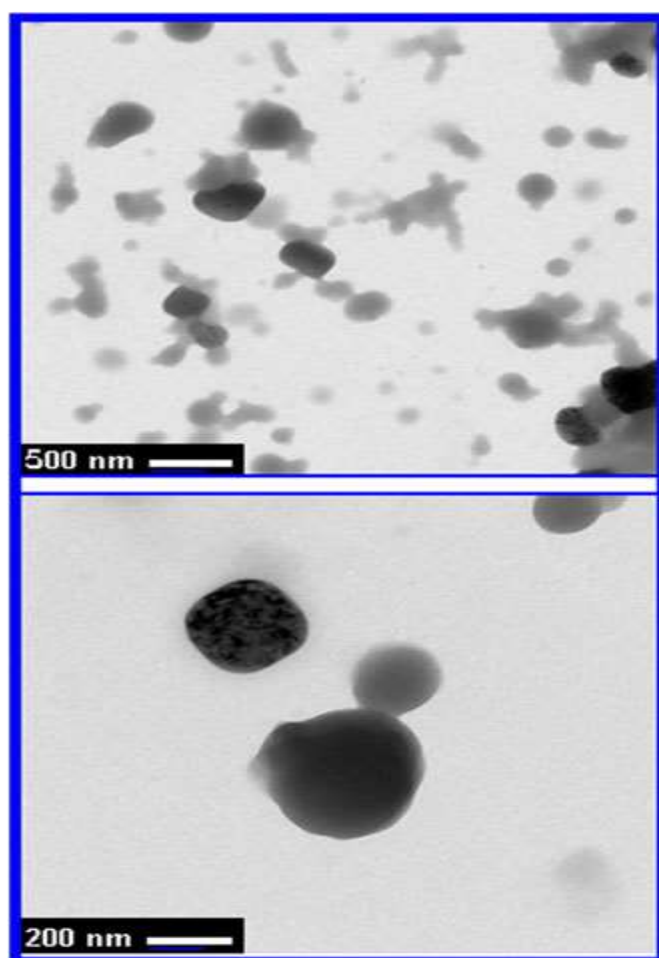


Figure. 4. 9. TEM images of copolymer-*g*-PLA/DMDA-MMT clay nanocomposite.

This considerable change observed in the morphology of these nanosystems can be explained by various characteristics of interfacial interactions such as chemical (first nanosystem) and physical (second nanosystem) in situ processing. Taking into consideration the chemical and physical in situ processing and hydrophilic/hydrophobic balance in the formation of nanocomposites, nanostructural model of the self-assembled micro- and nanoparticles with core-shell morphology can be schematically represented as follows (Figure 4.10): According to this structural model, the organoclay nanoparticles are easily wrapped in a copolymer-*g*-PLA shell due to favourable hydrophobic/hydrophilic interactions between graft copolymer and surfactant–intercalant that inorganic fragment of organoclay mineral forms the

nanocrystals containing core. This model is reasonably verified by the obtained results of FT-IR, XRD and TEM analyses, and can be utilized for the other encapsulated inorganic nanoparticles (Au, Ag, SiO₂, TiO₄, magnetic Fe₂O₃, etc.).

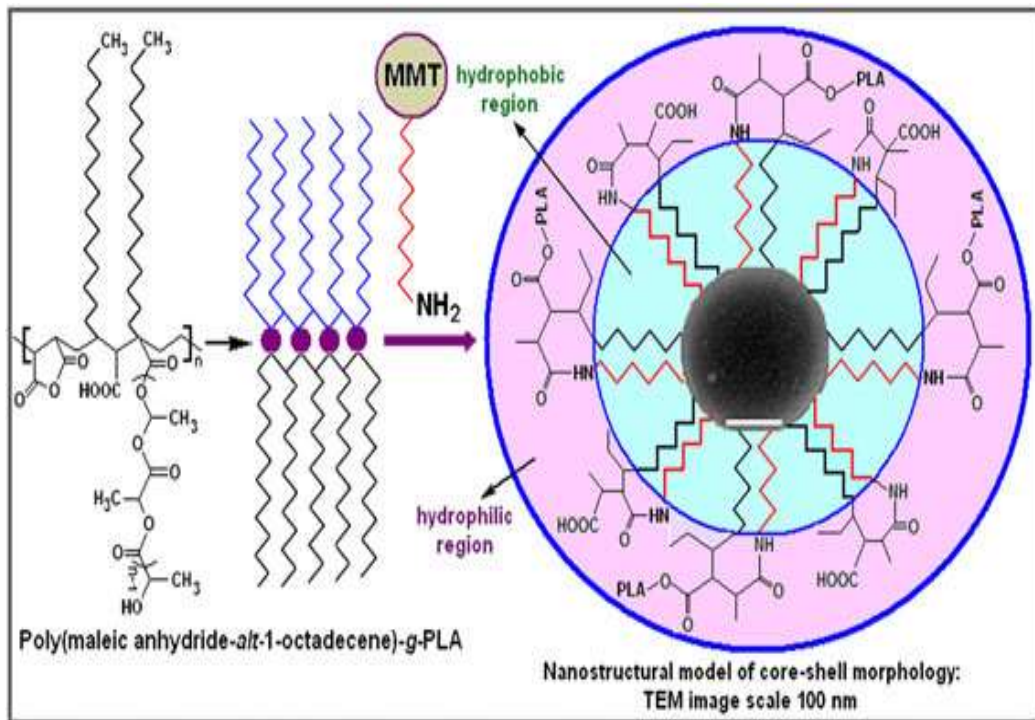


Figure. 4. 10. Nanostructural model of (micro) nanoparticles with core-shell morphology.

4.1.7. ζ -size and ζ -potential Parameters of (Micro) Nanoparticles

The obtained average values of ζ -size and ζ -potential of particles for nanocomposites and their individual components were determined in 1.0% chloroform solutions. The obtained particle parameters were summarized in Table 4.1. Relatively lower zeta potential (36.5 mV) obtained for non-reactive DMDA/MMT can be explained by steric hardness of two long dodecyl groups for self-assembly in the solution used. While this parameter significantly increased up to 94.2 mV after incorporation of this organoclay with copolymer-g-PLA due to formation of nano-size particles (0.09 μm) as a result of better self-assembly via in situ interaction of a quaternary ammonium cations with carbonyl/ carboxyl groups of monomer and graft copolymer during interlamellar

copolymerization. Observed lower zeta sizes and relatively higher zeta potential (76.5 mV) of pristine copolymer can be explained by surfactant structure of copolymer macromolecules in solution and their excellent hydrophobic/hydrophilic balance. Average particle sizes of two nanocomposites prepared with reactive and non-reactive organoclays were found to be 0.61 and 0.092 μm ($\Delta\zeta=150$ nm), respectively. The difference observed can be explained by the formation of partially agglomerated nanoparticles through in situ chemical (amidization) reactions in the first nanosystem and in situ physical interaction (H-bonding) in the second nanosystem. Similar difference ($\Delta\zeta=29.2$ mV) was observed in ζ -potential values of these systems. Thus, lower ζ -sizes (nano-level) and higher ζ -potential (>70 mV) values of particles increased the tendency towards the self-assembly of the macromolecular structures.

Table. 4. 1. Nanoparticle structure–composition– ζ -size/ ζ -potential relationships.

NCs and their individual components	ζ-size (μm)	ζ-potential (mV)
Poly(MA-<i>alt</i>-1-octadecene)	0.63	76.5
Copolymer-<i>g</i>-PLA	0.83	55.5
Copolymer-<i>g</i>-PLA/ODA-MMT	0.61	38.3
Copolymer-<i>g</i>-PLA/DMDA-MMT	0.09	71.7
ODA-MMT reactive organoclay	1.48	94.2
DMDA-MMT non-reactive organoclay	0.37	36.5

4.1.8. Thermal Behaviors (DSC and TGA/DTG)

In our group previous publications [95, 96, 139], we demonstrated that fully exfoliated nanostructures of the functional copolymer/organoclay nanocomposites exhibit low thermal stability compared to nanocomposites containing mixing intercalated/agglomerated and exfoliated nanostructures. Better thermal stability is observed in nanosystem consisting approximately 20 and 80% of intercalated and exfoliated structures, respectively [139].

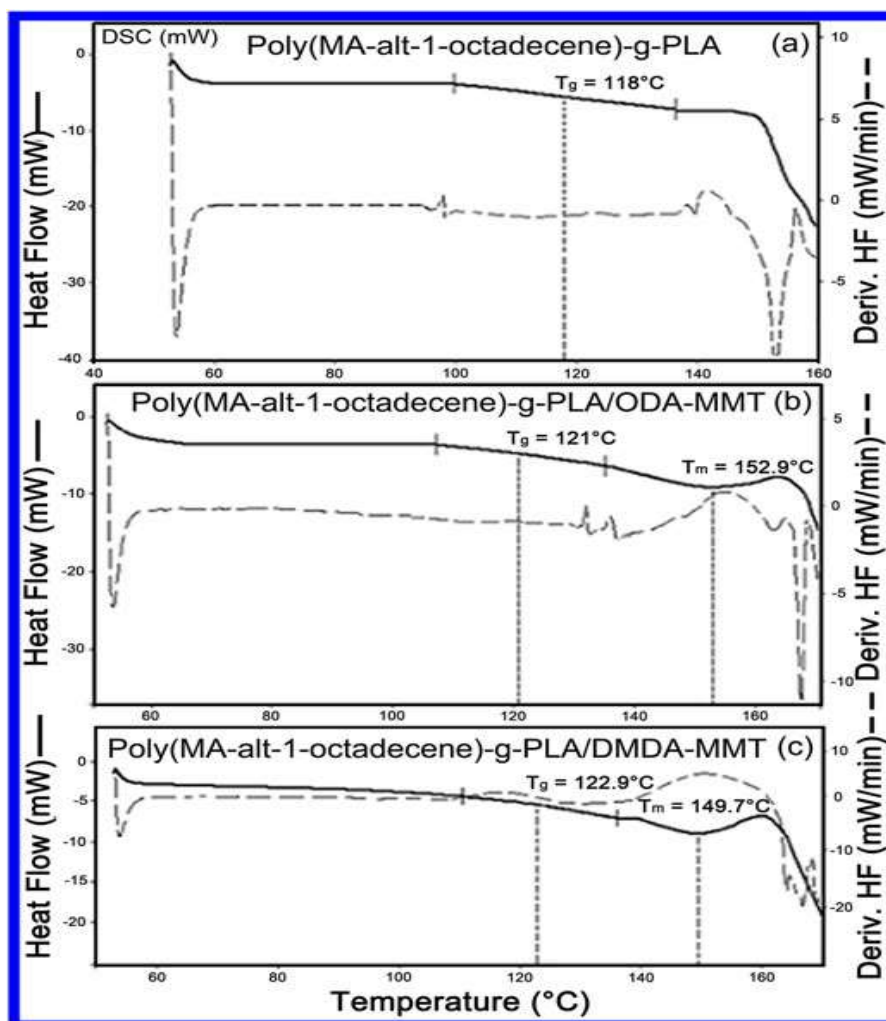


Figure. 4. 11. DSC traces of (a) copolymer-g-PLA and its nanocomposites incorporated with (b) ODA-MMT and (c) DMDA-MMT clays. Heating rate is 10°C/min under a nitrogen atmosphere.

The effect of incorporated organoclays on the thermal behaviors of nanocomposites were obtained from the comparative analysis of pristine graft copolymer and their nanocomposites using differential scanning calorimetry (DSC) and thermogravimetric-differential thermogravimetric (TGA-DTG) methods. The comparative analysis of DSC traces (Figure 4.11) indicated that pristine graft copolymer exhibits only glass-transition (T_g) at 117.6°C while nanocomposites show both T_g at 122.3, 116.7 and 122.8°C and melt-transition (T_m) endo-peaks at 158.4, 148.3 and 149.5°C, respectively. Therefore, obtained thermal parameters indicated that pristine graft copolymer exhibits amorphous structure (Figure 4.11-a) while nanocomposites (Figure 4.11-b and 4.11-c) show semi-crystalline structures. Incorporation of organoclays

increases the T_g values. Observed higher values of T_m for the nanosystems can be explained by a possible acceleration of crystallization process of the matrix copolymer with silicate layers of organoclay which plays the role of a nucleic agent. The thermal degradation parameters of copolymer-g-PLA and its layered silicate nanocomposites were evaluated by TGA-DTG analysis (Figure 4.12). Agreeing with these results, graft copolymer shows two-step degradation (Figure 4.12-A) where first step is associated with decarboxylation of matrix copolymer with 8.7% weight loss and second step is related to main chain degradation process. The nanocomposite containing 3.2 wt.% ODA-MMT degrades through one-step chain degradation mechanism (Figure 4.12-B) without decarboxylation at early stage.

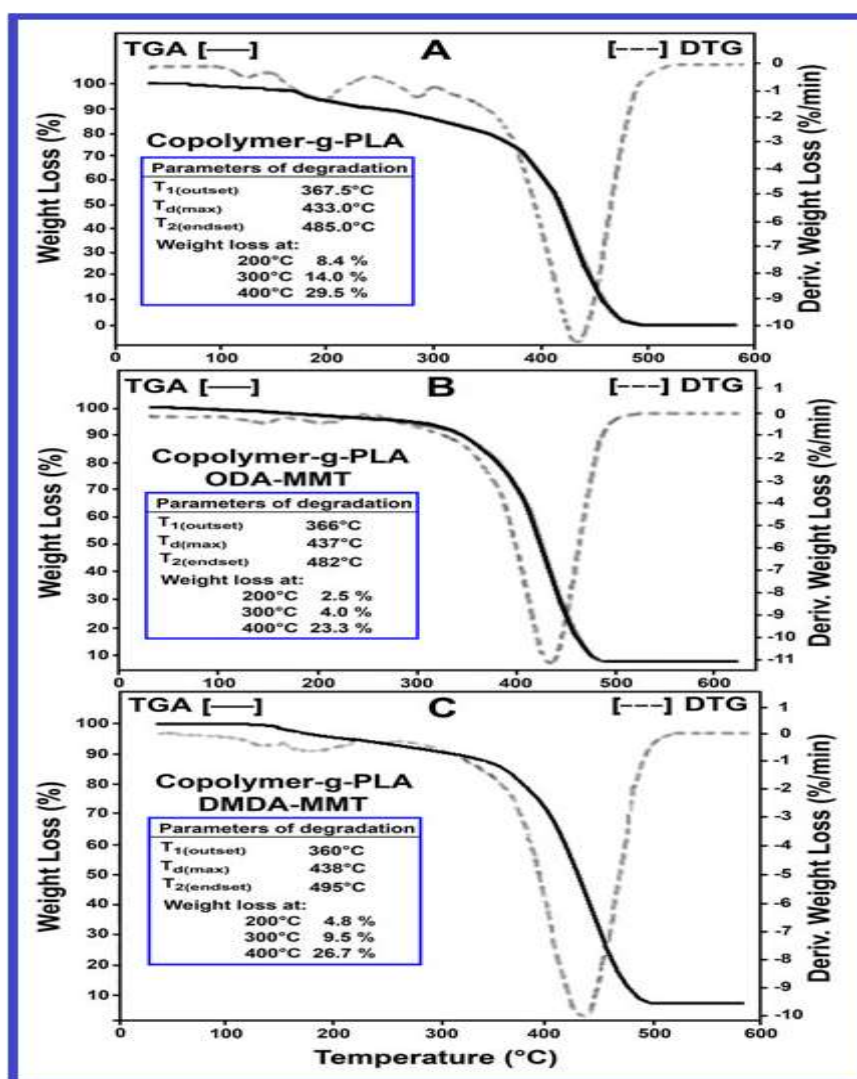


Figure. 4. 12. TGA-DTG curves of (A) pristine graft copolymer and its (B) ODA-MMT and (C) DMDA/MMT incorporated nanocomposites. Heating rate is 10°C/min under a nitrogen atmosphere

Thus, observed better thermal degradation parameters such as $T_{1(\text{outset})}$, $T_{d(\text{max})}$, $T_{2(\text{endset})}$ and weight loss at different temperatures (Table in Figure 4.12-B) for the obtained copolymer-*g*-PLA/ODA-MMT nanosystem can be explained by the occurrence of in situ interfacial amidization of anhydride unit with octadecyl amine before decarboxylated degradation of anhydride/carboxyl groups.

However, graft copolymer (Figure 4.12-A) and copolymer-*g*-PLA/DMDA-MMT (non-reactive organoclay) nanosystem (Figure 4.12-C) easily undergo to visible degradation via decarboxylation in the isothermal conditions via two-step chain degradation mechanism. We propose that intercalated and partially agglomerated structures may be improved with regard to thermal stability and barrier properties of nanocomposites due to their ability to prevent heat flow transport, emission of oxygen and other degraded volatile products.

4.1.9. Dynamic Mechanical Properties

DMA analysis method allows to determine a combination of important thermal, mechanical and rheological properties of polymer materials, as well as to evaluate the effects of in situ interfacial interactions and adhesion strength between matrix polymer chains and nanofillers on the formation of particle nanostructures and their dispersion processes. In this study, we used DMA technique to detect response of nanocomposites to oscillatory deformation as a function of α -relaxation temperature. Dynamic force (DF) and complex modulus (CM) were illustrated as functions of temperature in Figure 4.13.

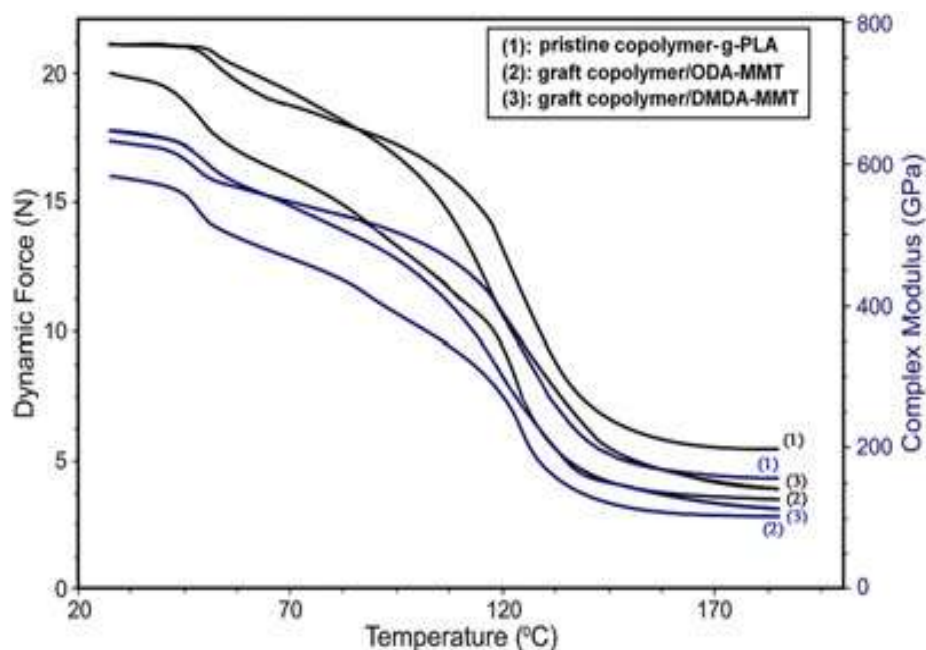


Figure. 4. 13. DMA spectra of (1) pristine copolymer-*g*-PLA, (2) copolymer-*g*-PLA/ODA-MMT and (3) copolymer-*g*-PLA/DMDA-MMT organoclays. Plots of dynamic force (black curves) and complex modulus (blue curves) versus α -relaxation temperature (T_α).

Significant difference (Δ) observed between these parameters [$\Delta = DF$ (nanocomposite) - DF (copolymer)] or [$\Delta = CM$ (nanocomposite) - CM (graft copolymer)] above T_g , relating to copolymer and its nanocomposite, can be described as a function of the formation of nano-structural architecture in poly(MA-*alt*-1-OD)-*g*-PLA/organoclay system. It can be proposed that Δ value also characterizes the interfacial adhesion strength depending on the flexibility and hydrophobic/hydrophilic balance of the functional graft copolymer chains and their ability to form amide fragments and complexes via in situ interfacial chemical and physical interactions, respectively. The maximum values of Δ were observed around 90–110°C for systems related to graft copolymer and its organoclay nanocomposites around 110–130°C at middle and lower values of DF and CM parameters, respectively.

4.2. Characterization of Poly(MA-*alt*-1-octadecene)-*g*-Poly L-lactic/Clay Nanohybrids and Catalyst Nanofillers

4.2.1. Self-Catalytic Effects of Clay Nanofillers

At first we observed that interlamellar graft copolymerisation of LA monomer onto alternating copolymer can occur in the presence of inorganic or organically modified MMT which execute the dual functions of: (1) a catalyst, for in situ graft copolymerisation and (2) a nanofiller, for the formation of the CPNs without utilizing the conventional catalysts such as hazardous tin(oct)₂. Synthesis pathways for the poly(MA-*alt*-1-octadecene)-*g*-PLA/organoclay nanocomposites represented as follows (Figure 4.14):

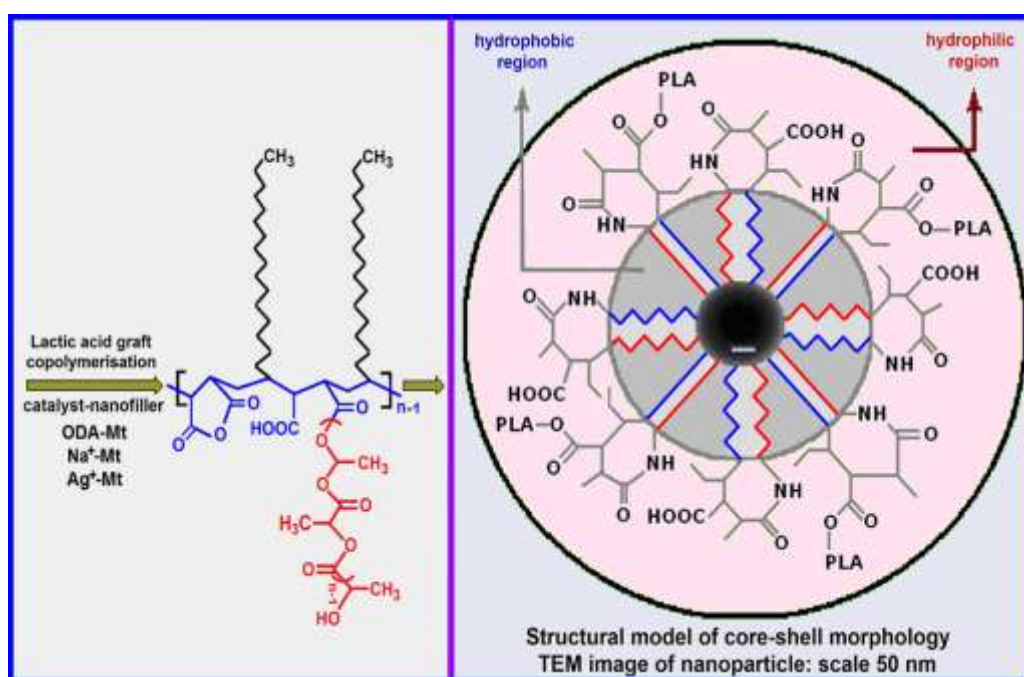


Figure. 4. 14. Schematic representation of synthetic pathways for copolymer-*g*-PLA intercalated silicate nano-composites in the presence of Na⁺-MMT, Ag⁺-MMT and ODA-MMT as catalysts of graft copolymerization of L-lactic acid onto poly(MA-*alt*-1-octadecene) and and nanofillers.

In this system, anhydride units of the copolymer play the role of a preventing agent, i.e., proceeds the first step grafting of LA monomer onto copolymer through monoesterification of anhydride unit (Figure 4.14). The catalytic effect provided by MMT...LA complexes containing activated positively charged groups. The activity of these catalysts strongly depends on the origin of used clay and correlated with the end reaction time as a function of fixed given

phase separation time for each catalyst system. Experimentally, we have found the following phase separation times (PST) for all tested MMT...LA catalysts with different clays: ODA-MMT 56 min, Na⁺-MMT 35min and Ag⁺-MMT 25min. These obtained results are also reasonably in agreement with zeta-size and zeta-potential parameters of the used inorganic and organic MMTs (Table 4.2).

Table. 4. 2. The ζ -size and ζ -potential of inorganic and organic MMT and their polymeric particles in CHCl₃ solution before and after sonication (p = 400 W, f = 40 KHz, t = 15 min)

Mineral clays and their organic derivatives (C = 0.01 g/mL)	Zeta-size (nm)		Zeta-potential (μ V)
	before	after	
Na ⁺ Mt (K-10, Aldrich)	2535	1133	73.3
Ag ⁺ Mt	983	577	103.0
L-Lactic acid-Mt	2410	777	9.6
ODA-Mt (Nanomer 1.30E)	1476	769	94.2
Copolymer-g-PLA/ODA-Mt	828	706	1.6
Copolymer-g-PLA/Na ⁺ Mt	645	604	38.2
Copolymer-g-PLA/Ag ⁺ Mt	588	557	45.2
Pristine Copolymer	628	109	76.5

Thus, the mechanism of self-catalysis in situ processing can be interpreted taking into consideration the origin of different clays employed the following factors: (a) lactic acid easily reacts with anhydride unit of the copolymer through monoesterification and forms intercalated complex with Na and Ag salts of MMT and/or organoclay (-COOH...NH₂-(CH₂)₁₇-CH₃-MMT) through cation exchange and complex formation interactions, respectively; (b) copolymer also easily intercalated between silicate galleries via formation of a complex and reacts with octadecyl amine intercalant with the formation of a maleamide side-chain fragment; (c) pre-intercalated complexes and used clays, having high values of ζ -potential (>70 mV), take the place of a catalyst for graft copolymerization of lactic acid onto mono-lactic ether of the copolymer in the

early stage of intercalation processing. It has been observed that intercalation/exfoliation of graft copolymer chains between silicate layers were accompanied by phase separation (formation of solid phase relating to higher molar mass of graft copolymers) after graft copolymerisation period up to 56 min. The phase separation time strongly depends on the origin of clays and their ζ -potential parameters and is significantly reduced (up to 25 min) by using Ag^+ -MMT as the catalyst-nanofiller which exhibits a relatively high ζ -potential (103 mV).

4.2.2. FT-IR Spectroscopy

The structures of graft copolymer and its silicate layered polymer nanocomposites were confirmed by FT-IR spectroscopy. The obtained results of the chemical structural analysis of pristine Ag^+ -MMT (Figure 4.15-a), copolymer-*g*-PLA/ Ag^+ -MMT (Figure 4.15-b), copolymer-*g*-PLA/ Na^+ -MMT (Figure 4.15-c) and copolymer-*g*-PLA/ODA-MMT (Figure 4.15-d) are illustrated in Figure 4.15. Ag^+ -MMT spectra shows the absorption band at 3619 cm^{-1} which is associated with OH group vibration of metal (Mg, Al and Fe) hydroxyl fragments in the octahedral sheet. The broad bands at 3386 cm^{-1} (H-O-H stretching) and 1627 cm^{-1} (H-O-H bending) confirm the presence of adsorbed water. The presence of a very strong band at 1022 and 520 cm^{-1} can be attributed to stretching and bending modes of Si-O-Si and O-Si-O (silica) groups, respectively. The conversional inorganic clays (Mt or bentonite) show similar absorption bands at 1031 and 524 cm^{-1} [149]. Observed visible shift of these bands, assigned to complex Si-O stretching vibration in the tetrahedral sheets, to relatively lower region can be explained by replacement of alkaline metals with Ag^+ cations. FTIR spectra of copolymer-*g*-PLA/clay nanocomposites, illustrated in Figure 4.15-b, c and d, contains the following characteristic absorption bands related to MA unit (for C=O at 1852 and 1770 cm^{-1} , for ester at 1755 cm^{-1} and for -COOH at 1710 cm^{-1}), branched octadecyl group (for CH_2 stretching at 2935 cm^{-1} and CH_2 bending at 1462 cm^{-1}), LA unit (for CH_3 stretching at 2860 cm^{-1} and CH_3 bending at 1372 cm^{-1}) and silicate layers (around 1200 - 908 and 550 - 595 , and 520 cm^{-1}). Absorption bands at 2860 cm^{-1} and 1372 cm^{-1} appearing in the spectra of all CPNs were associated with stretching C-H in CH_3 and bending vibration of CH_3 group from grafted

PLA units. Absorbance values of 1462 (bending CH₂ from octadecyl group of copolymer) and 1372 cm⁻¹ bands can be used for the determination of grafting degree of LA onto copolymer. As seen from spectral analysis (Figure 4.15), absorbance of CH₃ bands for the three samples of CPNs prepared with Ag⁺-MMT, ODA-MMT and Na⁺-MMT depends on the origin of clay and significantly decreases in range of 0.135, 0.112 and 0.096 (stretching), and 0.042, 0.021 and 0.012 (bending). Therefore, in situ graft copolymerization can easily occur in the presence of Ag⁺-MMT as compared with those for the ODA-MMT and Na⁺-MMT containing systems. The grafting degree (GD %) of PLA in the clay polymer nanocomposites was determined by a known method [150] using the values of absorption bending bands of CH₂ and CH₃ groups from copolymer and PLA and the following equation: $GD (\%) = [A(1372)/(A(1372)+A(1462))] \times 10^{-2}$. The calculated values of GD are 41.2, 31.8 and 24.0% for the Ag⁺-MMT, ODA-MMT and Na⁺-MMT containing polymer composites, respectively. Additionally, the rate of phase separation and therefore grafting process were significantly accelerated with Ag⁺-MMT and ODA-MMT as effective catalysts for interlamellar graft copolymerization.

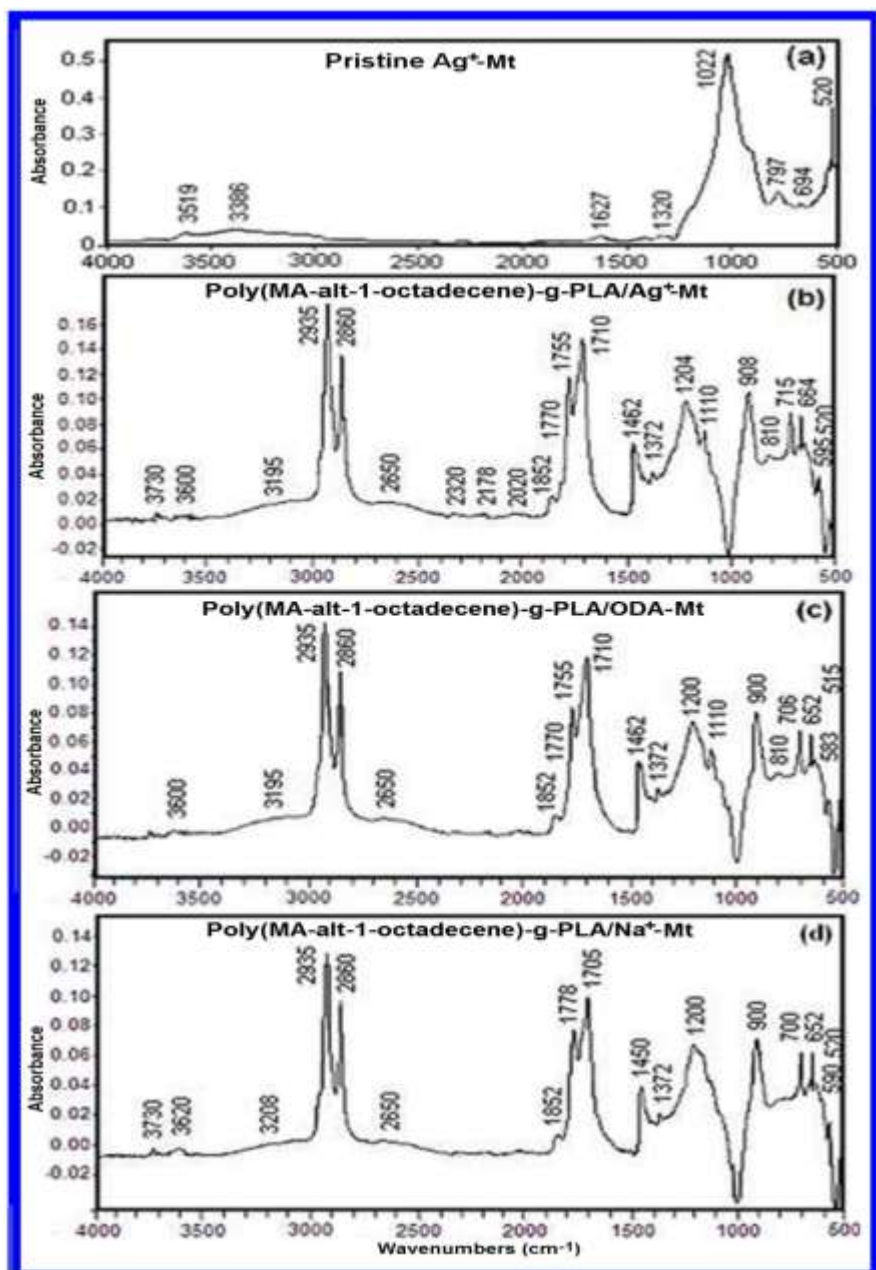


Figure. 4. 15. FT-IR spectra (KBr pellet) of (a) Ag⁺-MMT and nano-composites containing copolymer-g-PLA matrix polymer incorporated with (b) Ag⁺-MMT, (c) Na⁺-MMT and (d) ODA-MMT.

4.2.3. UV/VIS Spectrophotometer and Elemental (SEM/EDX) Analysis

The chemical structure and composition (elemental analysis) of Ag⁺-MMT nanoparticles were also confirmed by UV and SEM/EDX analysis methods (Figure 4.16). It is known that the silver nanoparticles have characteristic optical absorption peak at 420 nm in the UV-VIS region related to the surface plasmon resonance [151]. The UV-spectrum of a water solution of Ag⁺-MMT

(Figure 4.16-A) also indicates the presence of an optical absorption peak at 411.4 nm which can be attributed to the intercalated and in situ generated silver nanoparticles in Ag⁺-MMT clay mineral layer structure. Furthermore, the thermal treatment at 150°C for 10 min under nitrogen flow and drying at 80°C for 24 h under vacuum atmosphere significantly reduced silver nanoparticles and prevented the oxidation of silver with formation of only trace of AgO. Silver nanoparticles have promising applications in biotechnology and life sciences due to their remarkable optical, electrical and antimicrobial properties. The various synthetic methods have been developed for the fabrication of Ag-nanoparticles via in situ generation from silver salt cations, such as thermal decomposition [133], sonochemical synthesis [152], and chemical reduction [153].

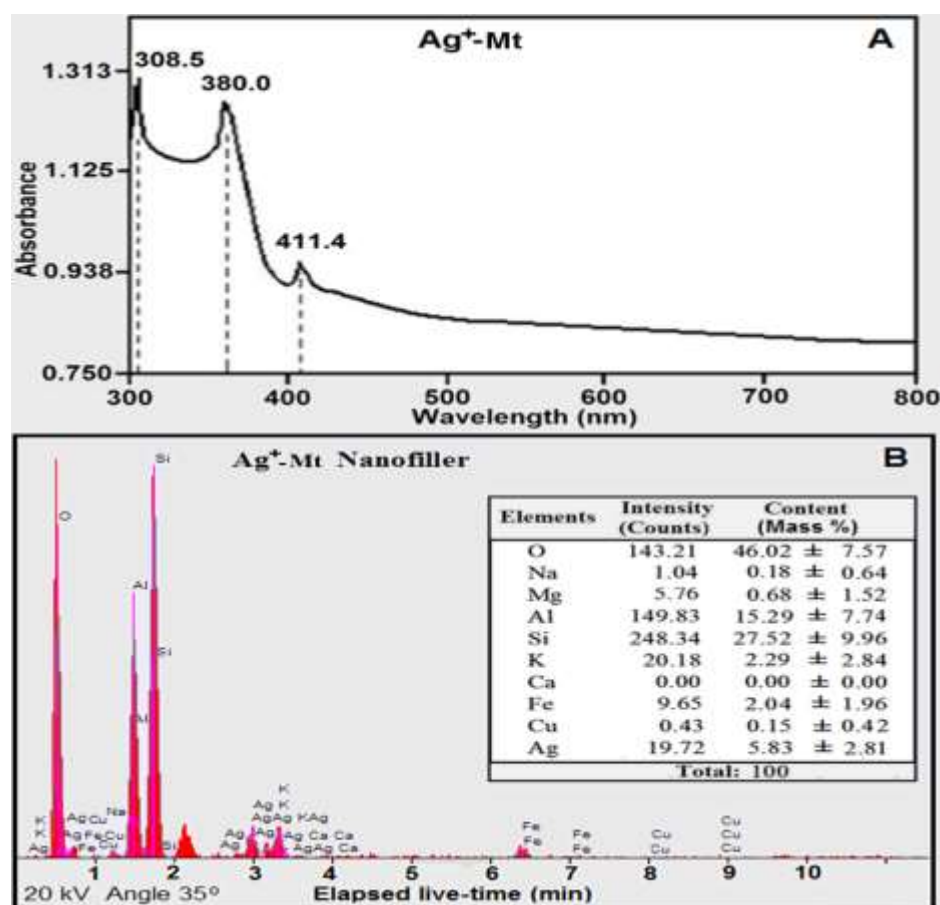


Figure. 4. 16. (A) UV-Vis spectrum and (B) SEM/EDX composition analysis of Ag⁺-MMT.

The results of SEM/EDX analysis (Figure 4.16-B) indicate the formation of intercalated silver particles with mass of 5.86% and essential reduce of mass for Na (0.18%) in Ag⁺-MMt. This results confirmed effective ion exchange reaction between Na and Ag cations.

4.2.4. ¹H, ¹³C and ¹³C-DEPT-135 NMR Analysis

The chemical structures of Copolymer-*g*-PLA fabricated without (in the presence of conventional tin octoate catalyst for the comparative analysis) and with Na⁺-MMT and ODA-MMT catalyst-nanofillers were also investigated by ¹H, ¹³C and ¹³C-DEPT-135 NMR analysis methods (Figure 4.17). NMR spectra of graft copolymer prepared with tin octoate catalyst in the similar reaction conditions (for 5.0 h grafting time up to phase separation) shows characteristic chemical shifts from CH and CH₃ groups of LA units with low intensities (Figure 4.17-A) as compared with those for the graft copolymers rapidly synthesized with Na⁺-MMt (Figure 4.17-B, grafting time 56 min) and ODA-MMT (Figure 4.17-C, grafting time 35 min). All chemical shifts from protons and carbon atoms of the functional groups relating to matrix copolymer and grafted PLA were observed in ¹H and ¹³C NMR spectra and additionally confirmed with ¹³C-DEPT-135 NMR analysis (CH₂, CH₃ and C=O in top and CH in bottom).

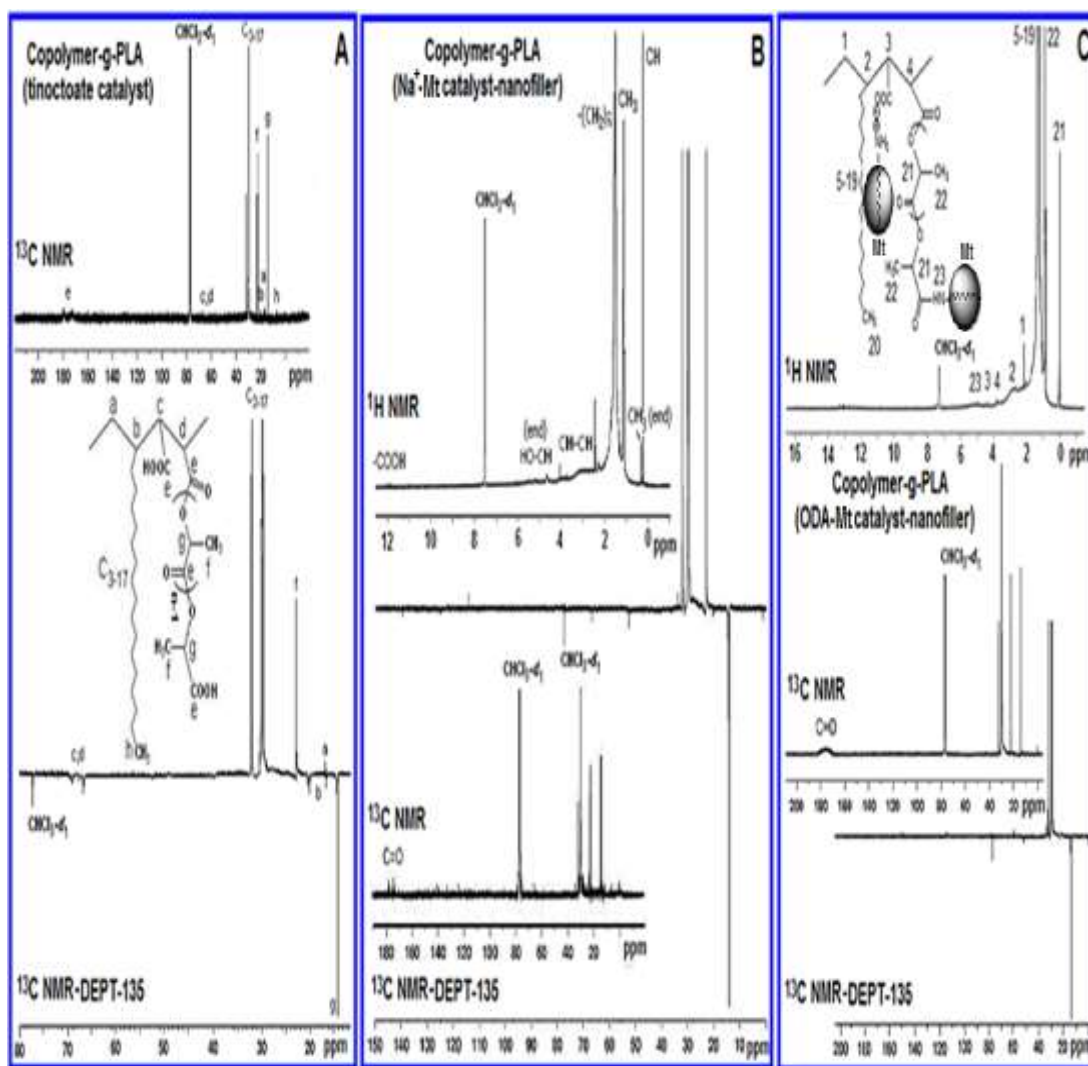


Figure. 4. 17. ^1H , ^{13}C and ^{13}C -DEPT-135 NMR spectra of Copolymer-g-PLA fabricated with (A) tinocatoate catalyst (grafting time 5 h), (B) Na^+ -MMT catalyst-nanofiller (grafting time 56 min) and (C) ODA-MMT catalyst-reactive nanofiller (grafting time 35 min).

4.2.5. X-ray Diffraction Analysis

The physical structures of CPNs were evaluated by X-ray diffraction (XRD) method (Figure 4.18 and 4.19). It is known that XRD is a method capable of probing long-range order in polymer crystals and it is therefore used for example to follow changes in the crystallinity of PLA monofilaments [52, 149, 154]. The XRD analysis of the polymer/organoclay nanosystems provides access to the interlayer stacking distance between clay sheets and to determine the crystallinity and ratio of amorphous and crystalline areas in the CPNs patterns. The well-known standard form of Scherrer equation was used

to calculate the crystallite size (T_{sh} , the mean thickness) of the coherent scattering domain of crystals from XRD full width data at half maximum (FWHM) intensity, employs a Scherrer constant (K_{sh} of 0.89). The obtained results are summarized in Tables are presented in Figure 4.18 and 4.19.

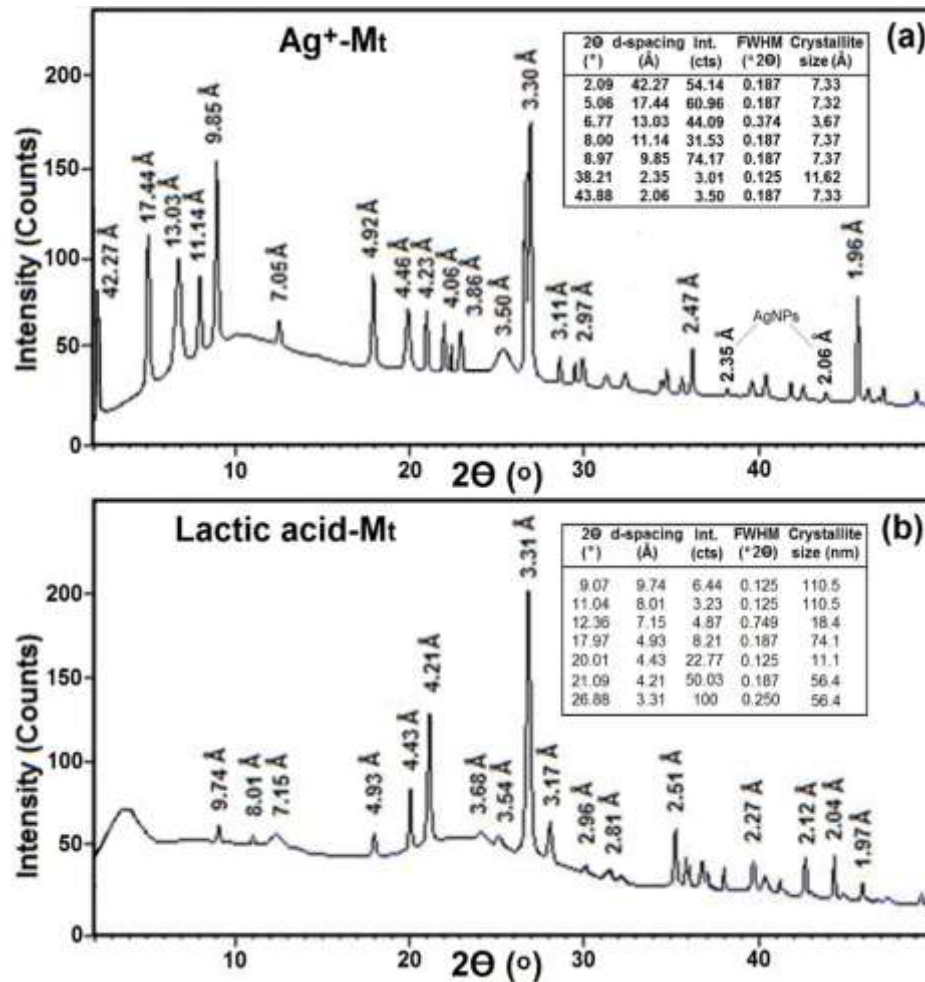


Figure. 4. 18. XRD patterns of Ag⁺-MMT and lactic acid-MMT.

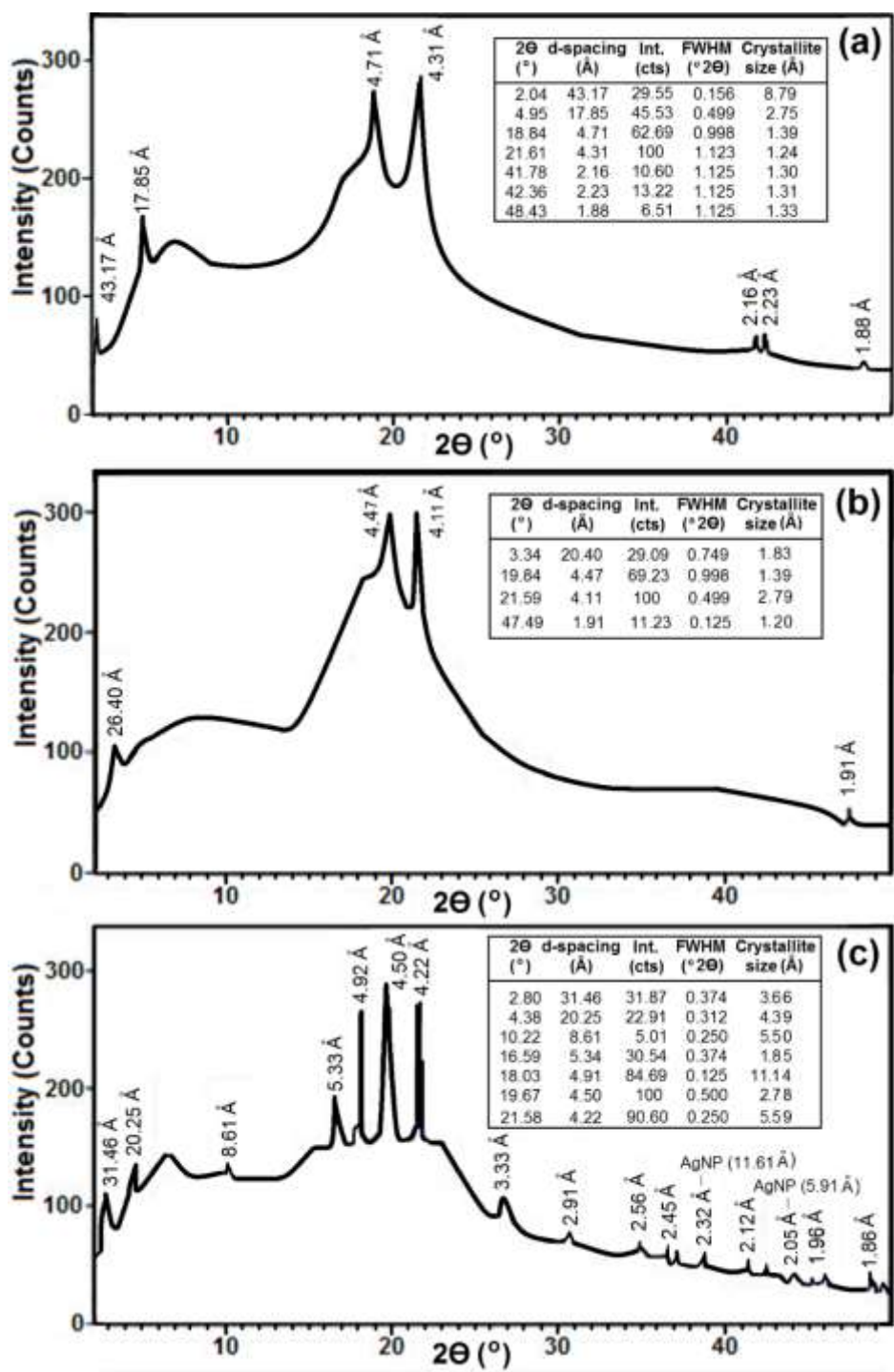


Figure. 4. 19. XRD patterns of poly(MA-*alt*-1-octadecene)-*g*-PLA incorporated with (a) ODA-MMT, (b) Na⁺-MMT and (c) Ag⁺-MMT nano-composites. Loading clay is 3.2 wt %.

The XRD patterns of the CPNs contain three characteristic traces from clay sheets, diffraction parameters (2θ, d-value and reflection intensity) of which are differed from those of the pristine inorganic and organic clays. The XRD

spectra of Ag⁺-MMT (Figure 4.18-a) contained reflection from silicate layers at 2.42° 2θ (d = 59.08 Å) and 7.3° 2θ (d = 13.03 Å). The presence of X-ray reflection at 2θ values of 38.24° (w) and 44.08° (m) with crystallite size of 1.16 and 7.33 Å, respectively (Figure 4.17-a), is associated with cub crystals of silver from dispersed Ag nanoparticles in CPN [155]. Preintercalated LA monomers as intercalate also executes the function of reactive compatibilizer between immiscible organic graft copolymer chains and inorganic clay phases and also expand the intergallery d-value from 10.17 Å for pristine Na⁺-MMT to 43.69 Å for Mt...LA organoclay (Figure 4.18-b). Observed shifted reflection with d = 8.74 Å from silica crystal (Si-OH at edges) can be explained by strong interaction of Si-OH and carboxyl group of intercalated LA. Agreeing with XRD patterns (Figure 4.19), all the CPNs predominantly exhibit amorphous structure with small crystalline phase from MMT. Higher diffraction reflection associated with a (001) plane from octahedral platelet of clay. Reflection with middle intensity related to (002) reflections from 2:1 tetrahedral sheets and low intensive reflection can be indexed as the (003) reflection from surface sheet containing Si-OH groups at edges. The CPN incorporated with Ag⁺-MMT (Figure 4.19-c) shows weak reflections from layered silicate fragments, suggesting that some clay mineral layers are exfoliated, but some non-exfoliated silicate layers may agglomerate and still remain in the graft copolymer matrix. The observed weak reflections at 38.71 and 44.16°2θ can be attributed to the AgNPs with nanosizes of 11.61 and 5.91 Å, respectively. A representative TEM image of copolymer-g-PLA/Ag⁺-MMT nanocomposite further confirms the exfoliation and/or partially agglomerated core-shell structures of layered clay in the graft copolymer matrix. Intercalating/exfoliating in situ processing only significantly changes the d-value parameters of 2:1 layered platelets (002) and silica crystals with Si-OH groups (003) at edges that are able to participate in the chemical and physical interfacial interactions with anhydride/carboxyl functional groups of the matrix graft copolymer, as well as to form complexes with metal cations especially silver cations.

4.2.6. Parameters of Particles: Structure ζ-size (potential) Relationships

Some important parameters obtained for the particles such as ζ-size and ζ-potential for the employed inorganic and organic clays and their polymer

nanocomposites are summarized in Table 4.2. The comparative analysis of these parameters for the Na⁺-MMT and Ag⁺-MMT and their modified LA derivatives indicates that the Ag-containing nanofillers are particles formed with relatively small size and large specific surface area, especially after sonication process. The ζ -sizes of all clays significantly reduced after microwave sonication in chloroform solution for 15 min while ζ -sizes of copolymer-*g*-PLA/clays composites (0.827 and 0.588 μm) were insignificantly reduced (0.706 and 0.557 μm). However, the particle size of pristine amphiphilic poly(MA-*alt*-1-octadecene) (0.828 μm) was essentially reduced up to nano scale (0.1 μm).

Higher ζ -potential values for Ag⁺-MMT (103 μV) and ODA-MMT (94.2 μV) clays were observed. The average values of ζ -potential also essentially depend on the origin of clays. ζ -potential values of the particles related to intercalated LA-Ag⁺-MMT (33.3 μV) and LA-Na⁺-MMT (9.6 μV) clays significantly increased up to 75.3 and 43.5 μV , respectively, after sonication for 15 min. The CPN incorporated with ODA-MMT shows lower ζ -potential due to neutralization of octadecyl amine cations with anhydride groups via in situ amidization processing. Origins of the clays, also, essentially influence the particle parameters of CPNs which decrease the average values of ζ -size and increase ζ -potential in the following order of clays: ODA-MMT < Na⁺-MMT < Ag⁺-MMT.

4.2.7. Effect of Clay Origin on the Morphology of Polymer Nanocomposites

The surface and inner morphologies of the copolymer-*g*-PLA layered silicate nanocomposites prepared by interlamellar catalytic graft copolymerization in the presence of different MMTs and ODA-Mt organoclay were examined by scanning electron microscopy (SEM) and Transmission Electron Microscopy (TEM). SEM images of all the CPNs prepared with above mentioned MMTs predominantly exhibit roughened, microporous (around 0.5-5.0 μm) and nanoporous (pore size approximately 20-35 nm in dark regions) surfaces (Figure 4.20 and 4.21) due to the elimination of traces of water molecules (nano-pores) and lactic acid (micro-pores). For the CPNs prepared with organoclay (Figure 4.20), the formations of non-evenly distributed smaller and rough fractures of

clay aggregates were observed. As evidenced from these results, organic intercalant relatively and more effectively participates in situ graft copolymerization via chemical interfacial interaction than its inorganic analogues. Relatively better distribution of surface micro and nanopores was observed for the CPNs incorporated with Ag⁺-MMT (Figure 4.21).

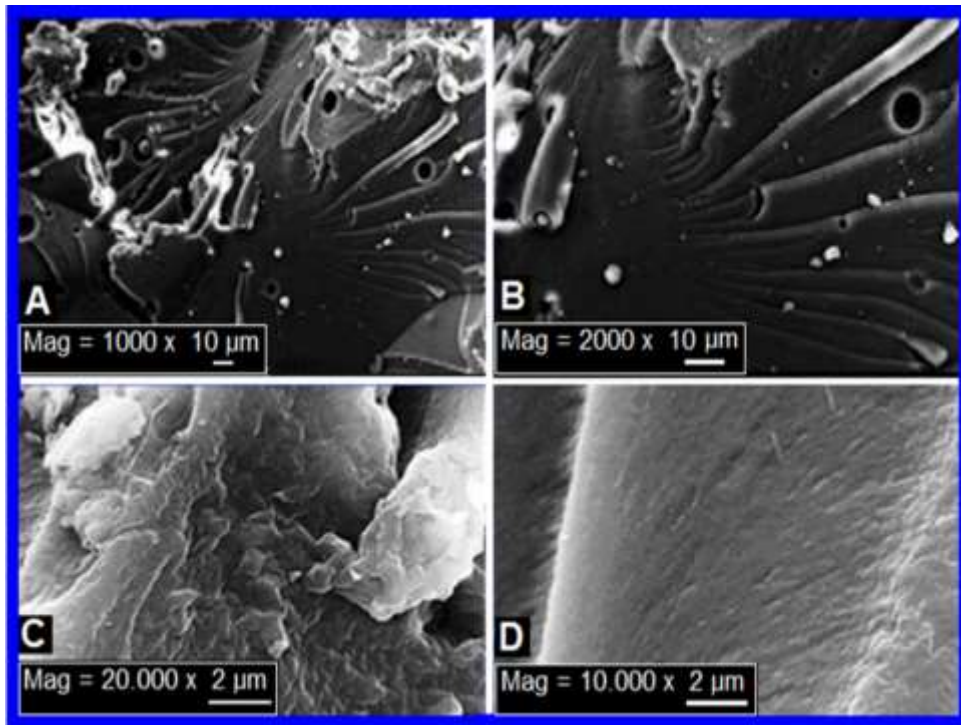


Figure. 4. 20. SEM images of poly(MA-*alt*-1-octadecene)-*g*-PLA/ODA-MMT nano-composites. Scale: (A) 1000 x, 10 μm, (B) 2000 x, 10 μm, (C) 20.000 x, 2 μm and (D) 10.000 x, 2 μm.

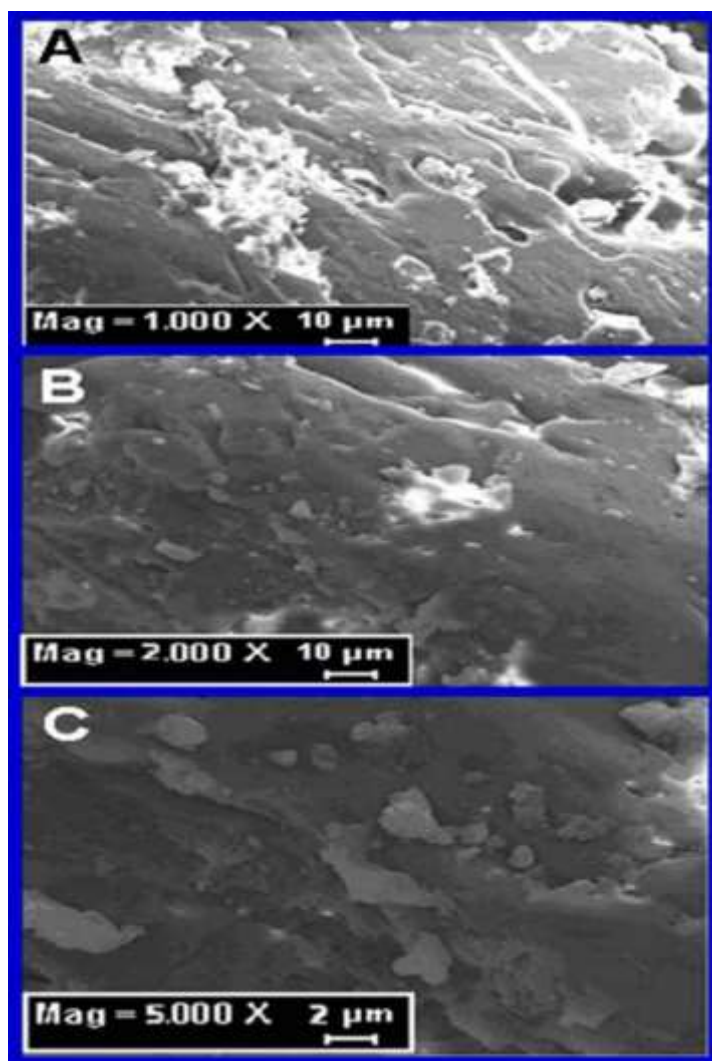


Figure. 4. 21. SEM images of poly(MA-*alt*-1-octadecene)-*g*-PLA/Ag⁺-MMT nanocomposites at different scales and magnifications.

The TEM morphology of the individual particles illustrated in Figure 4.22 indicates that the clay crystals clustered together with regularly form and the spherical particles covered with matrix graft copolymer in the form of nanoporous core-shell morphology. This phenomenon can be explained by the formation of better hydrophilic/hydrophobic balance in the used reactive copolymer-*g*-PLA/organoclay mixture, and therefore, occurrence of the self-organized in situ chemical and physical interfacial interactions in the chosen interlamellar graft copolymerization conditions. Agreeing with TEM images, the CPNs exhibit typical self-assembled core-shell morphology (Figure 4.22-25) and contain mixture of the fully (light spherical) and partially (dark spherical) covered nano and microparticles with polymer chains. The light spherical

particles show strong tendency to agglomeration predominantly through covalent bounding, especially for CPNs prepared with reactive ODA-MMT (Figure 2.23) and physical interaction for CPNs incorporated with inorganic clays (Figure 4.24 and 4.25).

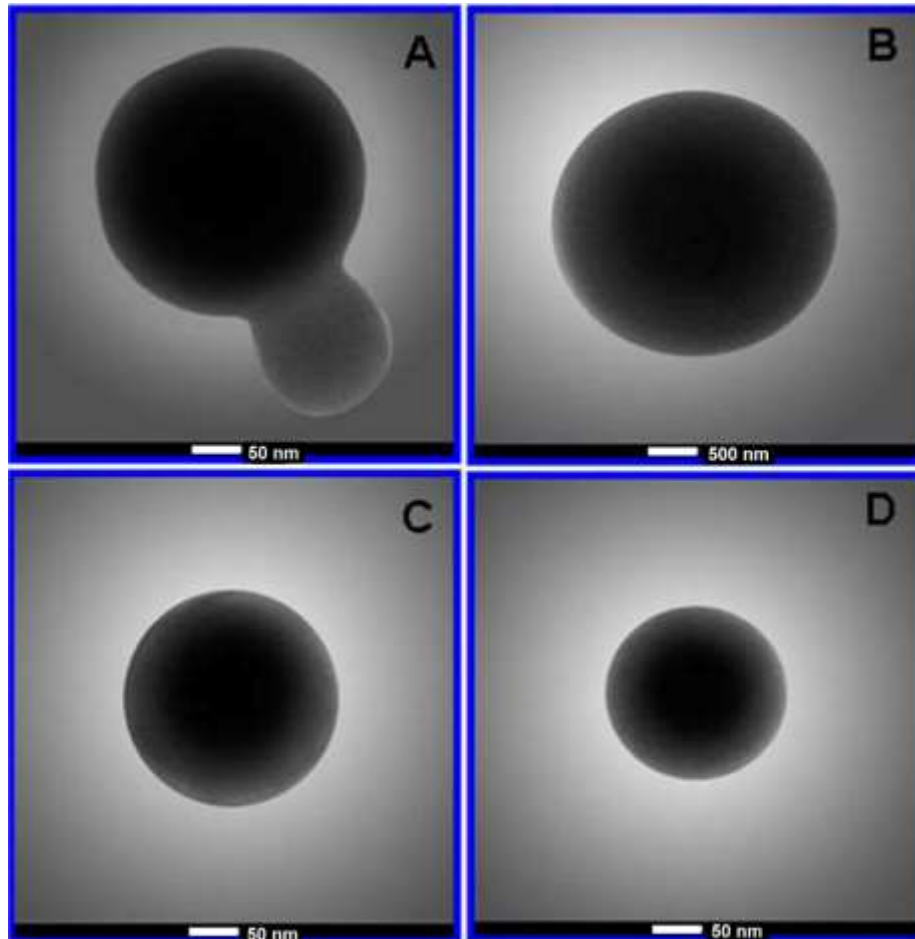


Figure. 4. 22. TEM images of individual particles of poly(MA-*alt*-1-octadecene)-*g*-PLA silicate layered nano-composites incorporated with (A and B) ODA-MMT, (C) Na⁺-MMT and (D) Ag⁺-MMT organic and inorganic clays in the presence of pre-intercalated MMT...LA complexes.

However, taking into consideration a fact that the inorganic clays (Ag⁺ and Na⁺) form the preintercalated complexes with LA monomer, i.e., easily transferred to organic clay forms in the reaction medium, they also exhibit a tendency to formation of nanostructures fragments with matrix graft copolymer chains. This proposes was reasonably confirmed by the obtained TEM morphology images (Figure 4.24 and 4.25) which include dispersed nano and micro size core-shell particles and agglomerated spherical microparticles. Some spherical self-

assembled core-shell microparticles formed in the background of numerous nanoparticles with core-shell like structure. The diameters of these particles changed around 200-300 nm and 30-100 nm for the micro and nanoparticles, respectively.

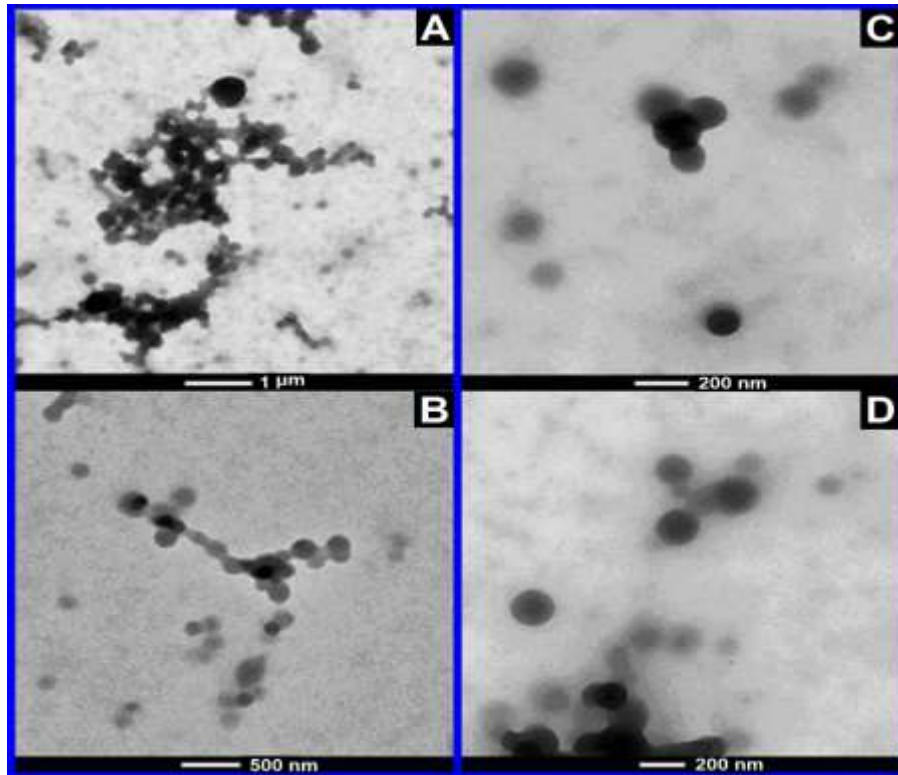


Figure. 4. 23. TEM images of poly(MA-*alt*-1-octadecene)-*g*-PLA/ODA-MMT nanocomposites. Scale: (A) 1 μm, (B) 500 nm and (C and D) 200 nm.

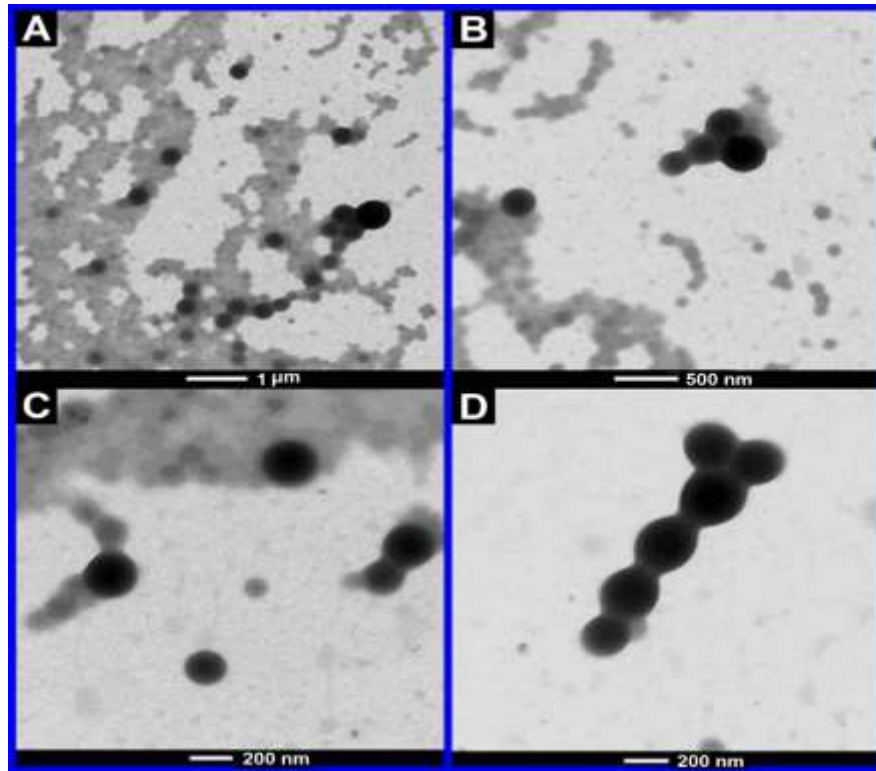


Figure. 4. 24. TEM images of poly(MA-*alt*-1-octadecene)-*g*-PLA/Ag⁺-MMT nanocomposites. Scale: (A) 1 μm, (B) 500 nm and (C and D) 200 nm.

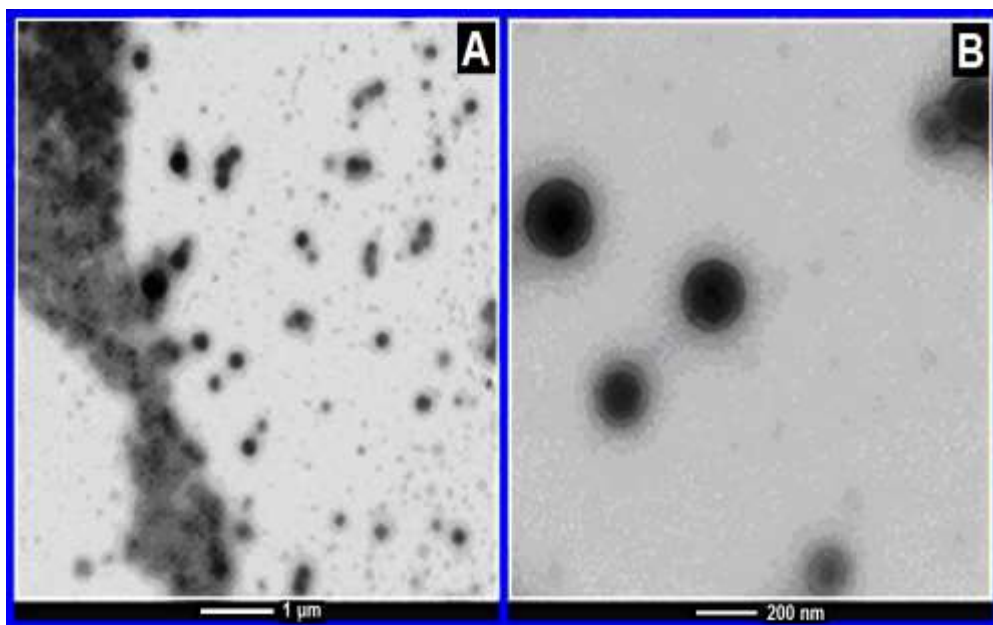


Figure. 4. 25. TEM images of poly(MA-*alt*-1-octadecene)-*g*-PLA/Na⁺-MMT nanocomposites. Scale: (A) 1 μm and (B) 200 nm.

4.2.8. Thermal Properties

The thermal properties of the origin clays and copolymer-*g*-PLA/clay nanocomposites were investigated using Differential Scanning Calorimetric (DSC) and thermogravimetric (TGA) analysis methods. The results of these analyses are illustrated in Figure 4.26 and 4.27. The thermal analysis results of the clays (Figure 4.27) demonstrate that the protonation and absorption of water molecules in the Ag⁺-MMT were strongly occurred compared with the Na⁺-MMT and ODA-MMT. Multi step degradation (elimination of water molecules) was observed for the Ag⁺-MMT due to elimination of surface absorbed and crystallization of water molecules, as well as degradation of metal-OH at edges with elimination of water molecules (Figure 4.27-A). A one step degradation with elimination of absorbed water (~2 mass %) and all various origins of the water molecules (29 mass %) was observed for Na⁺-MMT (Figure 4.27-B). The ODA-MMT degraded (Figure 4.27-C) by two steps: first step around 250-340°C associated with degradation of the organic octadecyl fragment and second step (more intensive DTG peak) included all eliminations of water molecules as an above mention mechanism.

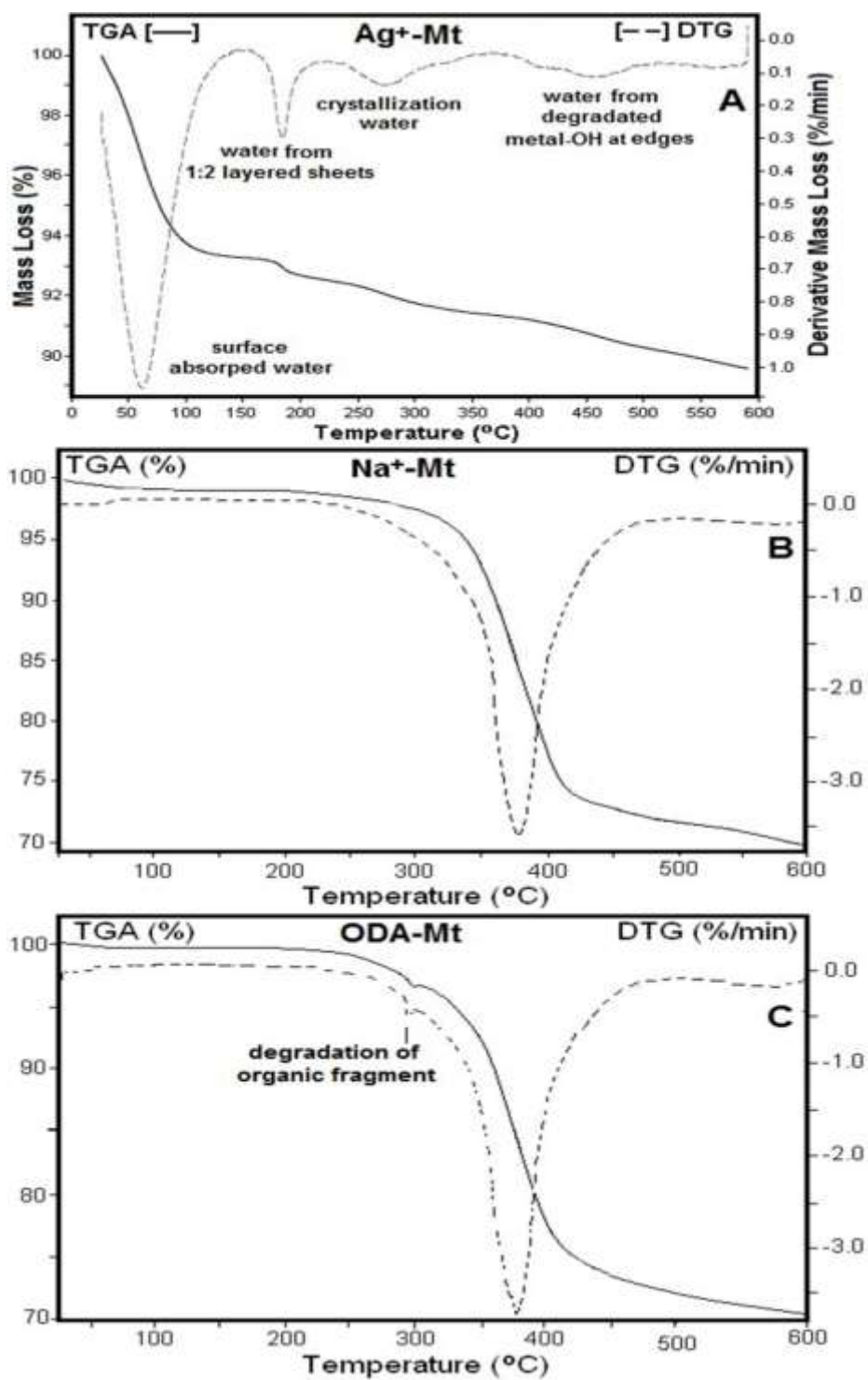


Figure. 4. 26. TGA-DTG curves of (A) Ag⁺-MMT, (B) Na⁺-MMT and (C) ODA-MMT. The heating rate is 10°C/min under nitrogen atmosphere.

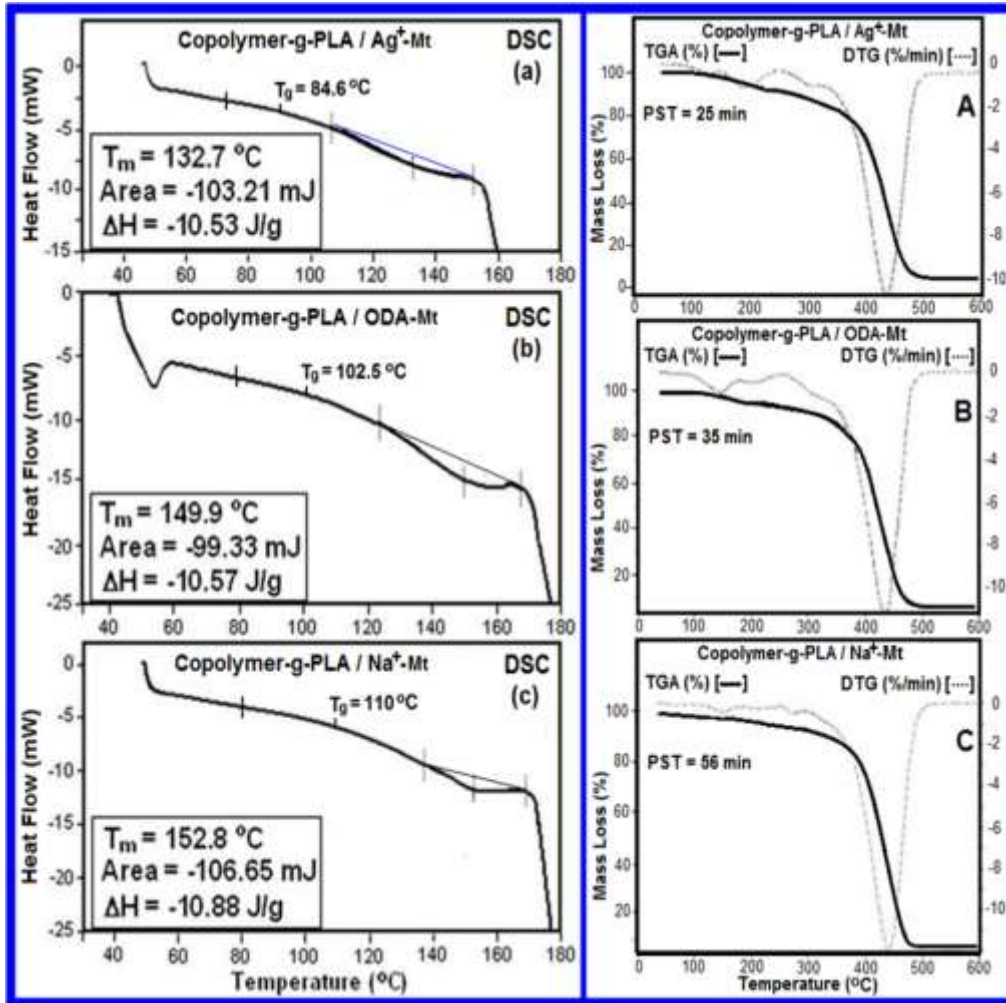


Figure. 4. 27. Thermal properties of copolymer-g-PLA/clay nano-composites. (A) DSC analysis of copolymer-g-PLA/Ag⁺-MMT, (B) DSC analysis of copolymer-g-PLA/ODA-MMT, (C) DSC analysis of copolymer-g-PLA/Na⁺-MMT, (a) TGA/DTG analysis of copolymer-g-PLA/Ag⁺-MMT, (b) TGA/DTG analysis of copolymer-g-PLA/ODA-MMT, (c) TGA/DTG analysis of copolymer-g-PLA/Na⁺-MMT.

Agreeing with DSC traces performed from the plots of heat flow (mW) versus temperature (Figure 4.26), origin of used the organic and inorganic clays apparently influenced on the glass-transition temperature (T_g) (around 90-110°C for the all CPNs) while essentially changes the melting transition (T_m) process which is appeared in the DSC traces as a broad endo-peaks around 138-152°C with peak areas around 100-106 mJ (Figure 4.26-A). It is known that high molar mass PLA exhibits lower T_m (around 170-180°C) as compared with those for the oligo-LA (207°C) due to the presence of enantiomeric and other impurities leading to imperfect crystals [52]. It was observed that CPNs

containing a matrix copolymer-*g*-PLA and different clay nanofillers (Ag⁺-MMT, ODA-MMT and Na⁺-MMT) also exhibit relatively lower T_m values as 132.7, 149.9 and 152.9°C, respectively. The observed relatively low value of T_m for Ag⁺-MMT containing polymer nanocomposite indicates significantly acceleration in-situ graft copolymerization by silver cations and formation of relatively high molar mass branched PLA. Moreover, these observations are in good agreement with evaluated phase separation times (PST) (Figure 4.26) as well as with results of above mentioned structural analyses by FTIR, (¹H and ¹³C) NMR and XRD methods. The lower degree of crystallinity (~11.5% for all clay polymer nanocomposites) was calculated using melting enthalpy values (around 10.53-10.88 J/g) for the CPNs (Figure 4.25) and known 100% crystalline PLA (93.1 J/g) [155]. Feijoo et al. [156] also reported the amorphous structures of PLA/Mt nanocomposites. Taking into consideration known fact that pristine poly(MA-*alt*-1-octadecene) exhibits amorphous structure with ~120°C softening point and undergo to degradation around 130-200°C through decarboxylation and above mentioned amorphous structure of PLA/clay nanocomposites, the CPNs of copolymer-*g*-PLA incorporated with different clays with similar compositions may be formed the analogous amorphous structures. This propose is partially confirmed by DSC results. The obtained DSC parameters allow us proposed that the all CPNs predominantly exhibit amorphous structures containing lower parts of crystalline areas. However, we observed that grafting of PLA onto copolymer caused to decrease of T_g values up to 84.6, 102.5 and 110°C as compared with T_{soft} value (~120°C) of pristine copolymer due to internal plasticizing effect of polyester PLA side-chain linkages and provided the weak endothermic melt-transitions at 132.7, 149.9 and 152.8°C in the all CPNs incorporated with Ag⁺-MMT, ODA-MMT and Na⁺-MMT, respectively. Thus, DSC parameters of the copolymer-*g*-PLA/clay nanocomposites strongly depend on the inorganic and reactive organic origin of applied mineral clays due to the different structural factors and in situ interfacial interactions processing.

The TGA-DTG analyses of the CPNs were illustrated in Figure 4.26-B. The results from these analyses show that the origin of clays also influenced on the degradation processing and thermal stability of the CPNs. Two steps of

degradation were observed for all of CPNs. The first step relates to elimination of adsorbed water molecules, organic intercalate molecules (3.2-6.5%) and decarboxylation of anhydride units of copolymer fragments around 110-190°C (Figure 4.26-a) and second step associates with chain degradation of polymeric phase of nano-hybrids around 320-500°C with maximum values of degradation temperature ($T_{d(max)}$) around 400-450°C for ODA-MMT, Ag^+ -MMT and Na^+ -MMT containing polymer nanocomposites.

4.3. Characterization of St-g-PLA Copolymers Synthesized Through Supercritical Carbon Dioxide

4.3.1. Optimization of the Operational Parameters and Evaluation of Their Effect on the Grafting Degree

The synthetic pathway for the preparation of the St-g-PLA graft copolymer in a $scCO_2$ medium includes a two-step reaction schematically demonstrated as follows (Figure 4.28): Synthesis of the graft copolymer was performed by gelatinization of the starch (first step) and graft copolymerization of LA monomer onto the starch in a $scCO_2$ medium (second step).

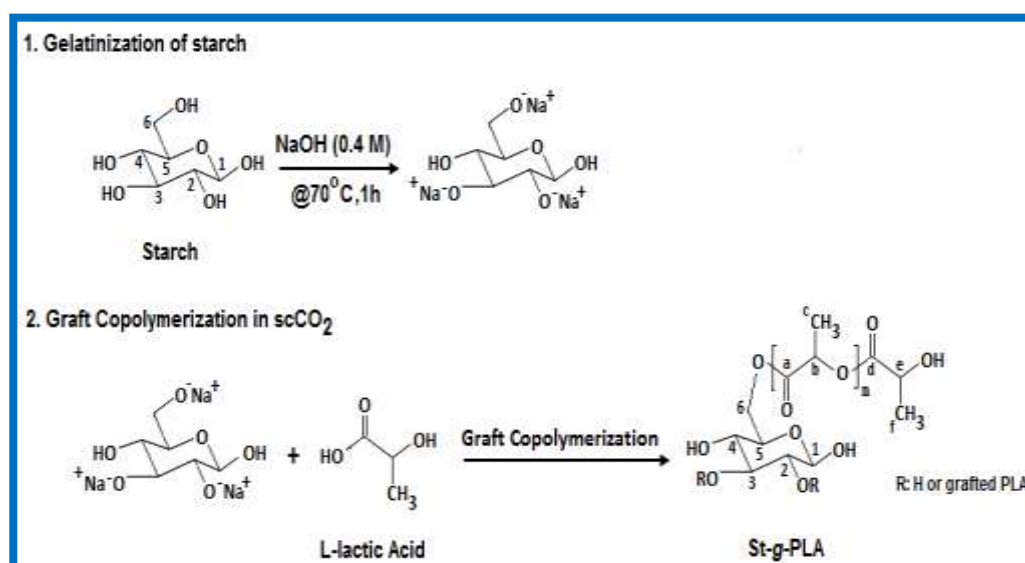


Figure. 4. 28. The synthetic pathways of St-g-PLA copolymer.

To optimize the operational parameters of the reaction (St/LA feed ratio, temperature, pressure, $scCO_2$ flow rate and reaction time) and evaluate their effects on the grafting degree, graft copolymerizations were investigated in

detail, and the results are summarized in Table 4.3. We observed that these operational parameters significantly influenced the graft copolymerization and thus the grafting degree (content of branched PLA). It was found that St-*g*-PLA with a maximum grafting degree (52 mol%) is formed using the following reaction conditions: a St/LA feed ratio of 1:3, 100°C, 200 bar, a scCO₂ flow rate of 10 g/min and a reaction time of 6 h. The grafted LA mole fraction (in mol%) of monomers (m_1 and m_2) in the St-*g*-PLA copolymer was calculated by using FTIR absorption bands from St and grafted PLA with the following equations [150]:

$$m_1 = \frac{A_{1336}/M_1}{A_{1336}/M_1 + A_{1735}/M_2} \times 100 \quad (2)$$

$$m_2 = \frac{A_{1735}/M_2}{A_{1336}/M_1 + A_{1735}/M_2} \times 100 \quad (3)$$

Where A_i donates the absorption area for the characteristic peaks and M_1 and M_2 are the molecular weights of the repeating St and LA units, respectively. The results are summarized in Figure 4.29. To determine the contents of the starch and LA units in the copolymer, absorption band value ratios between the characteristic bands of 1735 cm⁻¹ (for the LA C=O ester peak) and 1336 cm⁻¹ (for the St-CH₂ peak) were employed.

Table. 4. 3. Effects of reaction parameters on grafting degree.

St/LA feed ratio (w/w)	<i>T</i> (°C)	<i>P</i> (bar)	time (h)	scCO ₂ flow rate (g/min)	Grafted LA (mol %) ^a
<i>Effect of St/LA ratio</i>					
1:0.5	100	200	6	10	32
1:1	100	200	6	10	41
1:3	100	200	6	10	52
1:5	100	200	6	10	43
<i>Effect of temperature</i>					
1:3	70	200	6	10	32
1:3	90	200	6	10	49
1:3	100	200	6	10	52
1:3	110	200	6	10	41
<i>Effect of scCO₂ flow rate</i>					
1:3	100	200	6	1	28
1:3	100	200	6	5	36
1:3	100	200	6	10	52
1:3	100	200	6	15	40
<i>Effect of pressure</i>					
1:3	100	70	6	10	21
1:3	100	100	6	10	43
1:3	100	200	6	10	52
1:3	100	300	6	10	52
<i>Effect of reaction time</i>					
1:3	100	200	1.5	10	26
1:3	100	200	3	10	48
1:3	100	200	6	10	52
1:3	100	200	9	10	52

The effects of the graft copolymerization parameters, i.e., temperature, reaction time, scCO₂ flow rate and pressure, are shown in Figure 4.29, and related data are summarized in Table 4.3. The effect of the temperature on the graft copolymerization is shown in Figure 4.29-A. There is an inverse relationship between the temperature and the grafted LA mole fraction; at temperatures above 100°C, the grafted LA mole fraction decreased due to the breaking of grafted LA. It is obvious that over the starch gelatinization point, the starch structure puffed up, and this led to the partial separation of the amylose and amylopectin, which resulted in an increase in the activated groups (especially OH groups) available to react with the excess lactic acid in the polymerization media [157]. Especially of note is that at extremely high temperatures, the tendency of the lactic acid to homo-polymerize increased remarkably, which adversely caused a clear fall in the grafted PLA mole percent. Figure 4.29-B depicts the effect of time on graft copolymerization. It is clear that increasing the reaction time from 1.5 h to 6 h changed the grafted PLA mole percent significantly, and the maximum amount of grafted PLA (52%) was achieved after 6 h of reaction time. A further increase in the polymerization time had almost no effect on the grafted percentage.

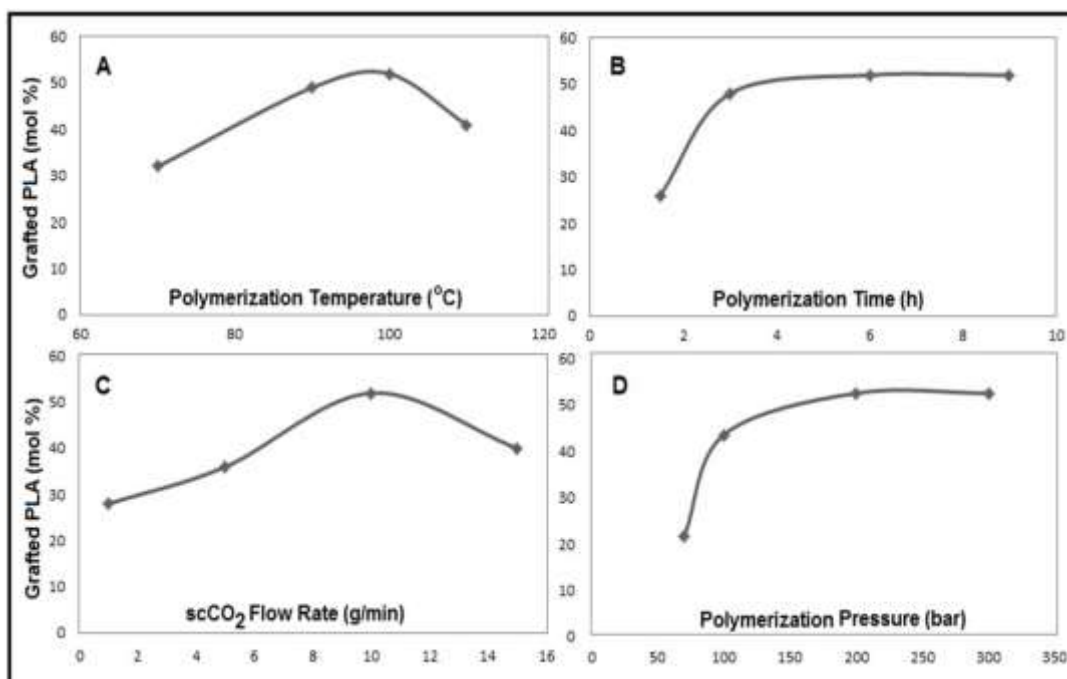


Figure. 4. 29. Influence of variable conditions on grafted LA mol percent. (A) polymerization temperature, (B) polymerization time, (C) scCO₂ flow rate and (D) polymerization pressure.

The effects of the scCO₂ flow rate and the polymerization pressure on the graft copolymerization are shown in Figure 4.29-C and D, respectively. The maximum grafted PLA mol percent (52%) was attained by increasing the scCO₂ flow rate to 10 g/min and the polymerization pressure to 200 bar. Furthermore, to demonstrate the reproducibility of our pro-posed system, we performed 10 consecutive trials at maximum grafting degree conditions (6 h, 100°C, 200 bar, 10 g/min scCO₂ flow rate and a 1:3 (w/w) ratio of St/LA). Relative standard deviation (RSD) analysis via Microsoft-Excel-2013 resulted in quite acceptable RSD value (4%) for the related data which is a strong proof of the proposed graft copolymerization procedure.

4.3.2. ATR-FTIR Spectroscopy

The FTIR spectra of starch and St-*g*-PLA are shown in Figure 4.30. Two characteristic peaks appear at 1000 and 1200 cm⁻¹ in the FTIR spectra of corn starch (Figure 4.30-A), which are associated with the C O band stretching of ether groups [158]. The characteristic peak at 1642 cm⁻¹ is related to the bending of the OH group of absorbed water. The observed shift of this peak indicated that the gelatinization of the starch prior to copolymerization led to a decrease in the hydrogen bonding in the starch backbone. In the case of St-*g*-PLA, a decrease in the OH groups as a result of the gelatinization process and graft copolymerization reaction resulted in a broad band being observed at 3320 cm⁻¹ that was related to hydrogen bonded hydroxyl groups (Figure 4.30-B).

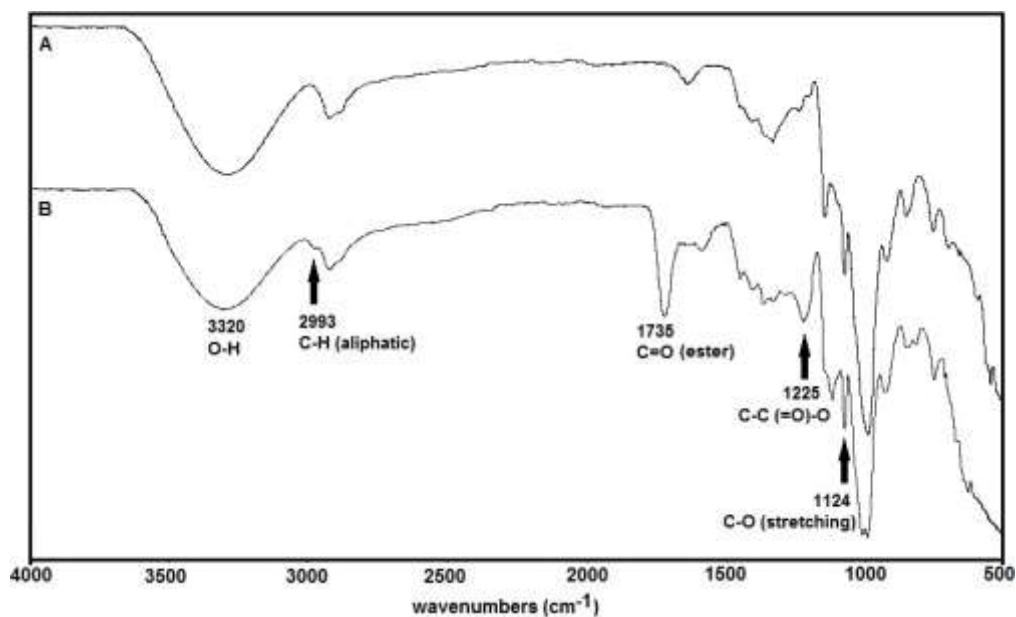


Figure. 4. 30. FTIR spectra of (A) starch and (B) St-*g*-PLA copolymer for the following reaction conditions; 1:3 polymer/monomer ratio, 100°C, 200 bar, 6 h (see Table 4.3).

In addition, in the spectra of the graft copolymer the appearance of a peak at 2993 cm^{-1} associated with C H (aliphatic) stretching indicated the occurrence of PLA grafting. A new strong characteristic C O stretching band at 1735 cm^{-1} in the spectra of St-*g*-PLA (Figure 4.30-B), which is not detected in the spectra of starch (Figure 4.30-A), can be attributed to the ester carbonyl group (Chang et al.,2009). From these FTIR analysis results, it was concluded that an efficient graft polymerization of LA monomer onto a starch backbone was achieved.

4.3.3. $^1\text{H-NMR}$ and $^{13}\text{C CP/MAS-NMR}$ Analysis of Graft Copolymers

The chemical structure of the graft copolymer was also confirmed by NMR analysis. Fig. 4 shows the $^{13}\text{C/CPMAS}$ NMR spectra of the starch and St-*g*-PLA copolymer made using a 1:3 starch to LA monomer ratio under the following polymerization conditions: 10 g/min scCO_2 flow rate at 100°C, 200 bar and 6 h. The chemical shifts (ppm) of the major peaks are presented on the insets of Figure 4.31-A and B. The signals at 26.1 and 27 ppm are attributed to the aliphatic group (CH_3) of the poly(L-lactic acid) chain. Additionally, the signals at 57.68 and 67.85 ppm are assigned to C-6 (CH_2OH) and the C-2, 3 and 5 groups of the starch chain, respectively. The broad peak at 77.28 ppm corresponds to the C-4 group of the starch chain while the peak between 94.73

and 98.21 ppm corresponds to the C-1 group. The presence of peaks at 172 and 178.3 ppm is of great importance. These peaks indicate the grafting of lactic acid to the starch and correspond to the ester carbonyl (C=O) peaks of the poly(L-lactic acid) chain.

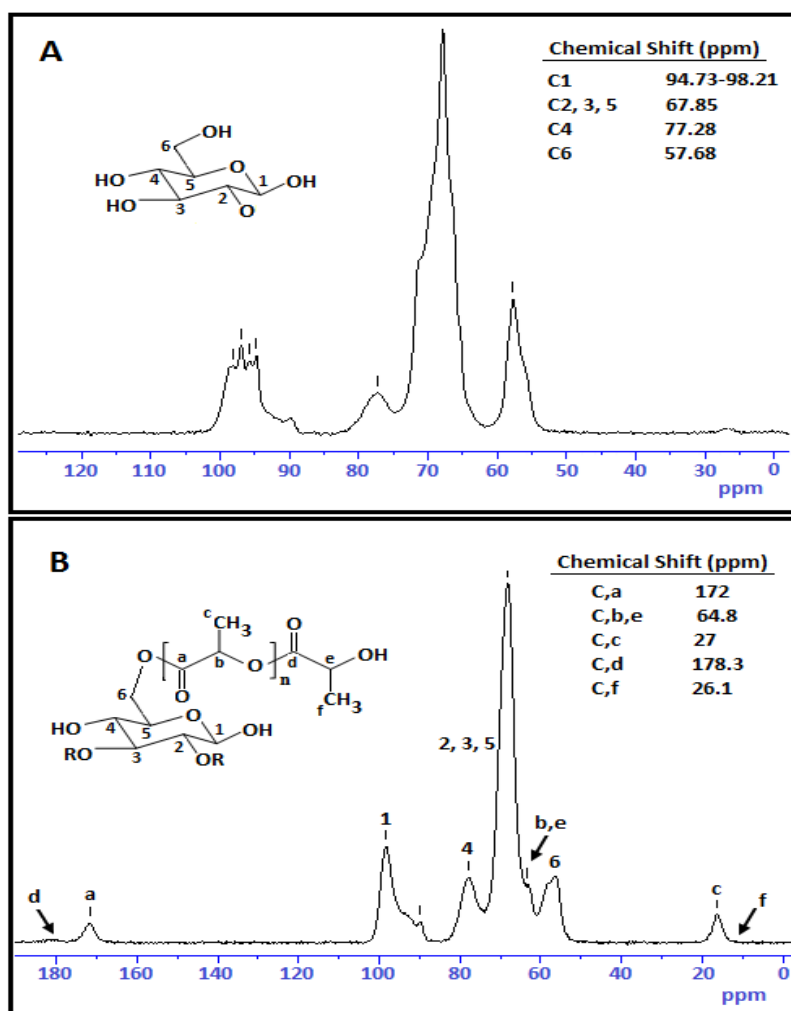


Figure. 4. 31. ^{13}C CP/MAS NMR spectra of (A) starch and (B) St-*g*-PLA copolymer prepared at 100°C, 200 bar, 6 h with 1:3 St/LA feed ratio.

^1H NMR analysis was also applied to determine the composition of the graft copolymers synthesized with different feed ratios of $M_1:M_2$ ranging from 1 to 0.2 (Figure 4.32 and Table 4.4). In this approach, the integrated peak areas (A_{mi}) of the proton from the (CH)[1H^+] group of the m_2 unit (LA) and the (CH₂) [2H^+] group of the m_1 unit (St) (Figure 4.32) in the spectra of the polymers were calculated using the following equations [159]:

$$Am_1(\text{CH})A_{\text{total}}=n_1m_1(a_1m_1+b_2m_2) \quad (4)$$

$$Am_2(\text{CH}_2)A_{\text{total}}=n_2m_2(a_2m_2+b_2m_2) \quad (5)$$

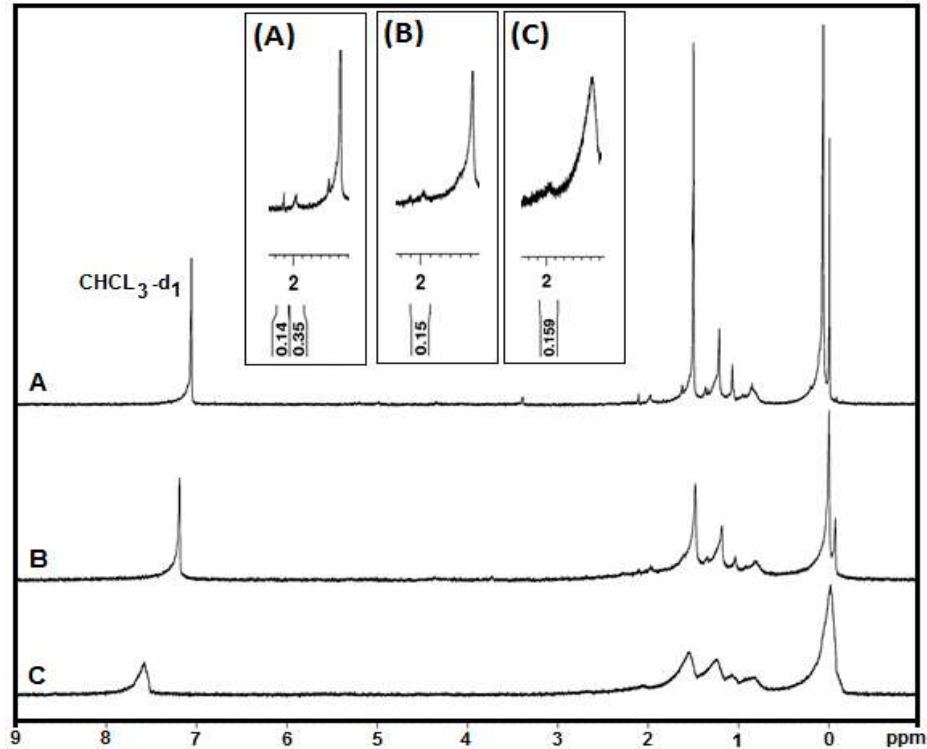


Figure. 4. 32. $^1\text{H-NMR}$ (400 MHz) spectra of St-g-PLA copolymers in $\text{CHCl}_3\text{-d}_1$ at 100°C , 200 bar, 6h. (A) 1:5; (B) 1:3 and (C) 1:1 monomer ratio.

where A_{m_1} and A_{m_2} are the normalized peak areas per H from the corresponding functional groups of the monomer unit; A_{total} is the total peak area of the protons in the copolymer; n_1 and n_2 are the integer number of protons in the functional groups of the monomer; and a and b are the integer number of protons in the monomer units (m_1 and m_2) in the case of $(m_1 + m_2) = 1$. Monomer unit ratios can be calculated from Eqs. (2) and (3) using the following equation:

$$m_1 / m_2 = f = [n_2 A_{m_1}(\text{CH})] / [n_1 A_{m_2}(\text{CH}_2)] \quad (6)$$

Where $n_1 = 1$ and $n_2 = 2$ are the number of protons in the chosen analytical groups from each monomer unit with integrated areas. From Eq. (3) the molar monomer unit ratio in samples was found to be $m_1(\text{LA}):m_2(\text{St}) = 60:40$ for a 1:3

monomer ratio [160]. These values have reasonable agreement with the FTIR results and are supported by the data of the grafted PLA mol% (see Table 4.2).

Table. 4. 4. ¹H-NMR analysis data to determine the composition of St-*g*-PLA for different feed ratios.

St/LA feed ratio (w/w)	Am_1 (St unit) ^a	Am_2 (LA unit) ^b	Copolymer Composition (mol %)	
			¹ H-NMR analysis	
			[m_1]	[m_2]
1:1	0.115	0.159	40	60
1:3	0.115	0.15	39.5	60.5
1:5	0.115	0.35	60	40

^a the integral area for CH₂ chemical shift of St unit.

^b the integral area for CH chemical shift of LA unit.

4.3.4. Acid Number Analysis of the Precipitate Phase

To obtain the grafting degree, we utilized the standard alkali titration method for determining the acid number (AN) of the precipitated phase. The AN (in mg KOH/g) was calculated using Eq. (7) as follows:

$$AN = [Mw(KOH) \times V(KOH) \times N(KOH)] / m \quad (7)$$

Where Mw (KOH)=56.1 g/mol; V(KOH)= consumed titrant; m = 0.4 g polymer; N(KOH)= 0.05 and the COOH end group concentration(C(COOH)) was determined via Eq. (8).

$$C(COOH) = [(AN) \times (Mw(COOH))] / Mw(KOH) \quad (8)$$

The acid number and COOH end group concentration of the unreacted LA monomer and oligomers soluble in methanol was calculated and is summarized in Table 4.4. All of the precipitated phases with acid numbers more than 20 indicate that as the lactic acid monomer (from a 1:1 ratio to 1:3 and 1:5 ratios) increases, the COOH groups increase, and the consumed volume of KOH increases as well. This results is well in accordance with the grafted PLA (mol%) data from Table 4.5, which indicates that lactic acid monomers and lactic acid oligomers have reacted with hydroxyl groups of the starch backbone under the scCO₂ pressure.

Table. 4. 5. End group analysis of St-*g*-PLA in precipitated phase.

St/LA weight ratios in precipitated phase	Consumed volume of KOH (ml)	AN (mg KOH/g)	COOH concentration (mg KOH.g ⁻¹)
1:0.5	2.9	20.33	16.30
1:1	5.1	35.76	28.68
1:3	6.0	42.07	33.75
1:5	7.2	50.49	40.50

4.3.5. X-ray Diffraction Analysis

A wide angle powder X-ray diffraction (XRD) method was employed to determine the crystalline and amorphous structures in St-*g*-PLA. The XRD patterns are illustrated in Figure 4.33. A significant change was observed in the crystallinity of native starch after being grafted with LA in a scCO₂ medium. The diffraction peaks present at $2\theta=14.98$, 17.08 and 23.04° are associated with crystalline structures of starch [44]. The crystallinity of the graft copolymer essentially disappeared as evidenced by the emergence of a broad peak at $2\theta=19.12^\circ$. This observation indicates the formation of a predominantly amorphous structure of the St-*g*-PLA copolymer. The partial gelatinization of starch crystalline regions a thigh pressure as well as the diffusion of scCO₂ solvent into St-*g*-PLA structures led to the disappearance of the characteristic crystalline peaks after graft polymerization.

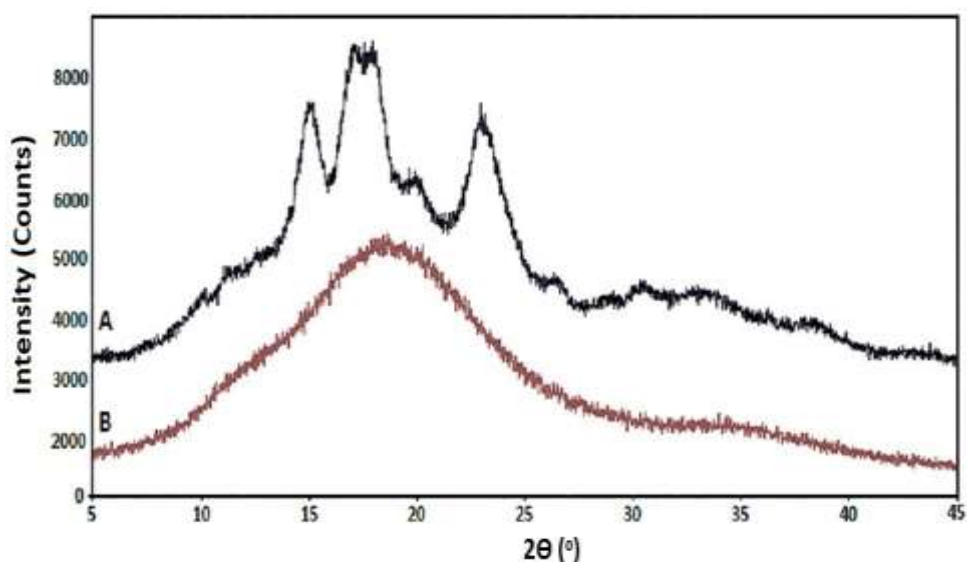


Figure. 4. 33. X-ray diffraction patterns of (A) starch and (B) St-*g*-PLA copolymer prepared at optimized reaction conditions; 1:3 St/LA ratio, 200 bar, 100°C for 6 h.

4.3.6. Reaction Parameters-Morphology Relationships

To determine the effect of scCO₂ on the morphology of starch granules under different reaction conditions, scanning electron microscopy (SEM) micrographs were taken, and representative SEM images are shown in Figure 4.34. According to the SEM images (Figure 4.34-A), it is obvious that starch granules exhibit a regular shape and a smooth surface morphology. The grafting of LA onto the starch backbone resulted in a dramatic change in the morphology of the product. These notable changes in the St-*g*-PLA morphology can be attributed to the interaction of the inner part of the starch structure with LA units under the high pressure of scCO₂ fluid, which is easily observed in the structures of the granules (Figure 4.34-B–D). The effect of the LA/St ratio on the morphology of the graft copolymer was also easily detected. Increasing the LA/St ratio in the scCO₂ medium led to the degradation of macroscopic starch structures. Due to the low amount of LA, a poor interfacial adhesion was observed between LA and starch functional groups (Figure 4.34-B). A further increase in the ratio of LA/St increased the hydrophilic groups of LA in the polymerization medium with a high compatibility of the two phases, and the degassing of supercritical fluid from the reaction medium led to the formation of a microporous morphology in St-*g*-PLA (Figure 4.34-6C and D). The detailed SEM images with higher magnification (Figure 4.34-E and F) indicated that a St/LA feed ratio of 1:3 caused the formation of micropores with sizes ranging from 1 μm to 5 μm. In addition to micropores, nano-sized cracks on the starch backbone in the St-*g*-PLA copolymer were also observed due to the effect of scCO₂ on the morphology.

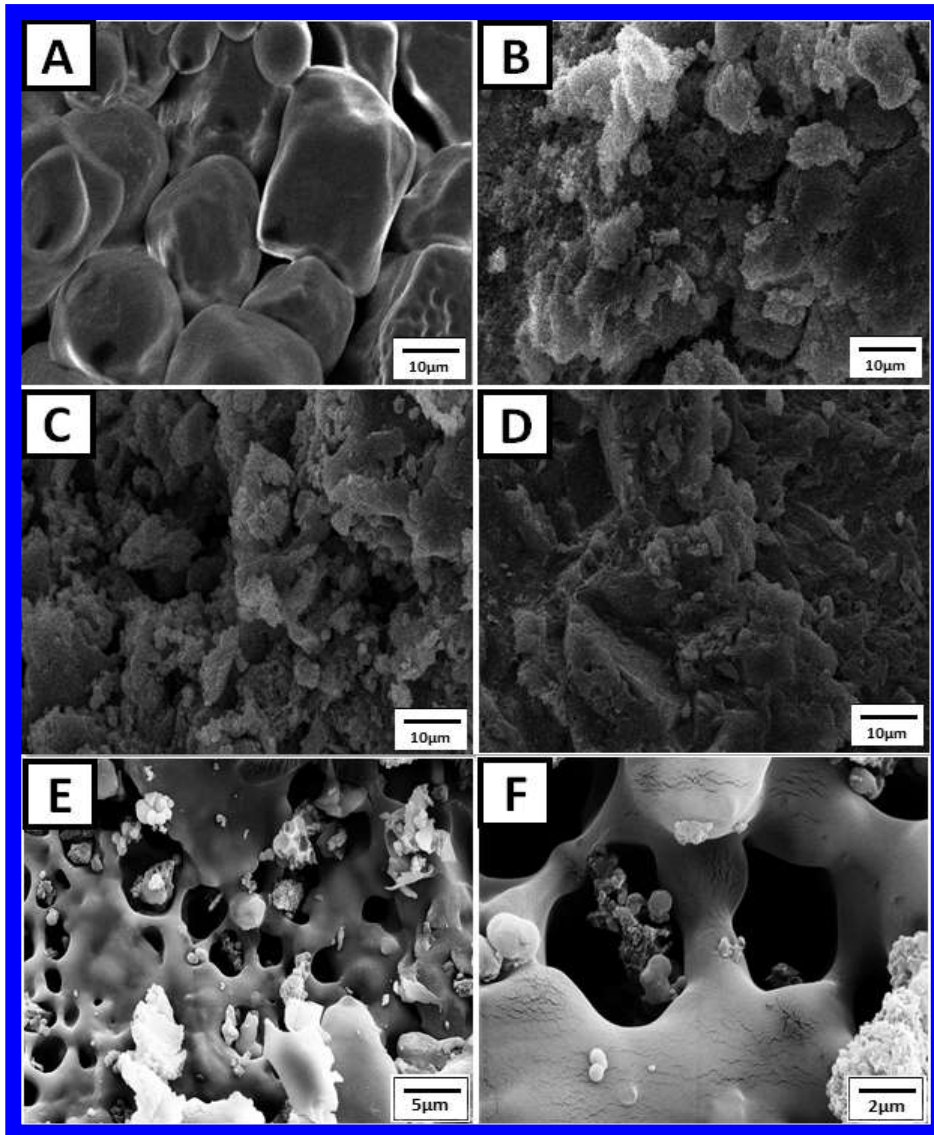


Figure. 4. 34. SEM images of (A) starch and St-g-PLA copolymers at (B) 1:1, (C, E and F) 1:3 and (D) 1:5 St/LA feed ratios. All of products were performed at 100°C, 200 bar, 6 h.

Thus, we can conclude that SEM images are in good agreement with the XRD spectra in the context of the polymer morphology. Both micro-pores and nano cracks in the products make the copolymer a potent candidate as a biomaterial for micro-sized fibers in wound closure materials and as scaffolds for tissue engineering applications due to the high biocompatibility of the grafted poly(lactic acid) [161].

4.3.7. Thermal Behavior of Graft Copolymers

The thermal stabilities of the St-g-PLA copolymers prepared indifferent LA/St ratios were investigated via TGA and DTG techniques (Figure 4.35). The TGA curves showed that the degradation of the graft copolymers occurs at $\sim 300^{\circ}\text{C}$ (Figure 4.35-a), which is remarkably higher than unprocessed starch (270°C) [162].

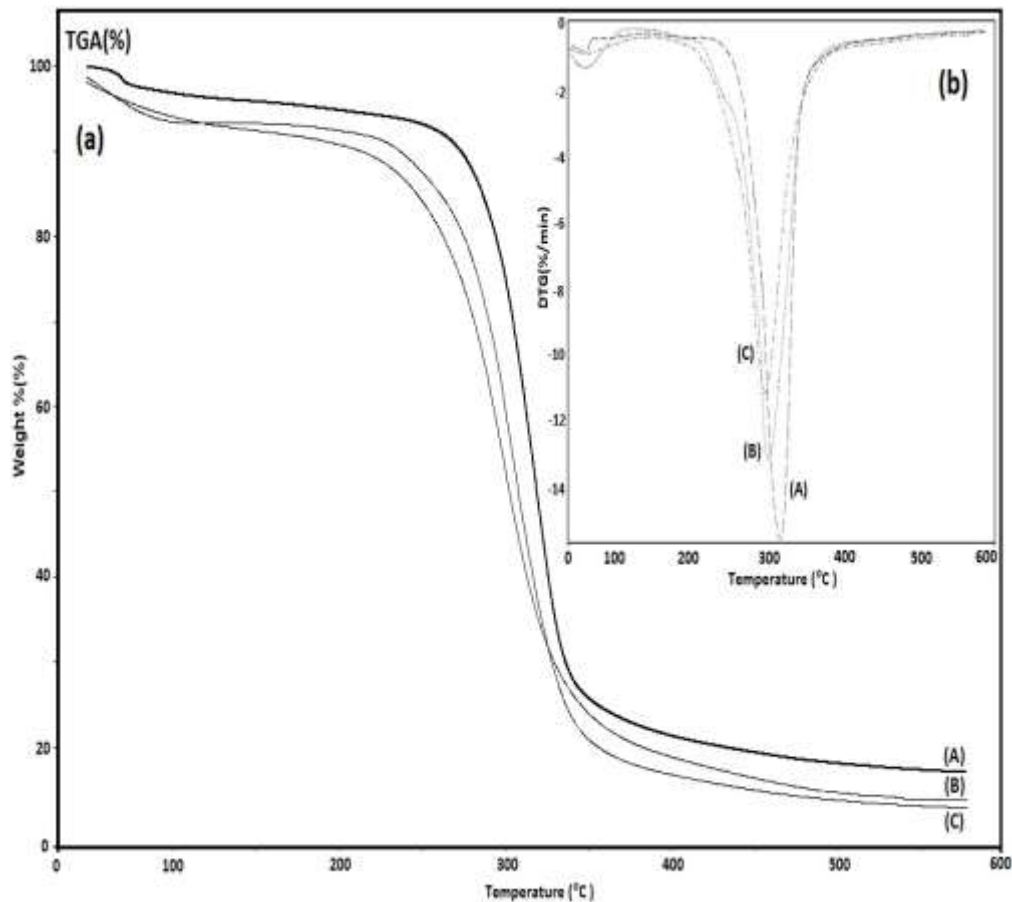


Figure. 4. 35. (a) TGA and (b) DTG thermograms of St-g-PLA copolymers prepared with the following different St/LA feed ratios: (A) 1:1, (B) 1:3 and (C) 1:5.

This may be due to the effect of supercritical carbon dioxide on the intermolecular interactions of several hydrogen bonds in the starch chain during the graft copolymerization with lactic acid [157]. TGA curves depicted two indicative mass loss events that occurred in the copolymer structure. The first mass loss (6%) in the range of 50 to 110°C can be related to the elimination of absorbed water molecules during the copolymerization procedure. Starch degradation was easily detected by the thermal degradation of the copolymer

over a broad temperature range of approximately 190–360°C. From the DTG curves (Figure 4.35-b), it could be concluded that the copolymers decomposed at 290°C, and the rapid and maximum of weight loss was observed at approximately 260–360°C with 60% chain degradation for second stage. Furthermore, the degradation was also reported for native starch, and it was lower than 65% and in the same temperature range. It is clear that the graft copolymerization led to enhancement of the thermal stability of the starch, which was essentially consistent with related literature. According to Xie et al. [13], a reduction in the amount of hydroxyl groups in the backbone of starch, which was confirmed by FTIR spectra, results in an increase in the thermal stability.

4.4. Characterization of St-g-PLA Copolymers Synthesized by Microwave Irradiation

4.4.1. ATR-FTIR Analysis

Figure 4.36 shows the FTIR spectra for starch (A) and St-g-PLA copolymers (B-D). From the FTIR spectrum of starch (Figure 4.36-A), it is clear that the absorption peak at 3351 cm^{-1} can be attributed to the stretching vibration of O-H groups, a peak at 2883 cm^{-1} is due to C-H stretching and the bands between 1000-1200 cm^{-1} are assigned to C-O-C stretching vibration of starch, respectively. The band at 1648 cm^{-1} is due to tightly bound water present in starch [163]. In the spectra of copolymers (Figure 4.36, B-D), the sharp and strong peak at 1732 cm^{-1} corresponds to the carbonyl group of ester, which confirms grafting of PLA chains onto the backbone of starch. The appearance of two peaks at 1228 and 2987 cm^{-1} due to the OH bending and C-H aliphatic groups of the PLA chain compared to starch, clearly indicates that the grafting of PLA chains onto the backbone of starch has successfully taken place by the microwave-assisted copolymerization method.

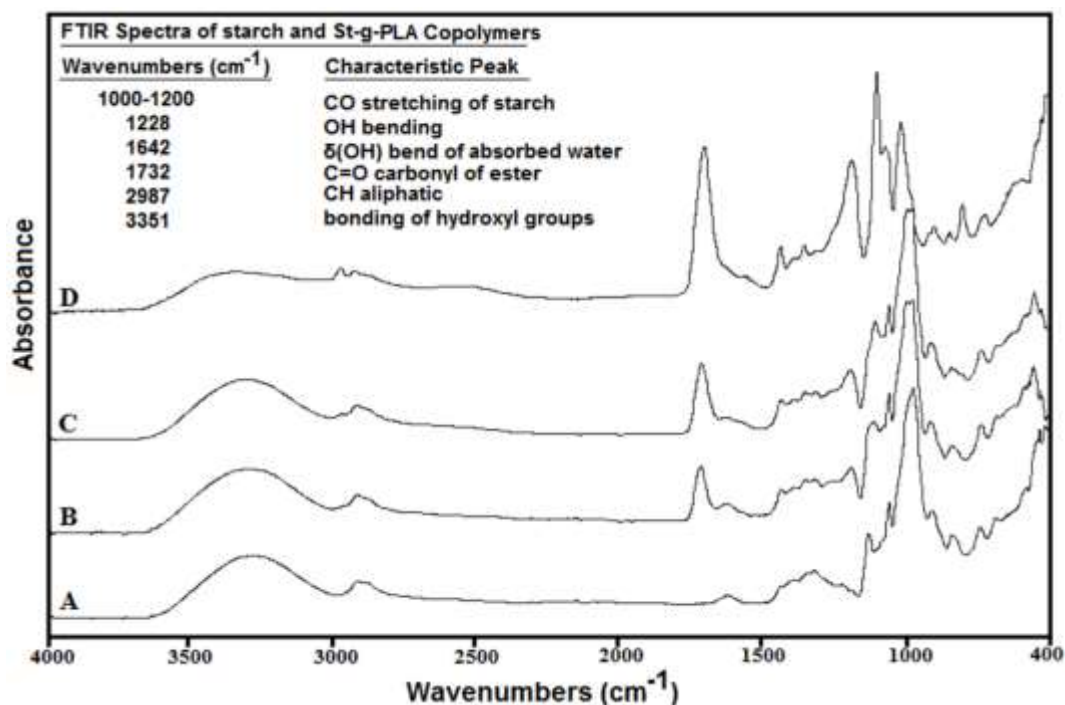


Figure. 4. 36. IR spectra of (A) starch, (B) St-g-PLA at 150W, (C) St-g-PLA at 300W and (D) St-g-PLA at 450W microwave irradiation.

4.4.2. ¹³C CP/MAS-NMR Analysis

To analyze the chemical structure of starch and St-g-PLA copolymer, ¹³C CP/MAS NMR spectroscopy was used (Figure 4.37). In Figure 2A, the region between 55 to 105 ppm is mostly assigned to the carbons of starch backbone (C-1 to C-6). The peaks between 94.73-98.21 ppm are attributed to the C-1 carbons. The peak at 57.68 ppm is related to the C-6 and the peak at 77.28 ppm belongs to the C-4 carbon of starch, respectively. In this region there was also a broad and sharp peak at 67.85 ppm which is assigned to C-2, C-3 and C-5. On the other hand, in Figure 4.37-B, the presence of two peaks at 173.8 and 19.6 ppm are related to the carbonyl group of ester (C=O) and methyl group (CH₃) of the PLA chain which indicated that the graft copolymerization reaction of PLA had successfully occurred on the starch backbone. In addition, the graft copolymerization reaction led to the decrease of the intensity of C-6 and C-2, 3, 5 peaks (Figure 4.37-B), which was because of the degradation of the granular shape of starch under microwave irradiation and the grafting of PLA from C-2, C-3 and C-6 hydroxyl groups. These results are consistent with FTIR, XRD, and SEM data. Finally, the hydroxyl groups in C-6 should be

attacked first by the carboxyl groups of L-lactic acid. This relates to the isomerism of functional groups (hydroxyl), which is proven by the decreasing intensity of C-6 resonances.

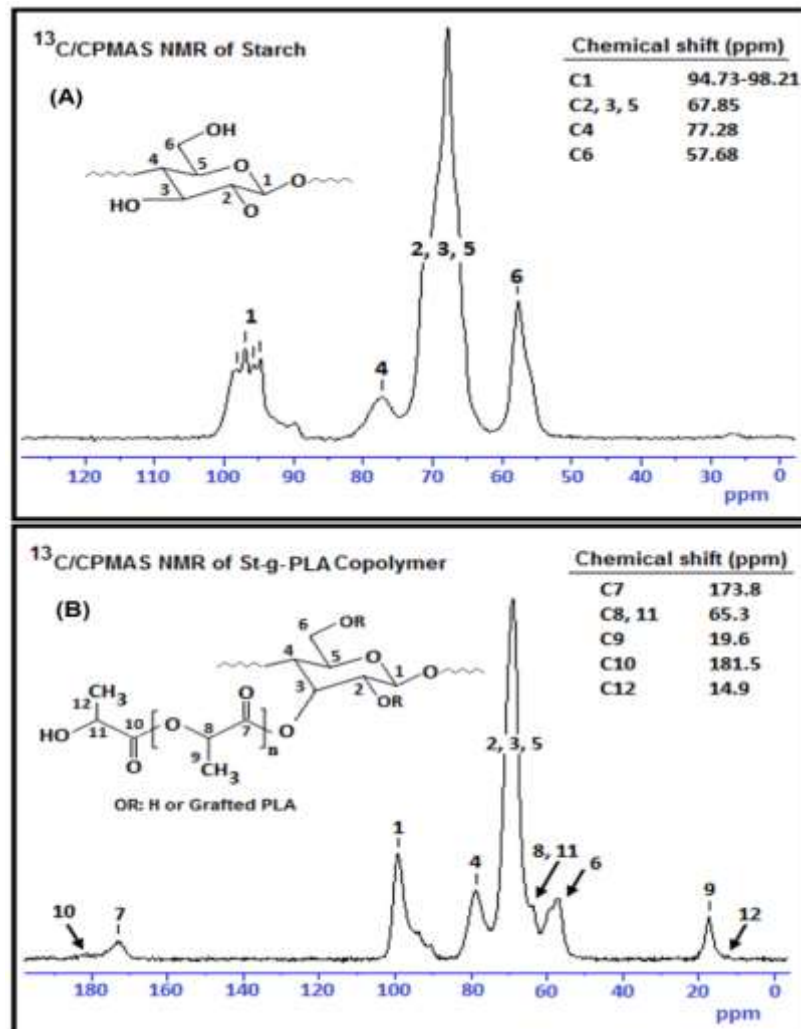


Figure. 4. 37. ¹³C CP/MAS NMR spectra of (A) starch and (B) St-g-PLA at 450W microwave irradiation.

4.4.4. X-ray Diffraction

Wide angle powder X-ray diffraction method (XRD) was used to determine the crystalline and amorphous structures in starch and St-g-PLA copolymers. Figure 4.38 depicts the XRD patterns of unreacted starch (Figure 4.38-A) and St-g-PLA copolymers (Figure 4.38-B-C). In Figure 3A, starch shows a crystalline structure with three diffraction peaks at 14.98°, 17.08° and 23.06° of

2θ . Absorption of microwave energy and transfer of this energy to heat led to the molecular friction of starch, so, excitation by radiation frequencies resulted in the disruption of the starch polar crystalline structure. However, PLA chains in the polymerization medium spoiled the excited starch functional groups and caused the loss of crystallinity. Elimination of starch crystalline peaks in St-g-PLA copolymers (from Figure 4.38, diffraction patterns B to C) is assigned to the grafting of PLA chains and the appearance of a wide broad peak at $2\theta=20.14^\circ$ proved that the St-g-PLA copolymers were existed in amorphous structure.

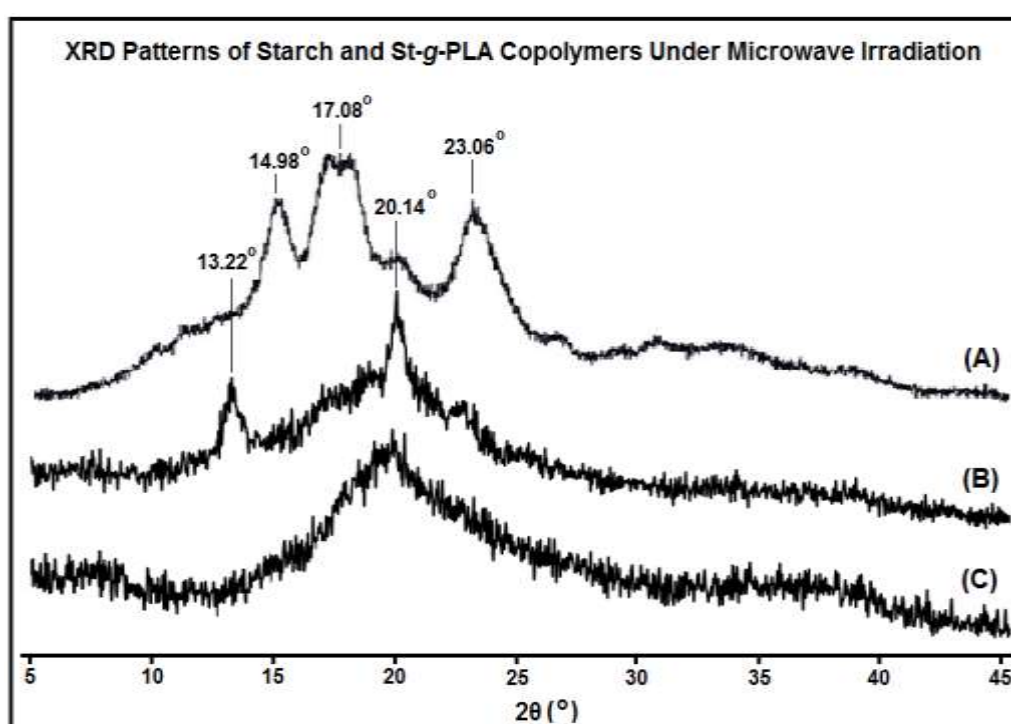


Figure. 4. 38. X-ray diffraction patterns of (A) starch, (B) St-g-PLA at 300W and (C) St-g-PLA at 450 W microwave irradiation.

4.4.5. Surface Morphology: SEM Analysis

Figure 4 shows the morphological analysis of St-g-PLA copolymers under different microwave irradiation that was performed by SEM. The changes in the surface morphology of the copolymers as an effect of PLA grafting with increasing of microwave energy is clearly revealed in the SEM micrographs. As can be seen, from Figure 4.39-A to 4.39-D, an increase in the microwave energy led to the formation of a continuous layer between St and PLA chains corresponding to successful graft copolymerization of LA which in turn affects the regular structural arrangement of starch.

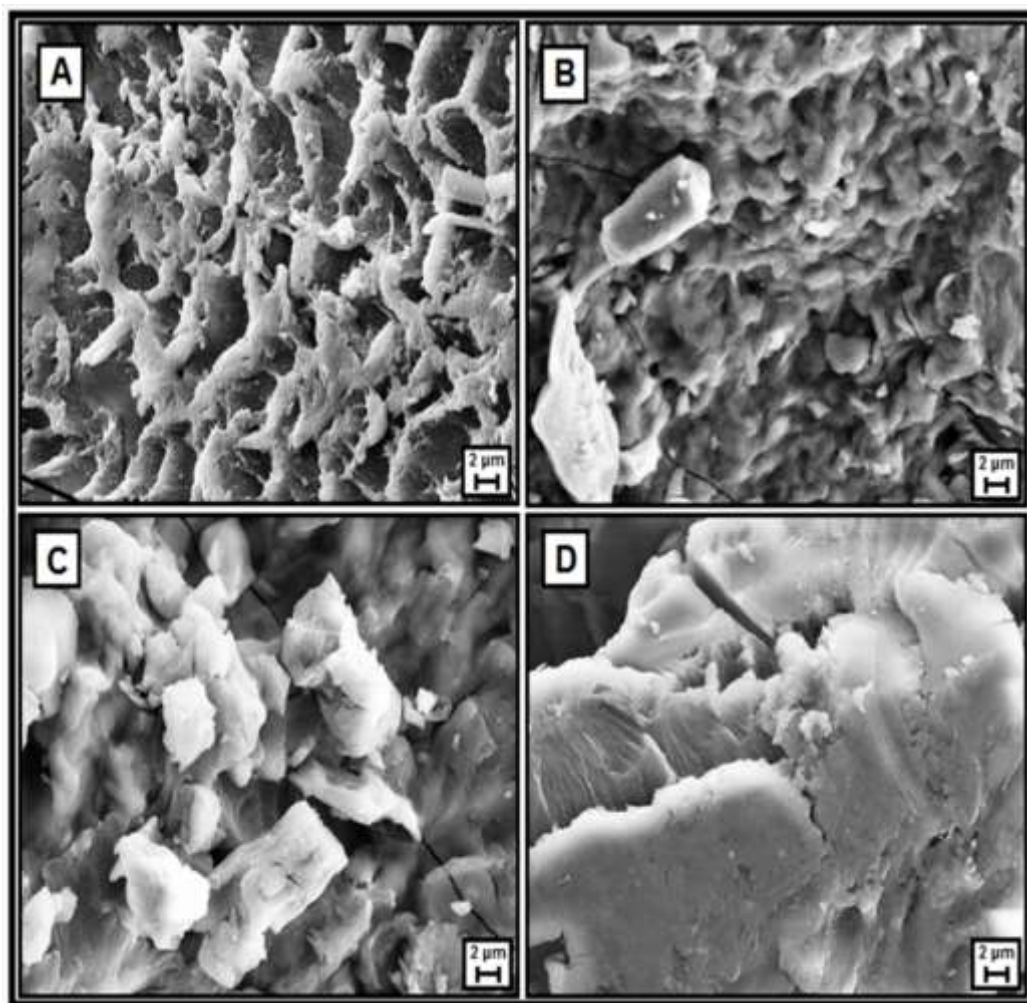


Figure. 4. 39. SEM images of (A) St-*g*-PLA at 300W, (B) St-*g*-PLA at 450W, (C) St-*g*-PLA at 600W and (D) St-*g*-PLA at 750W microwave irradiation.

4.4.6. Thermal Behavior: TGA/DTG Analysis

The thermogravimetric (TGA-DTG) curves of St-*g*-PLA copolymers prepared under different microwave irradiations are shown in Figure 4.40. The maximum thermal degradation of starch occurred at about 270°C with a total weight loss of 84% until 500°C while this value for PLA is higher than starch (~365°C) with total weight loss nearly 100% at ~390°C [150]. The TGA curves showed that the decomposition temperature of the St-*g*-PLA copolymers (Figure 4.40-A-D) begins at a higher temperature than starch (~330°C) and the completion of decomposition occurs at temperature near that of PLA. This demonstrates that the addition of LA and microwave irradiation causes a gradual thermal enhancement of St-*g*-PLA copolymers that can be attributed mainly to good

starch-lactic acid interactions and the thermal destruction of starch granules. As shown in Figure 5, there was two significant mass losses in the TGA curves. The first range (50-160°C) is assigned to the removal of adsorbed water molecules presented in starch and corresponds to the first step of the starch thermal degradation-dehydration process.

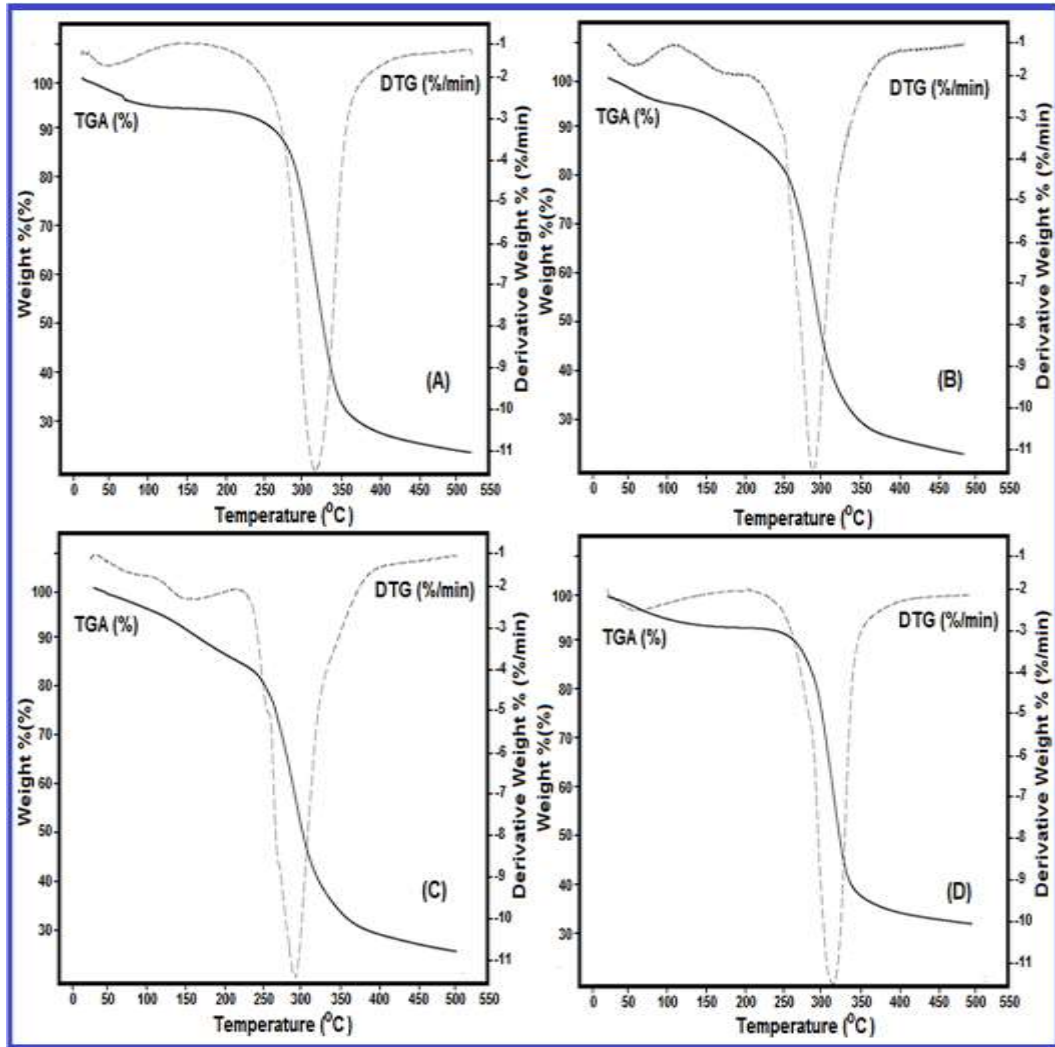


Figure. 4. 40. TGA and DTG diagrams of St-g-PLA Copolymers. (A) at 150 W, (B) at 300 W, (C) at 450 W and (D) at 600 W microwave irradiation.

At the second stage of thermal degradation (190-450°C), according to Liu et al., [164] heating of St-g-PLA copolymer above 300°C produced volatile products (CO, CO₂, H₂O, etc.) which caused the breakdown of strong bonds of the starch backbone and PLA polyester chains. Furthermore, it is clear that in the presence of microwave energy, 20% aqueous solution of LA and NaOH solution in polymerization media caused the irreversible gelatinization of starch

granules and changes included the swelling of starch polar molecule granules and, finally, there was an appearance of an amorphous copolymer with the grafting of LA on the starch backbone. However, this hypothesis indicates an increase in the thermal stability of St-*g*-PLA copolymers and is in agreement with SEM and XRD data.

4.4.7. Effect of Reaction Conditions on Graft Copolymerization

The effect of variable reaction parameters on grafting PLA mole percent was observed by changing the NaOH concentration (0.1-0.5 M), power of radiation (150-750 W) and monomer ratio (0.5-7 w/w) and summarized in Table 4.6, Figure 4.41, and figure 4.42. According to Pekel et al., the grafted PLA mole fraction (in mole %) of monomers (starch and lactic acid) in St-*g*-PLA copolymer was calculated using the absorption bands from the starch and LA units in the copolymer, and the band absorption value ratios between characteristic bands of 1732 cm⁻¹ (for LA C=O ester peak) and 1336 cm⁻¹ (for St -CH₂ peak) were employed [150].

To optimize the effect of NaOH concentration as co-catalyst in reaction media, a constant temperature regime (100°C) was applied and the duration of radiation (sec) was determined by observing the formation of a brownish viscous product. It was found that grafted PLA (mole %) increased with the decrease of the duration of radiation up to 0.4 M and, after this point, both of them decreased (Table 4.6). This may due to the large number of active radical groups (ONa⁺) on the C-2, 3, 6 carbons of starch during gelatinization of starch and the presence of excess amounts of LA resulting in a higher grafted PLA mole (%) at 0.4 M. On the other hand, grafting values over 0.4 M tend to reduce this phenomenon. It is believed that the accumulation of high amounts of NaOH on the starch backbone causes PLA chain scission leading to the formation of oligo and homopolymers of LA.

In Figure 4.41-A, the increase in the power of radiation from 150-750 W at fixed concentration of NaOH (0.4 M) and monomer ratio (amount of LA: 5g) showed that the gelatinized polar structure of starch excited with microwave power and the amylose-amylopectin separation occurred is evidence of the formation of more excited groups (free radicals) and resulted in grafting of PLA. The first

increase in the grafted PLA value 450 W and then a decrease may be due to the disruption of starch macromolecule structure and some depolymerization of the PLA chain.

Table. 4. 6. Synthesis parameters of St-g-PLA copolymers under different conditions.

Copolymers	Amount of LA (g)	NaOH Concentration (M)	MW Power (W)	Duration of Radiation (sec)	Grafted PLA (mole %)
Optimized effect of NaOH concentration (M) @ constant temperature (100°C) in microwave assisted synthesis (amount of starch=1 g)					
St-g-PLA	5	0.1	-	360	32 (±1.64)
	5	0.2	-	290	41 (±2.05)
	5	0.3	-	205	45 (±2.21)
	5	0.4	-	335	51 (±2.55)
	5	0.5	-	220	48 (±2.34)
Optimized effect of power of radiation in microwave assisted synthesis (amount of starch=1 g)					
St-g-PLA	5	0.4	150	556	40 (±2.03)
	5	0.4	300	540	57 (±2.83)
	5	0.4	450	337	62 (±3.12)
	5	0.4	600	305	49 (±2.45)
	5	0.4	750	195	49 (±2.42)
Optimized effect of monomer ratio in microwave assisted synthesis (amount of starch=1 g)					
St-g-PLA	0.5	0.4	450	89	38 (±1.91)
	1	0.4	450	110	41 (±2.04)
	3	0.4	450	200	46 (±2.33)
	5	0.4	450	336	62 (±3.16)
	7	0.4	450	448	50 (±2.53)

Figure 4.41-B shows the effect of monomer ratio in the range of 0.5-7g (amount of LA) on the optimized concentration of NaOH (0.4 M) and radiation power (450 W). The increase in monomer ratio led to increasing grafted PLA mole fraction and absorption of more microwave energy. However, the decrease in grafted PLA value may be due to the tendency of LA toward homopolymerization because of the excess amount of LA suitable for homopolymerization. Thus, the maximum grafted PLA mole fraction of 62% was obtained at a 0.4 M concentration of NaOH, 450 W power of radiation and 5g of LA.

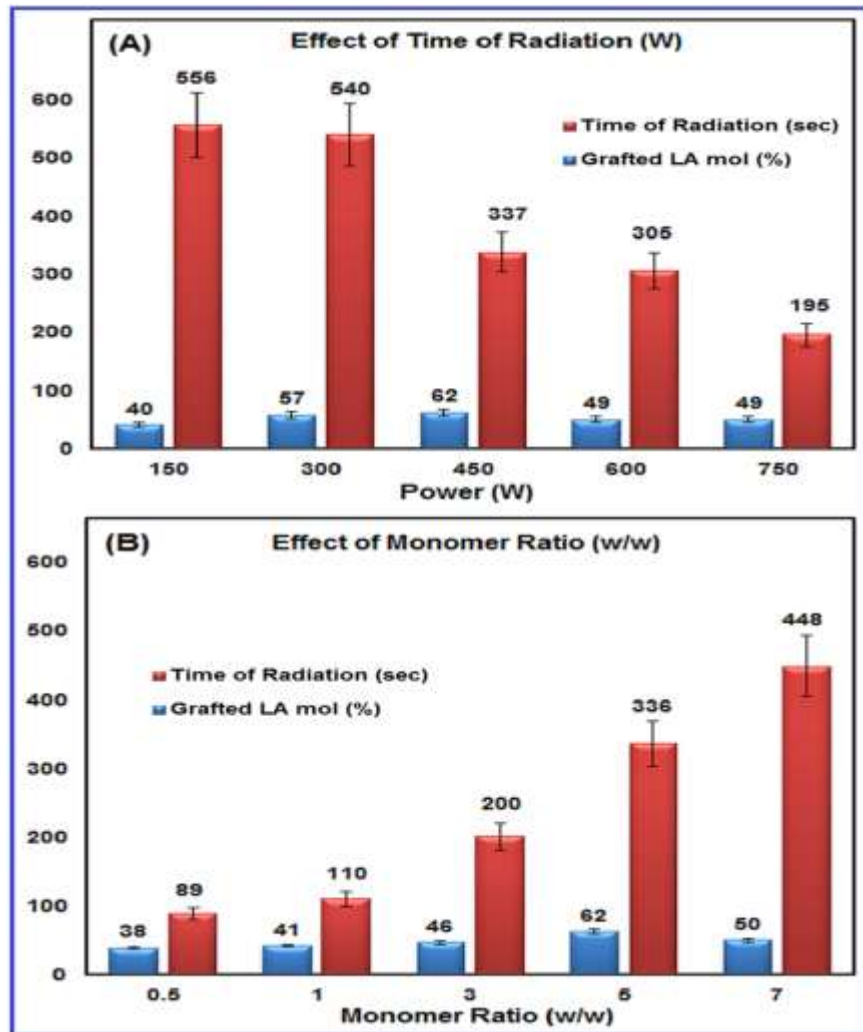


Figure. 4. 41. The effect of power of radiation (A) and monomer ratio (B) on duration of radiation and grafted PLA mole fraction (%).

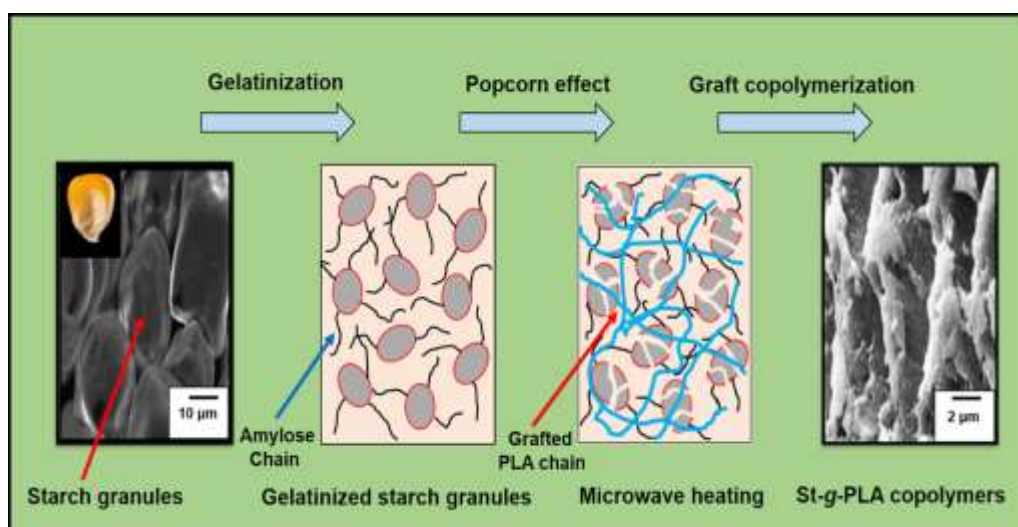


Figure. 4. 42. Microstructural model of St-g-PLA copolymers synthesized by microwave irradiation.

4.5. Characterization of St-*g*-PLA Copolymers and St-*g*-PLA/Organoclay Nanocomposites Synthesized Through Shear Mixing and Reactive Extrusion Methods

4.5.1. ATR-FTIR Spectroscopy

In this study, FT-IR spectroscopy has been utilized to confirm the chemical structures of the St-*g*-PLA copolymers with various compositions, grafted PLA mol percent, especially complexation of octadecyl amine-intercalant with the PLA unit and St-*g*-PLA/organoclay nanocomposite structure via $-\text{C}=\text{O}\dots\text{NH}_2-$ and $-\text{COOH}\dots\text{NH}_2-$ complex-formations, respectively. The obtained results are illustrated in Figure 4.43 and 4.44. The characteristic peaks at $1736\text{ (s)}\text{ cm}^{-1}$ are associated with the ester C=O groups of grafted PLA fragments which intensity of graft copolymers compositions containing the polyester groups increased with the increasing of step numbers of extrusion (Figure 4.43 and 4.44). The appearance of two peaks at 1228 and 2994 cm^{-1} due to the OH bending and C-H aliphatic groups of the PLA chain compared to starch, clearly indicates that the grafting of PLA chains onto the backbone of starch has successfully taken place by the shear mixing and reactive extrusion copolymerization methods (Figure 4.43). The grafted PLA mole fraction (in mole %) of monomers (starch and lactic acid) in St-*g*-PLA copolymer was calculated using the absorption bands from the starch (1227 cm^{-1} for St $-\text{CH}_2$ peak) and LA units (1736 cm^{-1} for LA C=O ester peak) in the copolymer [163] (Figure 4.43). The ester carbonyl and carboxyl groups from nanocomposite systems are highly responsive to ionic interactions. 1171 cm^{-1} (s), 1039 cm^{-1} (s-broad) and 924 cm^{-1} (m) bands related to Si-O-Si vibrations and Si-O stretching from delaminated clay mineral layers. (Figure 4.44).

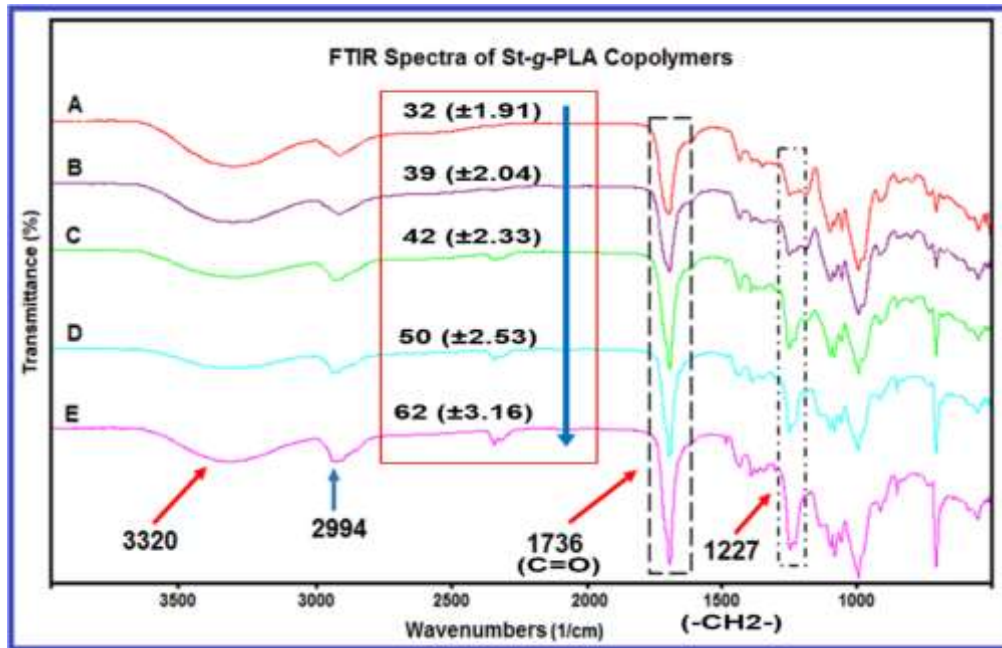


Figure. 4. 43. FTIR spectra of (A) St-g-PLA copolymer synthesized through shear mixer, (B) St-g-PLA copolymer blending by twin-screw extruder (1st step), (C) St-g-PLA copolymer blending by twin-screw extruder (2nd step), (D) St-g-PLA copolymer blending by twin-screw extruder (3rd step), St-g-PLA copolymer blending by twin-screw extruder (4th step).

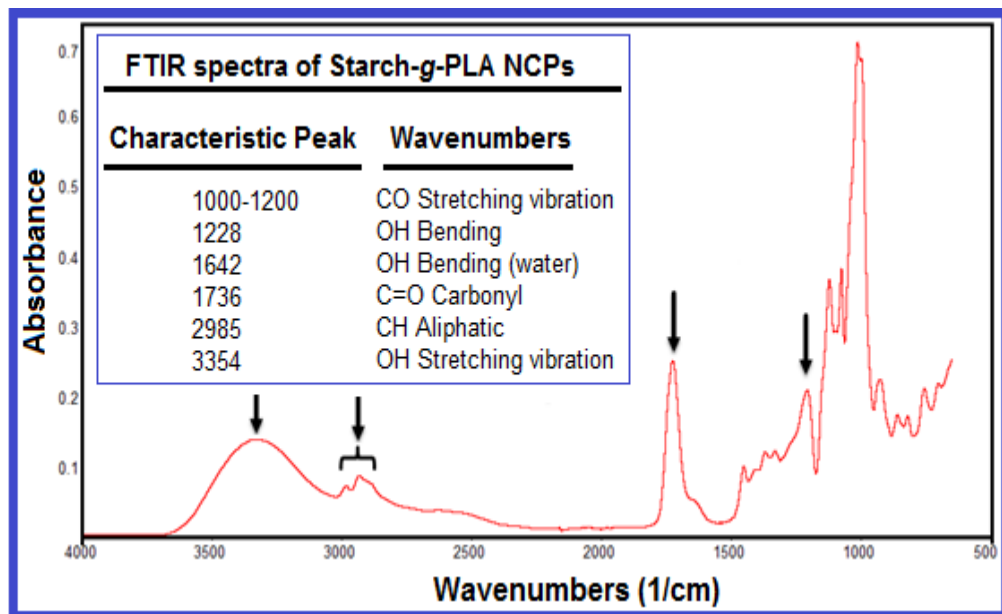


Figure. 4. 44. FTIR spectra of St-g-PLA/organoclay nanocomposite.

4.5.2. ^{13}C CP/MAS-NMR Analysis

The chemical structures of St-g-PLA and St-g-PLA/organoclay nanocomposites were also confirmed by ^{13}C CP/MAS-NMR analysis (Figure 4.45 and 4.46). In Figure 4.45, the presence of two peaks at 170.9-172.6 ppm (Figure 4.45) and 171-180.6 ppm (Figure 4.46) are related to the carbonyl group of ester (C=O). The peaks at 54.9 ppm (Figure 4.45) and 58.6 ppm (Figure 4.46) are attributed to methyl group (CH_3) of the PLA chain which indicated that the graft copolymerization reaction of PLA had successfully occurred on the starch backbone. In addition, the graft copolymerization reaction led to the decrease of the intensity of C-6 and C-2, 3, 5 peaks (Figure 4.45), which was because of the degradation of the granular shape of starch under shear mixing and the grafting of PLA from C-2, C-3 and C-6 hydroxyl groups. So, these results are consistent with FTIR, SEM data [163].(REF..Supercritic) The appearance of new chemical shifts at 14.28 ppm and 14.42 ppm (two types of C=O groups) were associated with the formation of new amide and carboxyl groups (complexes) as a result of the reaction of LA units with the octadecyl amine intercalant. Two signals from the carbon atoms of C=O groups (175 and 164 ppm) presented in the ^{13}C -NMR spectra and also confirmed the FTIR results. (Figure 4.46)

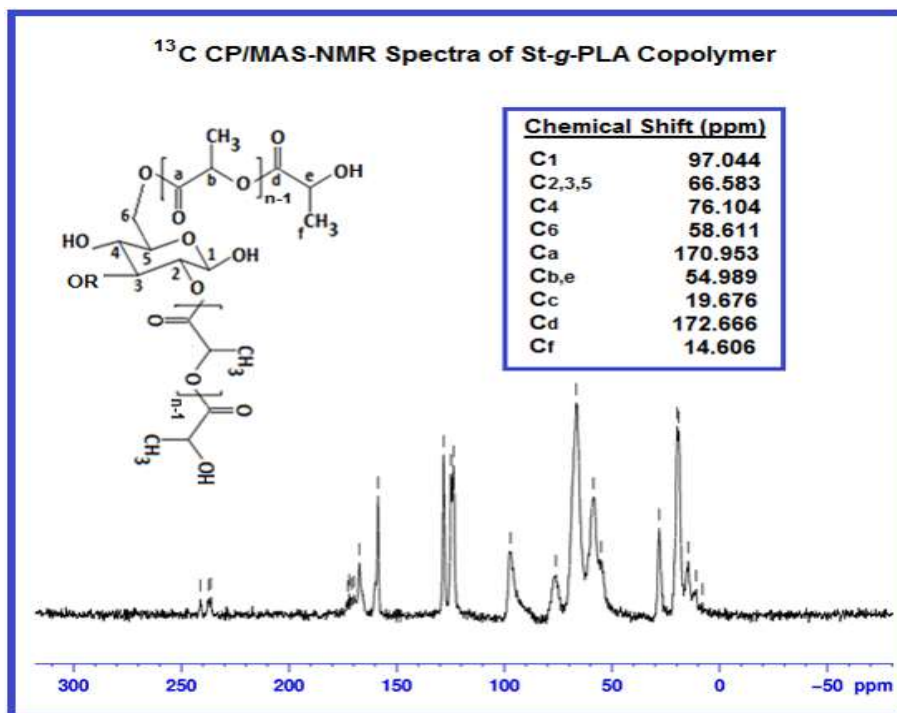


Figure. 4. 45. ^{13}C CP/MAS-NMR spectra of St-g-PLA copolymer.

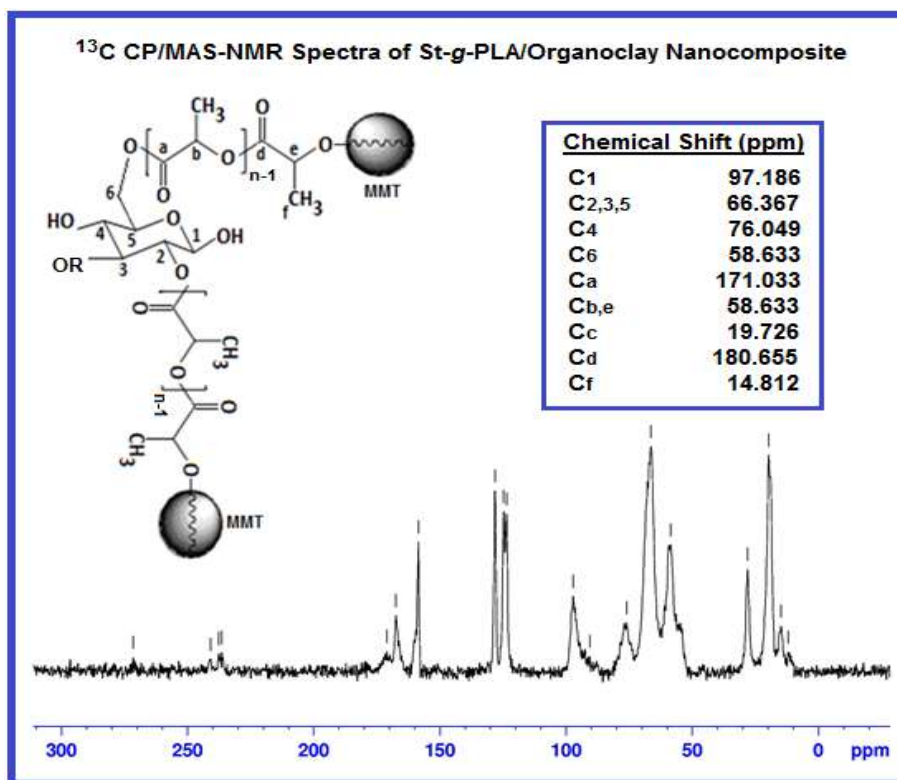


Figure. 4. 46. ¹³C CP/MAS-NMR spectra of St-g-PLA/organoclay nanocomposite.

4.5.3. X-ray Diffraction

The comparative analysis of the XRD patterns (to evaluate the physical structures, X-ray reflection parameters and amorphous and crystallinity areas) collected from the St-g-PLA copolymer and St-g-PLA/organoclay nanocomposites fabricated with shear mixer and reactive extrusion indicates the presence of X-ray reflection peaks from different fractions of the graft copolymer and organoclay (Figure 4.47).

During the processing of St-g-PLA copolymerization under turbo-mixing conditions, gelatinization was performed as the cumulative irreversible changes that occur to a starch granule in the presence of moisture (by LA with 20% aqueous solution content and), heat and shear. The changes include granule swelling due to absorption of moisture in the amorphous regions of the granule, leaching of small molecular weight polymers including amylose and loss of the crystalline order that cause both micropores and nano cracks in the starch

granules and finally confirms that the copolymer has a predominantly amorphous microstructure (Figure 4.46-A)

The clay characteristic reflections approximately 2θ values of $2-10^\circ$ exhibited a shift to a lower region, and their full disappearance (organoclay=5.0%) was observed confirming the presence of the intercalating/exfoliating nanostructures. The incorporation of organoclay slightly increases the intensity of the reflections becomes relatively stronger, which confirms the partial crystallization of the St-g-PLA/organoclay nanocomposites copolymer, especially at high organoclay loadings (Figure 4.47-B).

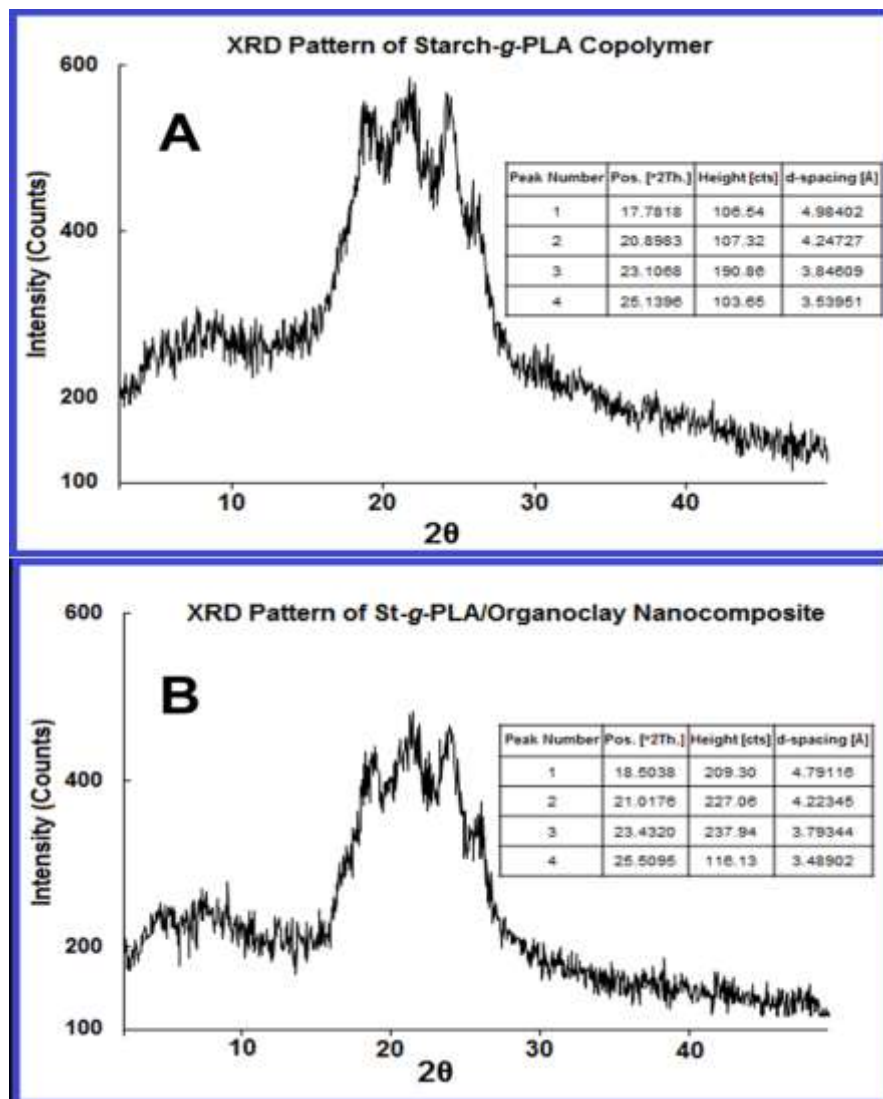


Figure. 4. 47. X-ray diffraction patterns of (A) St-g-PLA copolymer and (B) St-g-PLA/organoclay nanocomposite.

4.5.5. SEM Analysis

SEM analysis method was widely utilized for the investigation of surface morphology-property relationships of the starch granule shape and the final product on various length scales and provide direct evidence for morphology changes as a result of both chemical and physical interfacial interactions occurring between the polymer chains. The obtained SEM images of St-*g*-PLA copolymers prepared in the presence of different amounts of LA ratio as a reactive monomer by shear mixing and reactive extrusion methods were performed (Figure 4.48).

From Figure 4.48-A and B, the changes in the surface morphology of starch granules and the microstructure of St-*g*-PLA, it could be explained by considering that the applying of shear in the graft copolymerization led to micropores and nano sized cracks due to the moisture and heat in the polymerization media. As can be seen, Figure 4.48-C to F, it is evident that the granular morphology of starch is lost after grafting and transformed into lacy morphology by reactive extrusion method. This method increased the compatibility of the two phases, and the hydrophilic groups of starch and LA interacted with high value of interfacial adhesion that can be easily seen in Figure 4.48-E and F. Finally, the longer the extrusion step, the higher the amorphous ratio and the higher the interfacial attractions.

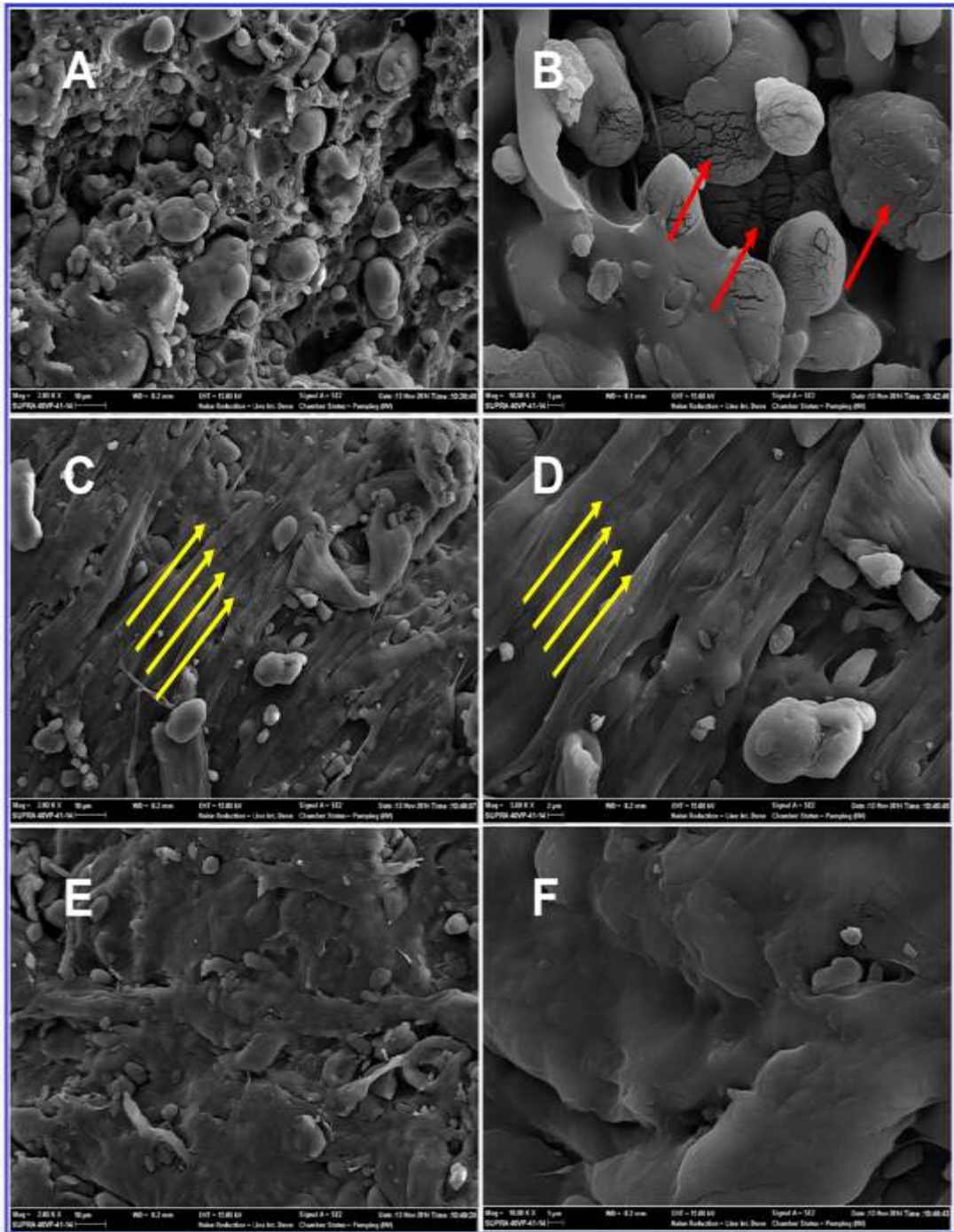


Figure. 4. 48. SEM images of St-g-PLA copolymers. Scale: (A) St-g-PLA copolymer synthesized through shear mixer; 2.00k x, 10 μm , (B) St-g-PLA copolymer synthesized through shear mixer; 10.00k x, 1 μm , (C) St-g-PLA copolymer blending by twin-screw extruder (1st step); 2.00k x, 10 μm , (D) St-g-PLA copolymer blending by twin-screw extruder (1st step), 5.00k x, 2 μm , (E) St-g-PLA copolymer blending by twin-screw extruder (4th step); 2.00k x, 10 μm and (F) St-g-PLA copolymer blending by twin-screw extruder (4th step); 10.00k x, 1 μm .

4.5.6. Thermal Analysis, Influence of the Processing Parameters and Composition

Thermal decomposition of starch during the processing is an important factor to estimate the behavior of starch based products. Thermogravimetric analysis (TGA) has been the conventional and most popular technique used to study the thermal stability and decomposition of starches [165]. A typical process of weight loss during heating of cornstarch, as measured by TGA technique is shown in Figure 4.49.

The TGA/DTG curves show that there are two major weight loss phases. The first phase represents the evaporation/dehydration of water that begins immediately after the temperature is increased and finishes at around 100°C. As can be concluded from the curves, the percentage weight loss in the first phase depends on the moisture content of the starch. In the second weight loss phase, thermal decomposition of starch has been occurred, which commences at around 304°C. From the past reported works [163] it can be understood that the evaporation of all of the initial water content from sample prior to reaching the decomposition temperature does not affect the onset of decomposition temperature.

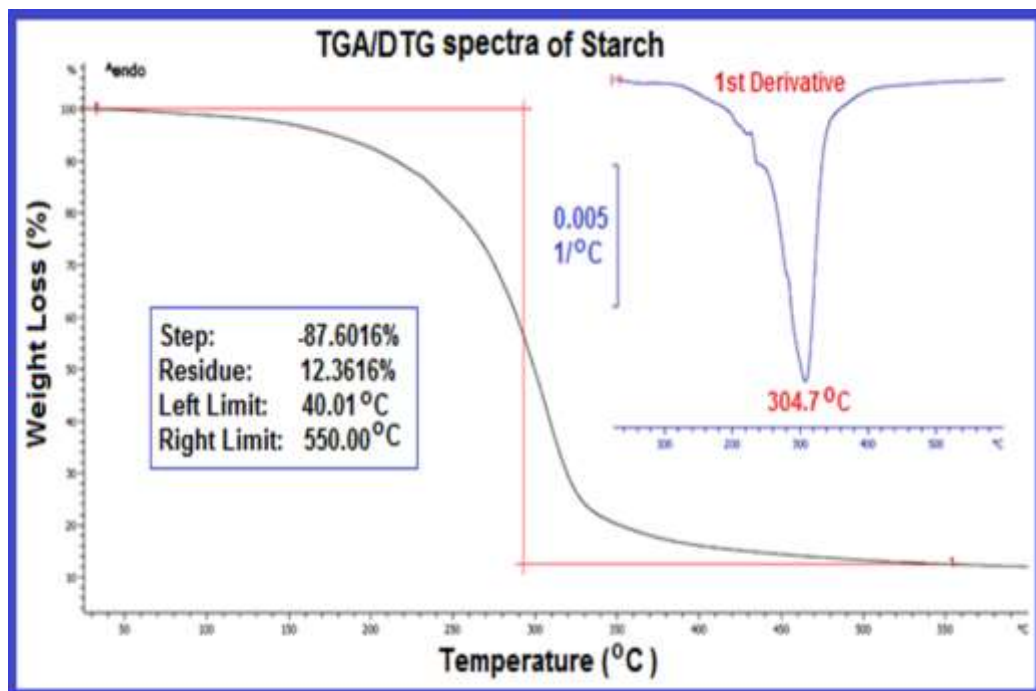


Figure. 4. 49. TGA-DTG curves of pristine starch.

The onset temperature of the degradation reaction (T_{onset}) and the temperature interval to which it extends (ΔT_d) for each sample are shown in Table 4.7, and some of the TGA curves of St-*g*-PLA and St-*g*-PLA/organoclay nanocomposites are presented in Figure 4.49 and 4.50, respectively. It can be seen that in addition to the above zones of weight loss for starch (Figure 4.50), have two extra zones of weight loss (340°C–460°C and 460°C–550°C), due to the grafted PLA chains (Table 4.7). As can be concluded from the TGA data in Table 4.7 and as illustrated in Figure 4.50, decomposition temperatures of the St-*g*-PLA/organoclay nanocomposites decreased linearly with increasing filler content. The decomposition of both the starch and St-*g*-PLA copolymers produced small polar molecules, which resulted in the breakdown of the polyester chains (PLA). Furthermore, decomposition temperatures of the St-*g*-PLA and St-*g*-PLA/organoclay nanocomposites blends were generally lower than those of the starch, suggesting that grafting of PLA and the presence of intercalated/exfoliated LA-organoclay have a greater effect on the thermal stability of the copolymers (Figure 4.51) [150].

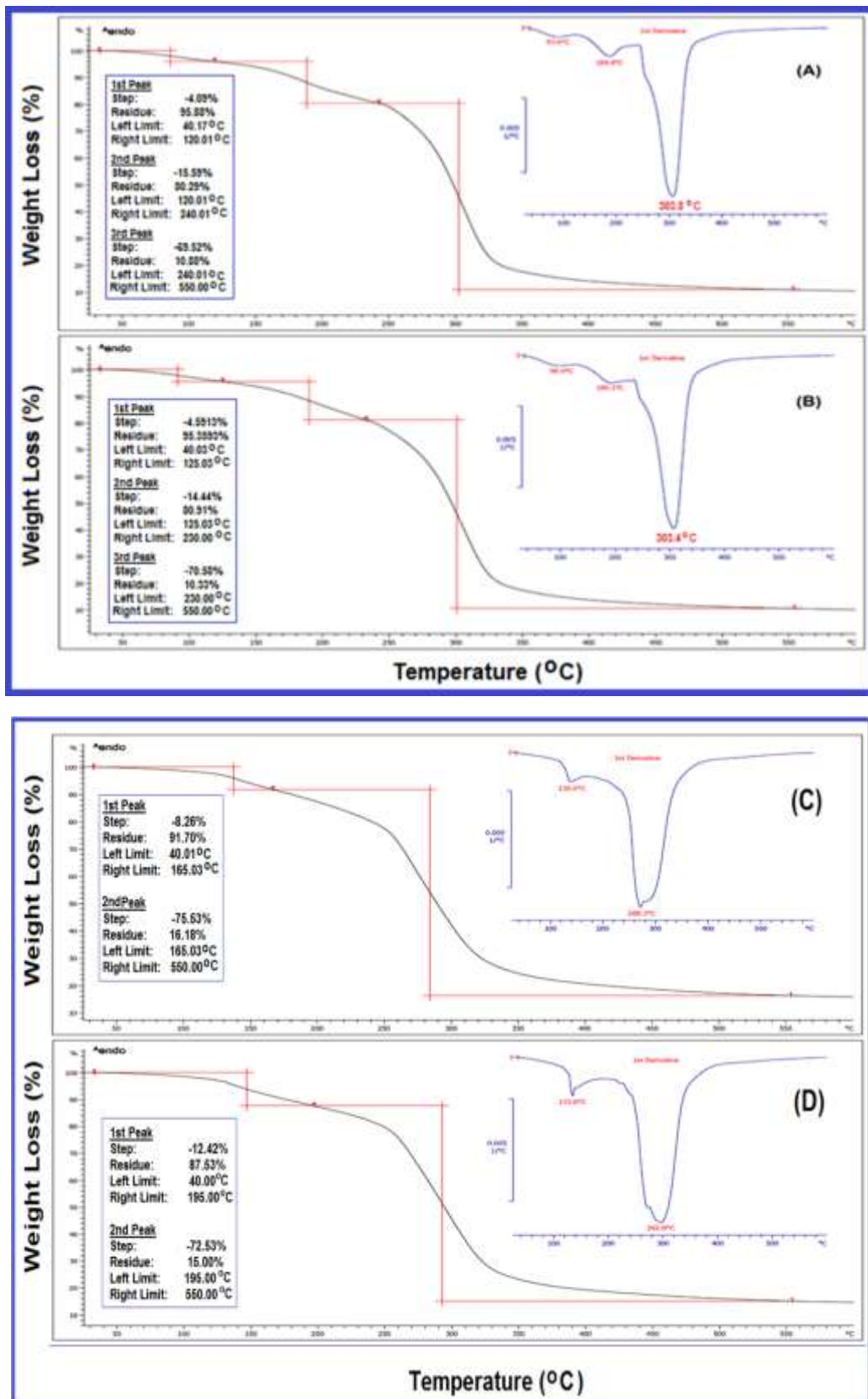


Figure. 4. 50. TGA-DTG curves of St-g-PLA copolymers. (A) blending by twin-screw extruder (1st step), (B) blending by twin-screw extruder (2nd step), (C) blending by twin-screw extruder (3rd step), (D) blending by twin-screw extruder (4th step).

Table. 4. 7. Degradation parameters of starch and St-g-PLA copolymers.

Sample	First Run	Second Run	Third Run	Degred. Point	1 st derivative Min. Point
Starch	Resi: 12.36%				
	L.T: 40 °C R.T: 550 °C	-	-	304.7°C	-
1	Resi: 95.88%	Resi: 80.28%	Resi: 10.76%		
	L.T: 40.17 °C R.T: 120 °C	L.T: 120 °C R.T: 240 °C	L.T: 240 °C R.T: 550 °C	303.8°C	184.9°C
2	Resi: 95.35%	Resi: 80.91%	Resi: 10.33 %		
	L.T: 40 °C R.T: 125 °C	L.T: 125 °C R.T: 230 °C	L.T: 230 °C R.T: 550 °C	303.4°C	190°C
3	Resi: 91.70%	Resi: 16.17%			
	L.T: 40 °C R.T: 165 °C	L.T: 165 °C R.T: 550 °C	-	268.4°C	139°C
4	Resi: 87.53%	Resi: 15%			
	L.T: 40 °C R.T: 195 °C	L.T: 195 °C R.T: 550 °C	-	292.8°C	133.8°C

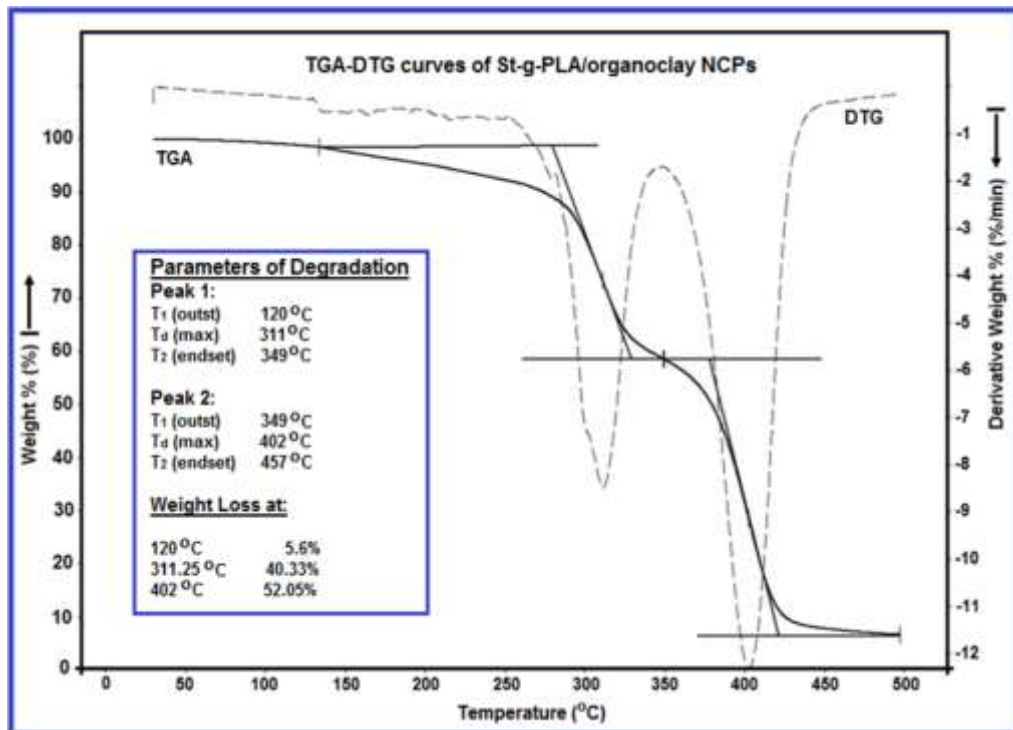


Figure. 4. 51. TGA-DTG curves of St-g-PLA/organoclay nanocomposite.

4.5.7.1. Mechanical Properties

The mechanical behavior of St-*g*-PLA and St-*g*-PLA/organoclay bio-nanocomposites was evaluated and tensile test results are reported in Table 4.8. The addition of organoclay as a matrix component into copolymerization media (Sample 3), produces an increase in Young's modulus values with respect to St-*g*-PLA, enhancing the reinforcement effect exerted by organoclay crystals (in agreement with XRD data). Moreover, an evident decrease in the elongation at break of the St-*g*-PLA based copolymer was also measured, thus confirming the brittle nature of these formulations (sample 1). The decrease of elongation at break with the addition of excess amount of LA in copolymerization media is a common trend observed in thermoplastic composites and PLA based bio-nanocomposites[166]. The elongation at break is affected by the volume fraction of the added organoclay phase, the dispersion in the intercalated/exfoliated organoclay-LA matrix (reinforcement). Finally, a well-developed polymer/clay nanocomposite results in highly increased mechanical strength in St-*g*-PLA/organoclay nanocomposite (Sample 3) compared to the St-*g*-PLA copolymer matrix (Sample 1 and 2) since uniform dispersion of the nano-sized clay particles produces an ultra-high interfacial area and ionic bonds between the nanoclay and main polymer structure [68, 69].

Table. 4. 8. Tensile properties of St-*g*-PLA and St-*g*-PLA/organoclay nanocomposite films

Samples	Tensile Strength (N/mm²)	Elongation at Break (%)	Young Modulus (N/mm²)
	MD	MD	MD
Sample 1	52.4	3.6	140
Sample 2	23	4.1	311
Sample 3	82.4	5.2	531

4.5.7.2. Permeability Properties

- Gas (CO₂ and O₂) Permeability

The O₂ and CO₂ permeability of St-*g*-PLA and St-*g*-PLA/organoclay nanocomposites are reported in Table 4.9 and Table 4.10, respectively. Table 4.9 shows that the O₂ permeability of samples were lower than those for CO₂, resulting in the selective action of starch based films components on gas permeability. There are a lot of works in the literature that reported the higher solubility of CO₂ in the St-*g*-PLA films [167]. In the present work the addition of intercalated/exfoliated organoclay-LA matrix improved barrier properties of St-*g*-PLA/organoclay nanocomposites films by avoiding pores and cracks as well as the shear rate applied from the turbo mixer. The obtained results are in agreement with SEM and XRD data. Permeability of St-*g*-PLA films was high because of the presence of pores and cracks in starch backbone and final copolymer structure (see SEM images). The increase of crystallinity with addition of organoclay-LA matrix markedly reduced the effect of pores. For example starch films CO₂ permeability decreased from 29.2x10⁻¹⁰ at initial time to 8.9x10⁻¹⁰ (cm³ m⁻¹ sec⁻¹ Pa⁻¹) after 20-d storage [167]. Synthetic materials show lower gas permeability like LDPE with 2.16x10⁻¹¹ for O₂ and 9.45x10⁻¹¹ (cm³ m⁻¹ sec⁻¹ Pa⁻¹) for CO₂ but have low selectivity between CO₂ and O₂, but the gas permeability of starch based films depend on the integrity of the film, the ratio between the partner polymer and the type/morphology of organoclay in the case of bio-nanocomposites.

Table. 4. 9. O₂ permeability of St-*g*-PLA and St-*g*-PLA/organoclay nanocomposite films.

Sample	Thickness (mic)	O₂ Permeability (cc/m².day)
Sample 1	120	4.73
Sample 2	145	2.84
Sample 3	152	3.2

Table. 4. 10. CO₂ permeability of St-g-PLA and St-g-PLA/organoclay nanocomposite films.

Sample	Thickness (mic)	CO₂ Permeability (cc/m².day)
Sample 1	120	5.73
Sample 2	145	1.42
Sample 3	152	2.9

- H₂O Vapor Permeability

The water vapor permeability (WVP) of all films are presented in Table 4.11. It was found that the organoclay addition as a matrix polymer caused a significant decrease in the water vapor permeability of graft copolymers (Sample 3). The decrease in water vapor permeability of the products is one of the most important factors for enhancing the possibilities for industrial application especially in the case of fresh fruits and vegetables by retarding the moisture loss. The decrease in the starch based nanocomposites film permeability by the incorporation of nanoclay has been frequently reported [168]. The distribution of organoclay-LA matrix in copolymer structure create multiple layers by nanosized clay platelets that caused to form a torturous path against the force gases due to the distribution of impermeable clay layers [169].

Furthermore, the optimum WVP rate is a balance between hydrophilic-hydrophobic ratio and crystalline-amorphous ratio. Thus, the permeability of nanocomposite films reported by determining of two important factors: diffusion and solubility coefficients. Effectively, reducing the transport of water by diffusion (incorporation of nanoclays, and absorption of water by hydrophilic part of copolymer) through a polymer reduces its permeability. In addition, the degree of dispersion of the clay within the polymer matrix is related to the resulting barrier properties. On the other hand, reducing the solubility coefficient in the film can also cause a significant reduction in the water vapor permeability [68, 168].

Table. 4. 11. Water vapor permeability (WVP) of St-g-PLA and St-g-PLA/organoclay nanocomposite films.

Sample	Thickness (mic)	WVP [x10¹⁰(g/m.s.Pa)]
Sample 1	120	8.4
Sample 2	145	12.87
Sample 3	122	3.2

4.5.7.3. Biodegradation and Composting Properties

Biodegradation by soil burial test was carried out to investigate the actual effect of a normal environment on the St-g-PLA based films, without any enzymatic and composting materials and man-made active compounds which is similar to the normal surrounding environment conditions. The degradation of PLA films were reported in the literature by using the composting materials and enzymatic under high temperature and controlled composting conditions [170, 171]. As it can be observed from figure. 4.52, the presence of starch in the St-g-PLA films structure accelerated the weight loss due to the sorption of microbe. The higher degradation in films compare to PLA films can be explained by the enzymatic degradation of starch backbone in the copolymer structure. The higher biodegradation rate is due to the lower crystallinity of the films since amorphous regions are more susceptible to degradation which is in agreement with XRD and water vapor permeability data. Furthermore, to compare the weight loss of the sample1 and sample2, the higher starch content as a hydrophilic component in sample 2 cause to the higher water adsorption into the film which effect the biodegradation rate. It can be concluded that the biodegradation rate of the St-g-PLA films were faster than that of PLA value.

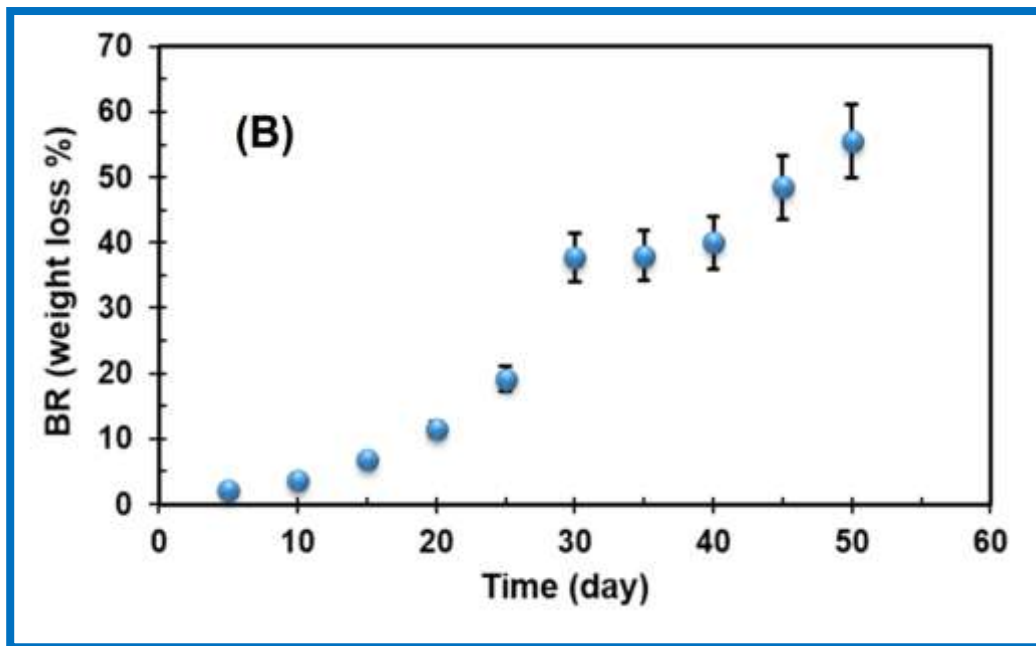
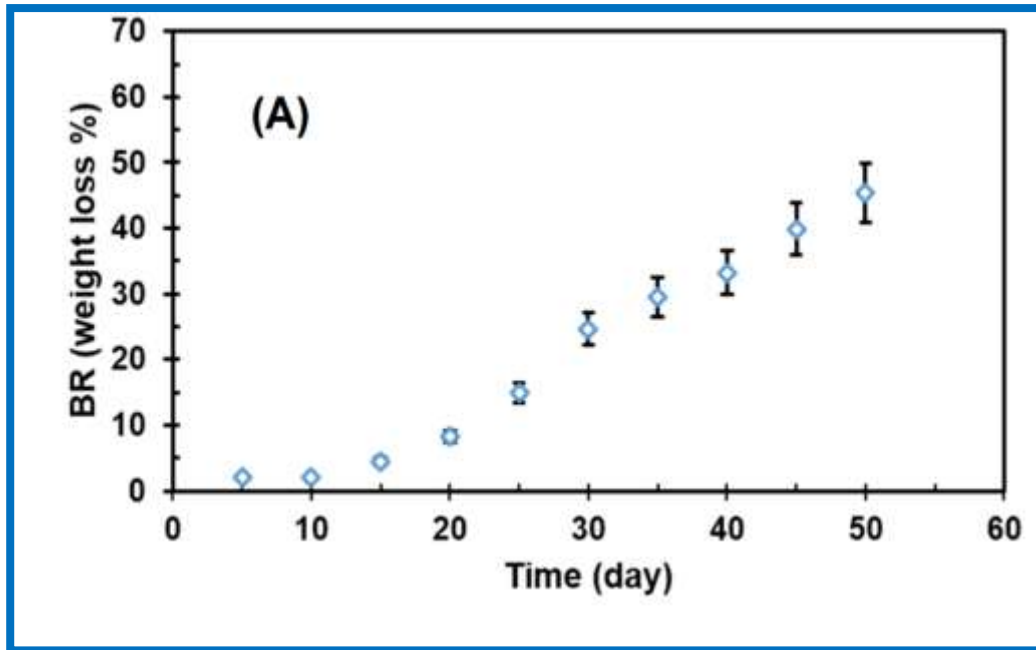


Figure. 4. 52. The Biodegradability and Time Relationship; (A) St-g-PLA (Sample 1), (B) St-g-PLA (sample 2).

4.5.7.4. Microbiological Tests and Food Contact Properties

To analyze the microbiological properties of films, all three samples were contaminated with *salmonella* (600 colonies) at +4°C by using an incubator. The results of the first and third days were gathered and colony counts were performed and reported in table 4.12.

Table. 4. 12. Microbiological results of samples.

	Sample 1	Sample 2	Sample 3
First day	320	230	230
Third day	240	240	160

In terms of reducing of the microbiological load, all of the samples represents the same results. The difference between the samples microbiologically is not significant and is negligible. Performed analysis showing the antibacterial activity of films.

The food contact analysis of the films were carried out using the conditions in which they spent the shelf life as samples were put into use in packaging. During the test, samples were analyzed by meat, cheese, and similar food simulants that represents this foods were used. After the test period completed, samples were removed from the simulants, evaporated, and the residual amount were determined by high sensitive gravimetric method. Regarding the Turkish Ministry of Food, Agriculture and Livestock packaging control laboratory reports, compliance results represents that the products are suitable for contact with fatty foods.

4.5.7.5. Real Field Application Properties

From the real field applications of the mulching films, it was found that the use of biobased/biodegradable materials (starch and LA based) can promote an environmentally friendly farming technology especially in rural areas. This biodegradable materials can reduce the contamination of the soil, increasing the use of sustainable/renewable raw materials such as starch, and protection of the environment from the waste pollution.

At the end of the mulching films lifetime, it was observed that the initial performances and stability of St-g-PLA films are consistent with their “safe” use for soil mulching in protected tomato and pepper cultivation (Figure 4.53). All the biodegradable films used during the 2 months of experiment, continued to

have their mulching function to avoid the direct contact of the tomatoes and peppers with the soil and hug the soil bed.



Figure. 4. 53. Real field applications of St-g-PLA mulching films.

5. CONCLUSIONS

The important results of this study can be concluded as follows:

- A facile and effective strategy for the design and synthesis of functional alternating copolymer-*g*-poly(L-lactic acid)/organoclays nanocomposites have developed using an interlamellar bulk graft copolymerization of lactic acid (LA) monomer onto pol (MA-*alt*-1-octadecene) in the presence of organoclays and $\text{Ti}(\text{Oct})_2$ catalyst.
- Agreeing with the $^1\text{H-NMR}$ analysis, intercalate organoclay cations significantly accelerated graft copolymerization as a co-catalyst. This is also confirmed with obtained value of molecular mass for the pristine copolymer and copolymer-*g*-PLA using MALDI-TOF-MS spectroscopy method.
- The obtain results of the comparative chemical, physical, thermal and morphology (SEM and TEM) analyses indicate that the preintercalate LA monomer...organoclay complexes play an important role in interlamellar copolymerization and intercalation/exfoliation in sit processing, as well as in the formation of self-assembled coreshell morphology with micro- and nanoporous structures and predominant intercalated nanostructures in these nanosystems.
- Complex-formation (H-bonding) and chemical reaction between anhydride/carboxyl unit and surface alkyl ammonium cations of organoclay essentially increase the force of interfacial adhesion between organic (copolymer chains) and inorganic clay phases as well as intercalating/exfoliating degree of graft copolymer chains between silicate galleries.
- The comparative DMA analysis (dynamic force and complex modulus at different T_α -relaxation temperatures) of pristine graft copolymer and its nanocomposite indicates significant difference (Δ) between DMA parameter

above T_g and can be described as a function for the formation of nano-structural architecture in poly(MA-*alt*-MA)-*g*-PLA/organoclay systems.

- Unlike known polymer/organoclay nanosystems, synthesized copolymer-*g*-PLA/organoclay nanocomposites exhibit self-assembled core-shell morphology due to surfactant character of matrix copolymer which easily forms the hydrophilic/hydrophobic balance in the reactive copolymer-*g*-PLA/organoclay systems and, therefore, the self-organized in situ chemical and physical interfacial interactions occur in the chosen interlamellar graft copolymerization conditions.
- Better self-assembled coreshell morphology structure achieved with nano-scale particle size around 25–100 nm due to physical in situ interfacial interaction and some agglomerated microparticles (300–400 nm) as a result of preferable chemical in situ processing as well as water absorption-swelling processes were observed in the poly(MA-*alt* 1-octadecene)-*g*-PLA incorporated with DMDA-MMT and ODAMM clays, respectively.
- Synthesis of functional copolymer-*g*-biopolymer layered silicate nanocomposites incorporated with different clays were carried out which are executed the dual functions as a catalyst and nanofiller.
- The origin of used clays and their LA preintercalate complexes as well as self-assembled structure of matrix graft copolymer with better hydrophilic/hydrophobic balance play an important role in the in-situ processing and in the formation and distribution of micro and nanoparticles.
- The chemical and physical structures confirmed the proposed steps and mechanism of interlamellar graft copolymerization in the presence of catalyst-nanofillers. The XRD and DSC patterns indicate that the CPNs predominantly exhibit amorphous structure with low degree of crystallinity (11.5%). The XRD patterns also provide access to the inter-layer stacking distance between clay plates.

- The obtain SEM results indicate that the origin of the clays influenced on domain size of particles, surface porosity and pore size. TEM images show the size distribution, diameter and thickness of the platelets which confirm the mixture of intercalated/exfoliated CPNs with fine disperse and partially agglomerated core-shell particles.
- The results from TGA-DT analyses indicate that the thermal stability ($T_{d(max)}=333.3\text{--}441.7\text{ }^{\circ}\text{C}$) depends on the type of used clays and changes in the following order: ODA⁺-MMT < Ag⁺-MMT < Na⁺-MMT.
- To increase thermal stability and processability of the starch-based products, we have developed a new approach for the synthesis of St-*g*-PLA copolymers by the catalytic graft copolymerization of an LA monomer onto starch in a scCO₂ medium.
- It was found that the St/LA feed ratio, temperature and pressure significantly affected the grafting degree, thermal stability and morphology of St-*g*-PLA.
- It was observed that higher pressure and temperature values, as well as an increase in the scCO₂ flow rate, led to decrease in the number of grafted LA units and a degradation of the granular starch morphology. An increase in the polymerization temperature is suitable for PLA chain length grow that a relatively low flow rate value.
- The chemical and physical structures, surface morphologies and thermal analyses reasonably confirmed the above-mentioned evaluated effects. The structures and compositions of the St-*g*-PLA copolymers were quantitatively confirmed by FTIR, ¹H (¹³C CP/MAS) NMR and alkali titration.
- The XRD results indicated the disappearance of characteristic crystalline peaks of starch after grafting LA onto starch chains and the formation of amorphous structures in the St-*g*-PLA copolymer. SEM images demonstrated the microporous morphology of St-*g*-PLA with a pore size of approximately 1–5 μm and nanosized cracks on the starch backbone due to the effect of scCO₂.

- Degradation of St-*g*-PLA copolymers has occurred in the temperature range of 260 to 360°C by a one-step chain degradation mechanism. The thermal stability of St-*g*-PLA depends on the St/LA feed ratio and decreases with an increasing amount of LA monomer in the reaction mixture.
- Microwave assisted synthesis of St-*g*-PLA copolymers describes also an alternative method to the conventional thermal heating process in the synthesis of St-*g*-PLA copolymers by using a microwave heating technique. The occurrence of graft copolymerization of PLA on the starch macromolecule backbone was confirmed by FTIR, ¹³C CP/MAS NMR and XRD. Thermal and SEM analyses indicate that there is a faster energy transfer by microwave heating and finally that the popcorn effect in starch macromolecule structure caused an increase of thermal stability in final amorphous graft copolymers.
- Furthermore, absorption of more microwave energy up to 450W by many activated radical groups from two main monomers (starch and LA) resulted in the maximum grafted PLA (62%) indicating that the higher the microwave power, higher the grafted PLA value. This study represents that microwave dielectric heating is not only a 'green' approach to graft copolymerization on starch, but also demonstrates the possibility of eco-friendly and economically feasible mass production.
- Processing of St-*g*-PLA copolymers and St-*g*-PLA/organoclay nanocomposites were also carried out by using a Turbo-mixing system. The extrusion of as prepared copolymers were done in a twin-screw extruder (Rondol, England) at a mass flow rate of about 200 g/min.
- During the processing by extrusion, the temperature of the viscous melt, pressure and torque inside the barrel were monitored and recorded by a computer. The extruded coils granulated and then placed into linear low density polyethylene (LDPE) bags for blown film production step.

- The film extrusion in a lab-scale of the St-*g*-PLA and St-*g*-PLA/organoclay based films was carried out by using a twin-screw extruder equipped by a film extrusion die and rotating film-uptake. The film quality was examined by selection the extrusion parameters based on the conditions of optimal extrusion trials. The film blowing was done at constant air flow cooling after the die and collected by a rotating roll and the film thickness was measured by a micrometer at several points of the film during the extrusion.
- Chemical and physical structures, thermal behavior and morphology of synthesized copolymers, as well as some parameters were performed by FTIR and ¹³C CP/MAS NMR spectroscopy, XRD, TGA/ DTG and SEM, respectively.
- Mechanical properties were evaluated from the tensile stress-strain test data. A well-developed polymer/clay nanocomposite results in highly increased mechanical strength in St-*g*-PLA/organoclay nanocomposite in compare of St-*g*-PLA based films.
- The effect of St/LA ratio and in situ intercalation/exfoliation process of organoclay on water vapour, O₂ and CO₂ permeabilities were measured. The O₂ permeability of samples were lower than those for CO₂, resulting in the selective action of starch based films components on gas permeability. Furthermore, the addition of intercalated/exfoliated organoclay-LA matrix improved barrier properties of St-*g*-PLA/organoclay nanocomposites films by avoiding pores and cracks as well as the shear rate applied from the turbo mixer.
- Films were exposed degradation tests buried soil conditions. From the results of biodegradability, it was concluded that the increasing of the starch ratio remarkably improved the biodegradability rate of St-*g*-PLA films. The St-*g*-PLA films buried in soil have also good degradability.

- Laboratory tests for biodegradation and real field applications indicated that the mechanical degradation of the films starts from the starch component of the products. The type of degradation is essentially microbiological in buried soil conditions.
- Antibacterial activities of the St-g-PLA based films were obtained. In terms of reducing of the microbiological charge, all of the samples represents the same results. The difference between the samples microbiologically is not significant and is negligible. Performed analysis showing the antibacterial activity of films.
- Finally, the food contact analysis of the films were carried out. During the test, samples were analyzed by meat, cheese, and similar food simulants that represents this foods were used. After the test period completed, samples were removed from the simulants, evaporated, and the residual amount were determined by high sensitive gravimetric method. The reports from Turkish Ministry of Food, Agriculture and Livestock packaging control laboratory showed that the products are suitable for contact with fatty foods.

REFERENCES

- [1] Otey FH, Westhoff RP. Biodegradable starch-based blown films. *Google Patents*; **1982**.
- [2] Bhattacharya M, Vaidya UR, Zhang D, Narayan R. Properties of blends of starch and synthetic polymers containing anhydride groups. II. Effect of amylopectin to amylose ratio in starch. *Journal of applied polymer science*. 57:539-54, **1995**.
- [3] Vaidya UR, Bhattacharya M, Zhang D. Effect of processing conditions on the dynamic mechanical properties of starch and anhydride functional polymer blends. *Polymer*. 36:1179-88, **1995**.
- [4] Plackett D. Maleated polylactide as an interfacial compatibilizer in biocomposites. *Journal of Polymers and the Environment*. 12:131-8, **2004**.
- [5] Avella M, Errico ME, Immirzi B, Malinconico M, Martuscelli E, Paolillo L, et al. Radical polymerization of poly (butyl acrylate) in the presence of poly (L-lactic acid), 1. Synthesis, characterization and properties of blends. *Die Angewandte Makromolekulare Chemie*. 246:49-63, **1997**.
- [6] Takizawa K, Nulwala H, Hu J, Yoshinaga K, Hawker CJ. Molecularly defined (L)-lactic acid oligomers and polymers: Synthesis and characterization. *Journal of Polymer Science Part A: Polymer Chemistry*. 46:5977-90, **2008**.
- [7] Mohanty A, Misra M, Hinrichsen G. Biofibres, biodegradable polymers and biocomposites: an overview. *Macromolecular Materials and Engineering*. 276:1-24, **2000**.
- [8] Gross RA, Kalra B. Biodegradable polymers for the environment. *Science*. 297:803-7, **2002**.
- [9] Petersen K, Væggemose Nielsen P, Bertelsen G, Lawther M, Olsen MB, Nilsson NH, et al. Potential of biobased materials for food packaging. *Trends in Food Science & Technology*. 10:52-68, **1999**.
- [10] Bertuzzi M, Armada M, Gottifredi J. Physicochemical characterization of starch based films. *Journal of food engineering*. 82:17-25, **2007**.
- [11] Carus M, Dammer L, Essel R. Options for Designing a New Political Framework of the European Bio-based Economy nova-Institute's contribution to the current debate.

- [12] Lawal OS, Lechner MD, Hartmann B, Kulicke WM. Carboxymethyl cocoyam starch: Synthesis, characterisation and influence of reaction parameters. *Starch-Stärke*. 59:224-33, **2007**.
- [13] Xie W, Zhang Y, Liu Y. Homogenous carboxymethylation of starch using 1-butyl-3-methylimidazolium chloride ionic liquid medium as a solvent. *Carbohydrate Polymers*. 85:792-7, 2011.
- [14] Kiatkamjornwong S, Thakeow P, Sonsuk M. Chemical modification of cassava starch for degradable polyethylene sheets. *Polymer Degradation and Stability*. 73:363-75, **2001**.
- [15] Thakore I, Desai S, Sarawade B, Devi S. Studies on biodegradability, morphology and thermo-mechanical properties of LDPE/modified starch blends. *European Polymer Journal*. 37:151-60, **2001**.
- [16] Chandra R, Rustgi R. Biodegradation of maleated linear low-density polyethylene and starch blends. *Polymer Degradation and Stability*. 56:185-202, **1997**.
- [17] Bikiaris D, Prinos J, Panayiotou C. Effect of EAA and starch on the thermooxidative degradation of LDPE. *Polymer degradation and stability*. 56:1-9, **1997**.
- [18] Yoo SI, Lee TY, Yoon JS, Lee IM, Kim MN, Lee HS. Interfacial adhesion reaction of polyethylene and starch blends using maleated polyethylene reactive compatibilizer. *Journal of applied polymer science*. 83:767-76, **2002**.
- [19] Rzaev ZM. Polyolefin nanocomposites by reactive extrusion. *Advances in Polyolefin Nanocomposites*. 87: **2011**.
- [20] Rzaev ZM. Graft copolymers of maleic anhydride and its isostructural analogues: High performance engineering materials. arXiv preprint arXiv:11051260, **2011**.
- [21] Zhang J-F, Sun X. Mechanical properties of poly (lactic acid)/starch composites compatibilized by maleic anhydride. *Biomacromolecules*. 5:1446-51, **2004**.
- [22] Heinze T, Liebert T. Unconventional methods in cellulose functionalization. *Progress in Polymer Science*. 26:1689-762, **2001**.
- [23] Willett J, Jasberg B, Swanson C. Rheology of thermoplastic starch: effects of temperature, moisture content, and additives on melt viscosity. *Polymer Engineering & Science*. 35:202-10, **1995**.

- [24] Harris R, Humphreys RW, Jureller SH, Kerschner JL, Trzasko PT. Polysaccharide modification in densified fluid. *Google Patents*, **1999**.
- [25] Cooper AI. Polymer synthesis and processing using supercritical carbon dioxide. *Journal of Materials Chemistry*. 10:207-34, **2000**.
- [26] Woods HM, Silva MM, Nouvel C, Shakesheff KM, Howdle SM. Materials processing in supercritical carbon dioxide: surfactants, polymers and biomaterials. *Journal of Materials Chemistry*. 14:1663-78, **2004**.
- [27] Aydin HM. A Three-Layered Osteochondral Plug: Structural, Mechanical, and in vitro Biocompatibility Analysis. *Advanced Engineering Materials*. 13:B511-B7, **2011**.
- [28] Davies OR, Lewis AL, Whitaker MJ, Tai H, Shakesheff KM, Howdle SM. Applications of supercritical CO₂ in the fabrication of polymer systems for drug delivery and tissue engineering. *Advanced drug delivery reviews*. 60:373-87, **2008**.
- [29] Gencer ZA, Odabas S, Sasmazel HT, Piskin E. Macroporous silicone biomaterials with modified surface chemistry: Production and characterization. *Journal of Bioactive and Compatible Polymers*. 0883911512455115, **2012**.
- [30] Kemmere MF, Meyer T. Supercritical carbon dioxide: in polymer reaction engineering: *John Wiley & Sons*; **2006**.
- [31] Muljana H, Picchioni F, Heeres HJ, Janssen LP. Green starch conversions: Studies on starch acetylation in densified CO₂. *Carbohydrate Polymers*. 82:653-62, **2010**.
- [32] Yin C, Li J, Xu Q, Peng Q, Liu Y, Shen X. Chemical modification of cotton cellulose in supercritical carbon dioxide: synthesis and characterization of cellulose carbamate. *Carbohydrate polymers*. 67:147-54, **2007**.
- [33] Yılmaz M, Eğri S, Yıldız N, Çalıklı A, Pişkin E. Dispersion polymerization of L-lactide in supercritical carbon dioxide. *Journal of Polymer Research*.;18:975-82, **2011**.
- [34] Fanta GF, Felker FC, Shogren RL. Graft polymerization of acrylonitrile onto spherocrystals formed from jet cooked cornstarch. *Carbohydrate polymers*. 56:77-84, **2004**.
- [35] Singh V, Kumar P, Sanghi R. Use of microwave irradiation in the grafting modification of the polysaccharides—A review. *Progress in polymer science*. 37:340-64, **2012**.

- [36] Bertolini A, Mestres C, Colonna P, Raffi J. Free radical formation in UV- and gamma-irradiated cassava starch. *Carbohydrate Polymers*. 44:269-71, **2001**.
- [37] Vahdat A, Bahrami H, Ansari N, Ziaie F. Radiation grafting of styrene onto polypropylene fibres by a 10MeV electron beam. *Radiation Physics and Chemistry*. 76:787-93, **2007**.
- [38] Singh V, Tiwari A, Pandey S, Singh S. Peroxydisulfate initiated synthesis of potato starch-graft-poly (acrylonitrile) under microwave irradiation. *Express Polymer Letters*. 1:51-8, **2007**.
- [39] Sen G, Kumar R, Ghosh S, Pal S. A novel polymeric flocculant based on polyacrylamide grafted carboxymethylstarch. *Carbohydrate Polymers*. 77:822-31, **2009**.
- [40] Sen G, Singh RP, Pal S. Microwave-initiated synthesis of polyacrylamide grafted sodium alginate: Synthesis and characterization. *Journal of applied polymer science*. 115:63-71, **2010**.
- [41] Sen G, Pal S. Microwave initiated synthesis of polyacrylamide grafted carboxymethylstarch (CMS-g-PAM): application as a novel matrix for sustained drug release. *International journal of biological macromolecules*. 45:48-55, **2009**.
- [42] Sen G, Mishra S, Jha U, Pal S. Microwave initiated synthesis of polyacrylamide grafted guar gum (GG-g-PAM)—Characterizations and application as matrix for controlled release of 5-amino salicylic acid. *International journal of biological macromolecules*. 47:164-70, **2010**.
- [43] Mishra S, Mukul A, Sen G, Jha U. Microwave assisted synthesis of polyacrylamide grafted starch (St-g-PAM) and its applicability as flocculant for water treatment. *International Journal of Biological Macromolecules*. 48:106-11, 2011.
- [44] Chang PR, Zhou Z, Xu P, Chen Y, Zhou S, Huang J. Thermoforming starch-graft-polycaprolactone biocomposites via one-pot microwave assisted ring opening polymerization. *Journal of applied polymer science*. 113:2973-9, **2009**.
- [45] Tong Z, Peng W, Zhiqian Z, Baoxiu Z. Microwave irradiation copolymerization of superabsorbents from cornstarch and sodium acrylate. *Journal of applied polymer science*. 95:264-9, **2005**.

- [46] Ebner C, Bodner T, Stelzer F, Wiesbrock F. One Decade of Microwave-Assisted Polymerizations: Quo vadis. *Macromolecular rapid communications*. 32:254-88, **2011**.
- [47] Hatakeyama T, Hatakeyama H. Thermal properties of green polymers and biocomposites: *Springer*; **2006**.
- [48] Carrasco F, Cailloux J, Sánchez-Jiménez P, MasPOCH ML. Improvement of the thermal stability of branched poly (lactic acid) obtained by reactive extrusion. *Polymer Degradation and Stability*. 104:40-9, **2014**.
- [49] Datta R, Henry M. Lactic acid: recent advances in products, processes and technologies—a review. *Journal of Chemical Technology and Biotechnology*. 81:1119-29, **2006**.
- [50] Holten CH. Lactic acid. Properties and chemistry of lactic acid and derivatives: Weinheim/Bergstr., W. Germany, Verlag Chemie GmbH; **1971**.
- [51] Lowe CE. PREPARATION. *Google Patents*; **1954**.
- [52] Inkinen S, Hakkarainen M, Albertsson A-C, Södergård A. From lactic acid to poly (lactic acid)(PLA): characterization and analysis of PLA and its precursors. *Biomacromolecules*. 12:523-32, **2011**.
- [53] Inkinen S, Stolt M, Södergård A. Stability studies on blends of a lactic acid-based hot melt adhesive and starch. *Journal of applied polymer science*. 110:2467-74, **2008**.
- [54] Jiang L, Wolcott MP, Zhang J. Study of biodegradable polylactide/poly (butylene adipate-co-terephthalate) blends. *Biomacromolecules*. 7:199-207, **2006**.
- [55] Yu J, Wang N, Ma X. Fabrication and characterization of poly (lactic acid)/acetyl tributyl citrate/carbon black as conductive polymer composites. *Biomacromolecules*. 9:1050-7, **2008**.
- [56] Bhardwaj R, Mohanty AK. Modification of brittle polylactide by novel hyperbranched polymer-based nanostructures. *Biomacromolecules*. 8:2476-84, **2007**.
- [57] Numata K, Finne-Wistrand A, Albertsson A-C, Doi Y, Abe H. Enzymatic degradation of monolayer for poly (lactide) revealed by real-time atomic force microscopy: Effects of stereochemical structure, molecular weight, and molecular branches on hydrolysis rates. *Biomacromolecules*. 9:2180-5, **2008**.

- [58] Zhang J, Beshra A, Domb AJ, Ozaki Y. d-Poly (lactide) and LHRH decapeptide stereointeractions investigated by vibrational spectroscopy. *European polymer journal*. 43:3016-27, **2007**.
- [59] Kister G, Cassanas G, Vert M, Pauvert B, Terol A. Vibrational analysis of poly (L-lactic acid). *Journal of Raman Spectroscopy*. 26:307-11, **1995**.
- [60] Younes H, Cohn D. Phase separation in poly (ethylene glycol)/poly (lactic acid) blends. *European polymer journal*. 24:765-73, **1988**.
- [61] Dorgan JR, Janzen J, Knauss DM, Hait SB, Limoges BR, Hutchinson MH. Fundamental solution and single-chain properties of polylactides. *Journal of Polymer Science Part B: Polymer Physics*. 43:3100-11, **2005**.
- [62] Lim L-T, Auras R, Rubino M. Processing technologies for poly (lactic acid). *Progress in Polymer Science*. 33:820-52, **2008**.
- [63] Tsai C-C, Wu R-J, Cheng H-Y, Li S-C, Siao Y-Y, Kong D-C, et al. Crystallinity and dimensional stability of biaxial oriented poly (lactic acid) films. *Polymer Degradation and Stability*. 95:1292-8, **2010**.
- [64] Fukushima K, Kimura Y. An efficient solid-state polycondensation method for synthesizing stereocomplexed poly (lactic acid) s with high molecular weight. *Journal of Polymer Science Part A: Polymer Chemistry*. 46:3714-22, **2008**.
- [65] Hirata M, Kobayashi K, Kimura Y. Enhanced Stereocomplexation by Enantiomer Adjustment for Stereo Diblock Polylactides with Non-Equivalent D/L Ratios. *Macromolecular Chemistry and Physics*. 211:1426-32, **2010**.
- [66] Huang J, Lisowski MS, Runt J, Hall ES, Kean RT, Buehler N, et al. Crystallization and microstructure of poly (l-lactide-co-meso-lactide) copolymers. *Macromolecules*. 31:2593-9, **1998**.
- [67] Weber C, Haugaard V, Festersen R, Bertelsen G. Production and applications of biobased packaging materials for the food industry. *Food Additives & Contaminants*. 19:172-7, **2002**.
- [68] Rzayev ZM, Salimi K, Eğri Ö, Pişkin E. Functional copolymer/organo-MMT nanoarchitectures. XIX. Nanofabrication and characterization of poly (MA-alt-1-octadecene)-g-PLA layered silicate nanocomposites with nanoporous core-shell morphology. *Polymers for Advanced Technologies*. 25:294-306, **2014**.

- [69] Salimi K, Rzayev ZM, Pişkin E. Functional organo-Mt/copolymer nanoarchitectures. XXII. Interlamellar graft copolymerisation of L-lactic acid onto poly (maleic anhydride-*co*-1-octadecene) in the presence of different clays as catalyst-nanofillers. *Applied Clay Science*. 101:106-18, **2014**.
- [70] Ogata N, Jimenez G, Kawai H, Ogihara T. Structure and thermal/mechanical properties of poly (L-lactide)-clay blend. *Journal of Polymer Science Part B: Polymer Physics*. 35:389-96, **1997**.
- [71] Paul M-A, Delcourt C, Alexandre M, Degée P, Monteverde F, Dubois P. Polylactide/montmorillonite nanocomposites: study of the hydrolytic degradation. *Polymer degradation and stability*. 87:535-42, **2005**.
- [72] Serizawa S, Inoue K, Iji M. Kenaf-fiber-reinforced poly (lactic acid) used for electronic products. *Journal of Applied Polymer Science*. 100:618-24, **2006**.
- [73] Oksman K, Skrifvars M, Selin J-F. Natural fibres as reinforcement in polylactic acid (PLA) composites. *Composites science and technology*. 63:1317-24, **2003**.
- [74] Huda MS, Drzal LT, Mohanty AK, Misra M. Chopped glass and recycled newspaper as reinforcement fibers in injection molded poly (lactic acid)(PLA) composites: a comparative study. *Composites Science and Technology*. 66:1813-24, **2006**.
- [75] Mathew AP, Oksman K, Sain M. Mechanical properties of biodegradable composites from poly lactic acid (PLA) and microcrystalline cellulose (MCC). *Journal of applied polymer science*. 97:2014-25, **2005**.
- [76] Mathew AP, Oksman K, Sain M. The effect of morphology and chemical characteristics of cellulose reinforcements on the crystallinity of polylactic acid. *Journal of applied polymer science*. 101:300-10, **2006**.
- [77] Dorgan JR, Janzen J, Clayton MP, Hait SB, Knauss DM. Melt rheology of variable L-content poly (lactic acid). *Journal of Rheology (1978-present)*. 49:607-19, 2005.
- [78] Celli A, Scandola M. Thermal properties and physical ageing of poly (L-lactic acid). *Polymer*. 33:2699-703, **1992**.
- [79] Witzke DR. Introduction to properties, engineering, and prospects of polylactide polymers: Michigan State University. *Department of Chemical Engineering*; **1997**.

- [80] Cai H, Dave V, Gross RA, McCarthy SP. Effects of physical aging, crystallinity, and orientation on the enzymatic degradation of poly (lactic acid). *Journal of Polymer Science Part B: Polymer Physics*. 34:2701-8, **1996**.
- [81] Giles Jr HF, Mount III EM, Wagner Jr JR. Extrusion: the definitive processing guide and handbook: *William Andrew*; **2004**.
- [82] Doi Y, Steinbüchel A. Biopolymers:[biology, chemistry, biotechnology, applications]. 4, Polyesters: 3. Applications and commercial products: *Wiley-Vch*; **2002**.
- [83] Lee JK, Lee KH, Jin BS. Structure development and biodegradability of uniaxially stretched poly (l-lactide). *European polymer journal*. 37:907-14, **2001**.
- [84] Conn RSE, Gruber PR, Hall ES, Kolstad JJ, Ryan CM. Melt-stable amorphous lactide polymer film and process for manufacturing thereof. *Google Patents*; **1996**.
- [85] Sodergard A, Selin J-F, Niemi M, Johansson C-J, Meinander K. Processable poly (hydroxy acids). *Google Patents*; **2003**.
- [86] RIEGERT TE, Stephens HM, TWEED EC. Polylactic acid blown film and method of manufacturing same. *Google Patents*; **2009**.
- [87] Jamshidian M, Tehrani EA, Imran M, Jacquot M, Desobry S. Poly-Lactic Acid: Production, Applications, Nanocomposites, and Release Studies. *Comprehensive Reviews in Food Science and Food Safety*. 9:552-71, **2010**.
- [88] Lehermeier HJ, Dorgan JR, Way JD. Gas permeation properties of poly (lactic acid). *Journal of membrane science*. 190:243-51, **2001**.
- [89] Dubois P, Alexandre M, Hindryckx F, Jérôme R. Polyolefin-based composites by polymerization-filling technique. **1998**.
- [90] Lagaly G. Introduction: from clay mineral-polymer interactions to clay mineral-polymer nanocomposites. *Applied Clay Science*. 15:1-9, **1999**.
- [91] Alexandre M, Dubois P. Polymer-layered silicate nanocomposites: preparation, properties and uses of a new class of materials. *Materials Science and Engineering: R: Reports*. 28:1-63, **2000**.
- [92] Goettler L, Lee K, Thakkar H. Layered silicate reinforced polymer nanocomposites: development and applications. *Polymer Reviews*. 47:291-317, **2007**.

- [93] Sinha Ray S, Pouliot S, Bousmina M, Utracki LA. Role of organically modified layered silicate as an active interfacial modifier in immiscible polystyrene/polypropylene blends. *Polymer*. 45:8403-13, **2004**.
- [94] Zanetti M, Lomakin S, Camino G. Polymer layered silicate nanocomposites. *Macromolecular Materials and Engineering*. 279:1-9, **2000**.
- [95] Rzayev ZM, Güner A, Söylemez EA, Kavlak S. Functional copolymer/organo-MMT nanoarchitectures. III. Dynamic mechanical behavior of poly (IA-co-BMA)-organo-MMT clay nanocomposites. *Polymers for Advanced Technologies*. 22:1349-58, **2011**.
- [96] Rzayev ZM, Şenol B, Denkbaş AB. Functional copolymer/organo-montmorillonite nanoarchitectures. IX. Synthesis and nanostructure–morphology–thermal behaviour relationships of poly [(maleic anhydride)-alt-(acrylic acid)]/organo-montmorillonite nanocomposites. *Polymer International*. 60:1446-54, **2011**.
- [97] Camino G, Tartaglione G, Frache A, Manfredi C, Costa G. Thermal and combustion behaviour of layered silicate–epoxy nanocomposites. *Polymer Degradation and stability*. 90:354-62, **2005**.
- [98] Kotsilkova R. Processing–structure–properties relationships of mechanically and thermally enhanced smectite/epoxy nanocomposites. *Journal of applied polymer science*. 97:2499-510, **2005**.
- [99] Altungöz E, Rzayev ZM, Alper E. Functional Copolymer/Organo-MMT Nanoarchitectures. XII. Polypropylene/Poly (MA-alt-1-octadecene)/Organoclay Based Biaxially Oriented Nanofilms Through Reactive Extrusion. *International Review of Chemical Engineering-Rapid Communications*. 3, **2011**.
- [100] Bozdoğan DD, Kibarer G, Rzayev ZM. Functional Copolymer/Organo-MMT Nanoarchitectures. XV. Interlamellar Complex-Radical Alternating Copolymerization of α -Olefins (C 6-12) with Maleic Anhydride in the Presence of Reactive and Non-Reactive Organoclays. *International Review of Chemical Engineering-Rapid Communications*. 4, **2012**.
- [101] Dilmani MA, Rzayev ZM, Alper E. Functional Copolymer/Organo-MMT Nanoarchitectures. XIII. EPDM Rubber/Poly [(MA-alt-1-octadecene)-g-PEO]/Organoclays Nanocomposites Through Reactive Extrusion. *International Review of Chemical Engineering-Rapid Communications*. 4, **2012**.

- [102] Rzaev ZM, Dincer S, Pişkin E. Functional copolymers of *N*-isopropylacrylamide for bioengineering applications. *Progress in Polymer Science*. 32:534-95, **2007**.
- [103] Rzaev ZM. Nano Methods in Polymer Synthesis and Processing: Carboxyl/Anhydride Functionalized Copolymers for Nanoengineering Applications. *International Review of Chemical Engineering-Rapid Communications*. 3, **2011**.
- [104] Di Corato R, Quarta A, Piacenza P, Ragusa A, Figuerola A, Buonsanti R, et al. Water solubilization of hydrophobic nanocrystals by means of poly (maleic anhydride-alt-1-octadecene). *Journal of Materials Chemistry*. 18:1991-6, **2008**.
- [105] Schmidt U, Zschoche S, Werner C. Modification of poly (octadecene-alt-maleic anhydride) films by reaction with functional amines. *Journal of applied polymer science*. 87:1255-66, **2003**.
- [106] Pellegrino T, Manna L, Kudera S, Liedl T, Koktysh D, Rogach AL, et al. Hydrophobic nanocrystals coated with an amphiphilic polymer shell: a general route to water soluble nanocrystals. *Nano Letters*. 4:703-7, **2004**.
- [107] William WY, Chang E, Sayes CM, Drezek R, Colvin VL. Aqueous dispersion of monodisperse magnetic iron oxide nanocrystals through phase transfer. *Nanotechnology*. 17:4483, **2006**.
- [108] Yu WW, Chang E, Falkner JC, Zhang J, Al-Somali AM, Sayes CM, et al. Forming biocompatible and nonaggregated nanocrystals in water using amphiphilic polymers. *Journal of the American Chemical Society*. 129:2871-9, **2007**.
- [109] Donescu D, Raditoiu V, Spataru CI, Somoghi R, Ghiurea M, Radovici C, et al. Superparamagnetic magnetite-divinylbenzene-maleic anhydride copolymer nanocomposites obtained by dispersion polymerization. *European Polymer Journal*. 48:1709-16, **2012**.
- [110] Gilding D. Biodegradable polymers. Biocompatibility of clinical implant materials. 2:209-32, **1981**.
- [111] Conn Jr J, Oyasu R, Welsh M, Beal JM. Vicryl (polyglactin 910) synthetic absorbable sutures. *The American Journal of Surgery*. 128:19-23, **1974**.
- [112] Heller J. The use of polymers in the construction of controlled-release devices. *NIDA research monograph*. 154:107-31, **1995**.

- [113] Carlson D, Nie L, Narayan R, Dubois P. Maleation of polylactide (PLA) by reactive extrusion. *Journal of applied polymer science*. 72:477-85, **1999**.
- [114] Carlson D, Dubois P, Nie L, Narayan R. Free radical branching of polylactide by reactive extrusion. *Polymer Engineering & Science*. 38:311-21, **1998**.
- [115] Ramkumar D, Bhattacharya M, Vaidya UR. Properties of injection moulded starch/synthetic polymer blends—II. Evaluation of mechanical properties. *European polymer journal*. 33:729-42, **1997**.
- [116] Li D, Ye C, Zhu Y, Qi Y, Gou Z, Gao C. Fabrication of poly (lactide-co-glycolide) scaffold embedded spatially with hydroxyapatite particles on pore walls for bone tissue engineering. *Polymers for Advanced Technologies*. 23:1446-53, **2012**.
- [117] Pan P, Liang Z, Cao A, Inoue Y. Layered metal phosphonate reinforced poly (l-lactide) composites with a highly enhanced crystallization rate. *ACS applied materials & interfaces*. 1:402-11, **2009**.
- [118] Vasanthan N, Ly H, Ghosh S. Impact of nanoclay on isothermal cold crystallization kinetics and polymorphism of poly (l-lactic acid) nanocomposites. *The Journal of Physical Chemistry B*. 115:9556-63, **2011**.
- [119] Yang Y, Wu D, Li C, Liu L, Cheng X, Zhao H. Poly (l-lactide) comb polymer brushes on the surface of clay layers. *Polymer*. 47:7374-81, **2006**.
- [120] Paul M-A, Alexandre M, Degée P, Henrist C, Rulmont A, Dubois P. New nanocomposite materials based on plasticized poly (L-lactide) and organo-modified montmorillonites: thermal and morphological study. *Polymer*. 44:443-50, **2003**.
- [121] Sinha Ray S, Maiti P, Okamoto M, Yamada K, Ueda K. New polylactide/layered silicate nanocomposites. 1. Preparation, characterization, and properties. *Macromolecules*. 35:3104-10, **2002**.
- [122] Maiti P, Yamada K, Okamoto M, Ueda K, Okamoto K. New polylactide/layered silicate nanocomposites: role of organoclays. *Chemistry of materials*. 14:4654-61, **2002**.
- [123] Bordes P, Pollet E, Avérous L. Nano-biocomposites: biodegradable polyester/nanoclay systems. *Progress in Polymer Science*. 34:125-55, **2009**.

- [124] Pluta M, Jeszka J, Boiteux G. Polylactide/montmorillonite nanocomposites: structure, dielectric, viscoelastic and thermal properties. *European Polymer Journal*. 43:2819-35, **2007**.
- [125] Yang K, Wang X, Wang Y. Progress in nanocomposite of biodegradable polymer. *Journal of Industrial and Engineering Chemistry-Seoul*. 13:485, **2007**.
- [126] Bourbigot S, Fontaine G, Duquesne S, Delobel R. PLA nanocomposites: quantification of clay nanodispersion and reaction to fire. *International Journal of Nanotechnology*. 5:683-92, **2008**.
- [127] Ferris JP. Mineral catalysis and prebiotic synthesis: montmorillonite-catalyzed formation of RNA. *Elements*. 1:145-9, **2005**.
- [128] Ferris JP, Huang C-H, Hagan Jr WJ. Montmorillonite: a multifunctional mineral catalyst for the prebiological formation of phosphate esters. *Origins of Life and Evolution of the Biosphere*. 18:121-33, **1988**.
- [129] Fukushima K, Tabuani D, Camino G. Nanocomposites of PLA and PCL based on montmorillonite and sepiolite. *Materials Science and Engineering: C*. 29:1433-41, 2009.
- [130] Gacitua W, Ballerini A, Zhang J. Polymer nanocomposites: synthetic and natural fillers a review. *Maderas Ciencia y tecnología*. 7:159-78, **2005**.
- [131] Kontou E, Niaounakis M, Georgiopoulos P. Comparative study of PLA nanocomposites reinforced with clay and silica nanofillers and their mixtures. *Journal of Applied Polymer Science*. 122:1519-29, **2011**.
- [132] Liu M, Zhang Y, Zhou C. Nanocomposites of halloysite and polylactide. *Applied Clay Science*. 75:52-9, **2013**.
- [133] Yang Y, Matsubara S, Xiong L, Hayakawa T, Nogami M. Solvothermal synthesis of multiple shapes of silver nanoparticles and their SERS properties. *The Journal of Physical Chemistry C*. 111:9095-104, **2007**.
- [134] Souza D, Dahmouche K, Andrade C, Dias M. Synthetic organofluoromica/poly (lactic acid) nanocomposites: Structure, rheological and thermal properties. *Applied Clay Science*. 80:259-66, **2013**.
- [135] Fernández MJ, Fernández MD, Aranburu I. Effect of clay surface modification and organoclay purity on microstructure and thermal properties of poly (l-lactic acid)/vermiculite nanocomposites. *Applied Clay Science*. 80:372-81, **2013**.

- [136] Bianchi A, Fernández M, Pantanetti M, Viña R, Torriani I, Sánchez R, et al. ODTMA⁺ and HDTMA⁺ organo-montmorillonites characterization: New insight by WAXS, SAXS and surface charge. *Applied Clay Science*. 83:280-5, **2013**.
- [137] Rzayev ZM, Söylemez AE. Functional copolymer/organo-MMT nanoarchitectures. VI. Synthesis and characterization of novel nanocomposites by interlamellar controlled/living radical copolymerization via preintercalated RAFT-agent/organoclay complexes. *Journal of nanoscience and nanotechnology*. 11:3523-32, **2011**.
- [138] Rzayev ZM, Söylemez EA, Davarcioğlu B. Functional copolymer/organo-MMT nanoarchitectures. VII. Interlamellar controlled/living radical copolymerization of maleic anhydride with butyl methacrylate via preintercalated RAFT agent–organoclay complexes. *Polymers for Advanced Technologies*. 23:278-89, **2012**.
- [139] Rzayev ZM, Güner A, Söylemez EA, Kavlak S. Functional copolymer/organo-MMT nanoarchitectures. II. Dynamic mechanical behavior of poly (MA-co-BMA) s-organo-MMT clay nanocomposites. *Journal of applied polymer science*. 118:2904-13, **2010**.
- [140] Söylemez E, Çaylak N, Rzayev M. Synthesis and characterization of functional copolymer/organo-silicate nanoarchitectures through interlamellar complex-radical (co) terpolymerization. *EXPRESS Polymer Letters*. 2:639-54, **2008**.
- [141] Önal M. Examination of some commercial sorptive organobentonites. *Turkish Journal of Chemistry*. 31:579-88, **2007**.
- [142] Kulkarni SK. Nanotechnology: principles and practices: *Springer*, **2007**.
- [143] Sivam AS, Waterhouse GI, Zujovic ZD, Perera CO, Sun-Waterhouse D. Structure and dynamics of wheat starch in breads fortified with polyphenols and pectin: An ESEM and solid-state CP/MAS ¹³C NMR spectroscopic study. *Food and Bioprocess Technology*. 6:110-23, **2013**.
- [144] Choucair A, Lavigueur C, Eisenberg A. Polystyrene-b-poly (acrylic acid) vesicle size control using solution properties and hydrophilic block length. *Langmuir*. 20:3894-900, **2004**.

- [145] Walther A, Goldmann AS, Yelamanchili RS, Drechsler M, Schmalz H, Eisenberg A, et al. Multiple morphologies, phase transitions, and cross-linking of crew-cut aggregates of polybutadiene-block-poly (2-vinylpyridine) diblock copolymers. *Macromolecules*. 41:3254-60, **2008**.
- [146] Ho R-M, Chiang Y-W, Lin C-C, Bai S. Block copolymer self-assembly induced compatibilization of PCL/PS-PEP blends. *Macromolecules*. 35:1299-306, **2002**.
- [147] de Wit J, van Ekenstein GA, Polushkin E, Korhonen J, Ruokolainen J, Ten Brinke G. Random Copolymer Effect in Self-Assembled Hydrogen-Bonded P (S-co-4VP)(PDP) Side-Chain Polymers. *Macromolecules*. 42:2009-14, **2009**.
- [148] Kaushlendra K, Asha S. Microstructural Reorganization and Cargo Release in Pyrene Urethane Methacrylate Random Copolymer Hollow Capsules. *Langmuir*. 28:12731-43, **2012**.
- [149] Cooper TR, Storey RF. Poly (lactic acid) and chain-extended poly (lactic acid)-polyurethane functionalized with pendent carboxylic acid groups. *Macromolecules*.; 1:655-62, **2008**.
- [150] Pekel N, Şahiner N, Güven O, Rzaev ZM. Synthesis and characterization of *N*-vinylimidazole–ethyl methacrylate copolymers and determination of monomer reactivity ratios. *European polymer journal*. 37:2443-51, **2001**.
- [151] Kulkarni S. Nanotechnology—Principles and Processes. Capital Publishing House, New Delhi; **2009**.
- [152] Salkar R, Jeevanandam P, Aruna S, Koltypin Y, Gedanken A. The sonochemical preparation of amorphous silver nanoparticles. *J Mater Chem*. 9:1333-5, 1999.
- [153] Lee P, Meisel D. Adsorption and surface-enhanced Raman of dyes on silver and gold sols. *The Journal of Physical Chemistry*. 86:3391-5, **1982**.
- [154] Casalini T, Rossi F, Santoro M, Perale G. Structural Characterization of Poly-L-lactic Acid (PLLA) and Poly (glycolic acid)(PGA) Oligomers. *International journal of molecular sciences*.;12:3857-70, **2011**.
- [155] Chitte HK, Bhat NV, Karmakar NS, Kothari DC, Shinde GN. Synthesis and Characterization of Polymeric Composites Embedded with Silver Nanoparticles. *World Journal of Nano Science and Engineering*. 2:19, **2012**.

- [156] Feijoo J, Cabedo L, Gimenez E, Lagaron J, Saura J. Development of amorphous PLA-montmorillonite nanocomposites. *Journal of materials science*. 40:1785-8, **2005**.
- [157] Muljana H, Picchioni F, Heeres HJ, Janssen LP. Supercritical carbon dioxide (scCO₂) induced gelatinization of potato starch. *Carbohydrate polymers*. 78:511-9, **2009**.
- [158] Ma X, Yu J, Wang N. Fly ash-reinforced thermoplastic starch composites. *Carbohydrate polymers*. 67:32-9, **2007**.
- [159] Cameron N, Cowie J, Ferguson R, McEwan I. Enthalpy relaxation of styrene–maleic anhydride (SMA) copolymers Part 1. Single component systems. *Polymer*. 41:7255-62, **2000**.
- [160] Gong Q, Wang L-Q, Tu K. In situ polymerization of starch with lactic acid in aqueous solution and the microstructure characterization. *Carbohydrate Polymers*.;64:501-9, **2006**.
- [161] Meshram M, Patil V, Mhaske S, Thorat B. Graft copolymers of starch and its application in textiles. *Carbohydrate Polymers*. 75:71-8, **2009**.
- [162] Muljana H, van der Knoop S, Keijzer D, Picchioni F, Janssen LP, Heeres HJ. Synthesis of fatty acid starch esters in supercritical carbon dioxide. *Carbohydrate Polymers*. 82:346-54, **2010**.
- [163] Salimi K, Yilmaz M, Rzayev ZM, Piskin E. Controlled graft copolymerization of lactic acid onto starch in a supercritical carbon dioxide medium. *Carbohydrate polymers*. 114:149-56, **2014**.
- [164] Liu X, Khor S, Petinakis E, Yu L, Simon G, Dean K, et al. Effects of hydrophilic fillers on the thermal degradation of poly (lactic acid). *Thermochimica Acta*. 509:147-51, **2010**.
- [165] Liu H, Xie F, Yu L, Chen L, Li L. Thermal processing of starch-based polymers. *Progress in Polymer Science*. 34:1348-68, **2009**.
- [166] Tsuji H, Ikada Y. Stereocomplex formation between enantiomeric poly (lactic acid) s. XI. Mechanical properties and morphology of solution-cast films. *Polymer*. 40:6699-708, **1999**.
- [167] Garcia M, Martino M, Zaritzky N. Lipid Addition to Improve Barrier Properties of Edible Starch-based Films and Coatings. *Journal of food science*. 65:941-4, **2000**.

- [168] Müller CM, Laurindo JB, Yamashita F. Effect of nanoclay incorporation method on mechanical and water vapor barrier properties of starch-based films. *Industrial Crops and Products*. 33:605-10, **2011**.
- [169] Akbari B, Bagheri R. Deformation mechanism of epoxy/clay nanocomposite. *European polymer journal*. 43:782-8, **2007**.
- [170] Ochi S. Mechanical properties of kenaf fibers and kenaf/PLA composites. *Mechanics of materials*. 40:446-52, **2008**.
- [171] Ohkita T, Lee SH. Thermal degradation and biodegradability of poly (lactic acid)/corn starch biocomposites. *Journal of applied polymer science*. 100:3009-17, **2006**.

CURRICULUM VITAE

Credentials

Name, Surname : Kouroush Salimi
Place of Birth : 12 February 1986, İran
Marital Status : Single
Email : salimi@hacettepe.edu.tr
Adress : Alsancak Mah., Alsancak Sok, 15/07, Etimesgut, ANKARA.

Education

High School : Rahe Danesh High School, İran, (1999-2003)
BSc. : Polymer Engineering, İran, (2004-2008)
MSc. : Chemical Engineering, Hacettepe University, (2011-2012)
PhD. : Chemical Engineering, Hacettepe University, (2012-2015)

Foreign Languages

Azerbaijanese- Mother tongue

Persian- Mother tongue

Turkish- Mother tongue

Arabic- Elementary

English- Proficient

Work Experience

Tonggouyan Petrochemical Co., poly F unit, PET production line, Process Control Engineer Assistant, Mahshahr Petrochemical Zone, Mahshahr, İran, June-September 2008.